GDL/GMF-90-01

Structure of Monopropellant Spray Flames at Elevated Pressures

by

G.M. Faeth, T.-W. Lee, M.E. Kounalakis
and L.-K. Tseng

FINAL REPORT

15 January 1990

U.S. Army Research Office
Contract No. DAAL03-86-K-0154

Department of Aerospace Engineering
The University of Michigan

Approved for Public Release; Distribution Unlimited

REPORT DOCUMENTATION PAGE

Form Approved OMB No. 0704-0188

1a. REPORT SECURITY CLASSIFICATION: Unclassified	1b. RESTRICTIVE MARKINGS
2a. SECURITY CLASSIFICATION AUTHORITY	3. DISTRIBUTION / AVAILABILITY OF REPORT: Approved for public release; distribution is unlimited.
2b. DECLASSIFICATION / DOWNGRADING SCHEDULE	
4. PERFORMING ORGANIZATION REPORT NUMBER(S)	5. MONITORING ORGANIZATION REPORT NUMBER(S)
6a. NAME OF PERFORMING ORGANIZATION: Dept. of Aerospace Engineering, The University of Michigan 6b. OFFICE SYMBOL (If applicable)	7a. NAME OF MONITORING ORGANIZATION: U.S. Army Research Office
6c. ADDRESS (City, State, and ZIP Code): 217 Aerospace Engineering Building, Ann Arbor, MI 48109-2140	7b. ADDRESS (City, State, and ZIP Code): P.O. Box 12211, Research Triangle Park, NC 27709-2211
8a. NAME OF FUNDING / SPONSORING ORGANIZATION: U.S. Army Research Office 8b. OFFICE SYMBOL (If applicable)	9. PROCUREMENT INSTRUMENT IDENTIFICATION NUMBER: DAAL03-86-K-0154
8c. ADDRESS (City, State, and ZIP Code): P.O. Box 12211, Research Triangle Park, NC 27709-2211	10. SOURCE OF FUNDING NUMBERS: PROGRAM ELEMENT NO. / PROJECT NO. / TASK NO. / WORK UNIT ACCESSION NO.

11. TITLE (Include Security Classification)
Structure of Monopropellant Spray Flames at Elevated Pressures (U)

12. PERSONAL AUTHOR(S)
G.M. Faeth, T.-W. Lee, M.E. Kounalakis and L.-K. Tseng

13a. TYPE OF REPORT	13b. TIME COVERED	14. DATE OF REPORT (Year, Month, Day)	15. PAGE COUNT
Final	FROM 9/1/86 TO 12/31/8	15 January 1990	81

16. SUPPLEMENTARY NOTATION The view, opinions and/or findings contained in this report are those of the author(s) and should not be construed as an official Department od the Army position, policy, or decision, unless so designated by other documentation.

17. COSATI CODES		
FIELD	GROUP	SUB-GROUP

18. SUBJECT TERMS (Continue on reverse if necessary and identify by block number)
Spray combustion
Liquid propellants
Monopropellant combustion

19. ABSTRACT (Continue on reverse if necessary and identify by block number)

The combustion properties of HAN-based monopropellants (LGP1845 and 1846) were studied, considering: liquid surface properties and conditions required for the thermodynamic critical point to be reached, drop combustion properties in combustion gas environments at pressures of 0.2-7.0 MPa, and pressure-atomized spray combustion properties in combustion gas environments at pressures of 3-9 MPa. Computations of liquid surface properties in flame environments indicated unusually high liquid surface temperatures, ca. 1000K, and critical combustion pressures, ca. 250 MPa, since these propellants have thermodynamic properties similar to molten salts. Drop burning was dominated by subsurface reaction leading to bubble formation and microexplosions which mechanically removed liquid, at low pressures (less than 2.1 MPa); and conventional hetereogeneous combustion from the surface at high pressures (greater than 2.1 MPa). The resulting apparant burning rates were relatively independent of pressure and were large, ca. 10 mm/s, which is consistent with earlier strand burning rate measurements of jelled propellants at pressures greater than 10 MPa by McBratney (1980, 1981). Measurements of drop size distributions, liquid flow rates, and liquid mass fluxes in combusting sprays were consistent with the individual drop burning rate measurements and exhibited strong effects of separated flow. Deterministic and stochastic separated flow models were developed which yielded predictions that were similar to each other and were in reasonably good agreement with the measurements. A locally-homogeneous flow model was also developed to provide estimates of spray behavior as thermodynamic critical conditions are approached; this approach indicates strong effects of the degree of flow development at the injector exit on combustion properties, with fully-developed turbulent flow yielding the smallest combustion volumes.

20. DISTRIBUTION / AVAILABILITY OF ABSTRACT	21. ABSTRACT SECURITY CLASSIFICATION
☒ UNCLASSIFIED/UNLIMITED ☒ SAME AS RPT. ☐ DTIC USERS	Unclassified
22a. NAME OF RESPONSIBLE INDIVIDUAL: David M. Mann	22b. TELEPHONE (Include Area Code): (919) 549-0641 / 22c. OFFICE SYMBOL

DD Form 1473, JUN 86 — Previous editions are obsolete. — SECURITY CLASSIFICATION OF THIS PAGE

Table of Contents

List of Tables

List of Figures

Nomenclature

Symbol	Description
c	reaction progress variable
d	injector diameter
L	injector passage length
p	pressure
SMD	Sauter mean diameter
u	streamwise velocity
x	streamwise distance
α_f	liquid volume fraction

Subscripts

c	centerline value
p	drop properties
0	initial condition

Superscripts

$\bar{(\,)}$	time-averaged mean quantity
$\tilde{(\,)}$	Favre-averaged mean quantity

List of Appendices

1. Statement of Problem

Combusting monopropellant sprays are an important fundamental combusting flow, since they are the premixed counterpart of more widely studied spray diffusion flames. Additionally, combusting monopropellant sprays have applications to regenerative liquid-propellant guns, throttable thrustors, and underwater propulsion systems. Motivated by these observations, the present investigation considered monopropellant combustion properties both as individual drops and pressure-atomized sprays. The investigation was limited to hydroxyl-ammonium-nitrate (HAN)-based monopropellants (LGP1845 and 1846) that are of interest for several high-pressure monopropellant combustion systems.

The general nature of a combusting pressure-atomized monopropellant spray is illustrated in Fig. 1. This involves injection of liquid from a passage into a combustion chamber where gas velocities are modest near the injector exit. Heat losses from practical monopropellant combustion systems are small; therefore, gas temperatures are near the adiabatic combustion temperature of the propellant. The atomization breakup regime is illustrated, where drops begin to form from the surface of the liquid right at the injector exit, since this condition is most important in practice. Atomization breakup yields a liquid core, much like the potential core of a single-phase jet, surrounded by a multiphase mixing layer containing drops and other irregular liquid elements (Ruff et al., 1989, 1990). Beyond the end of the liquid core, the flow becomes a dilute spray which has a finite length due to the combustion of the drops. Since monopropellant burning rates are relatively high (with liquid regression rates never much lower than 10mm/s for HAN-based monopropellants) flame thicknesses over liquid surfaces are small (ca. 1μm) so that the actual combustion process occurs in thin heterogeneous reaction zones which cover all liquid surfaces — separating liquid reactants and combustion product gases (Lee et al. 1988, 1989; Lee and Faeth, 1990). Major issues with respect to combusting monopropellant sprays involves the extent of the liquid-containing region and the rate of energy release, so that adequate combustion volumes can be provided; the presence and nature of combustion instabilities; and requirements for ignition and extinction of the spray. None of these issues can be addressed, however, without some understanding of drop combustion properties and spray structure; therefore, these simpler problems were the main focus of the present investigation.

Several questions concerning monopropellant drops and spray combustion must be resolved for an adequate understanding of the process. First of all, monopropellant combustors operate over a wide range of relatively high pressures, which implies that liquid surfaces can approach or exceed their thermodynamic critical point (Faeth, 1972, 1987; Kounalakis and Faeth, 1988). Combustor pressures when the critical point is reached must be identified, since below this pressure a multiphase flow like Fig. 1 is present, while above it the flow becomes a single-phase dense fluid flow with very different properties. Secondly, the combustion properties of individual drops must be known, for the pressure range where drops are present, since drop combustion mainly controls combustion rates of the spray. Next, information concerning the structure of combusting sprays is needed; particularly the extent of the liquid-containing region, drop sizes that are present, and the importance of separated-flow phenomena like the relative velocities between the drops and the gas and the combustion rates of drops within a combusting spray. Finally, the wide range of operating conditions for combusting monopropellant sprays precludes exhaustive testing to find spray structure for all conditions — effective models of the process are needed.

The present investigation sought to make a contribution to each of these issues, with the following specific objectives:

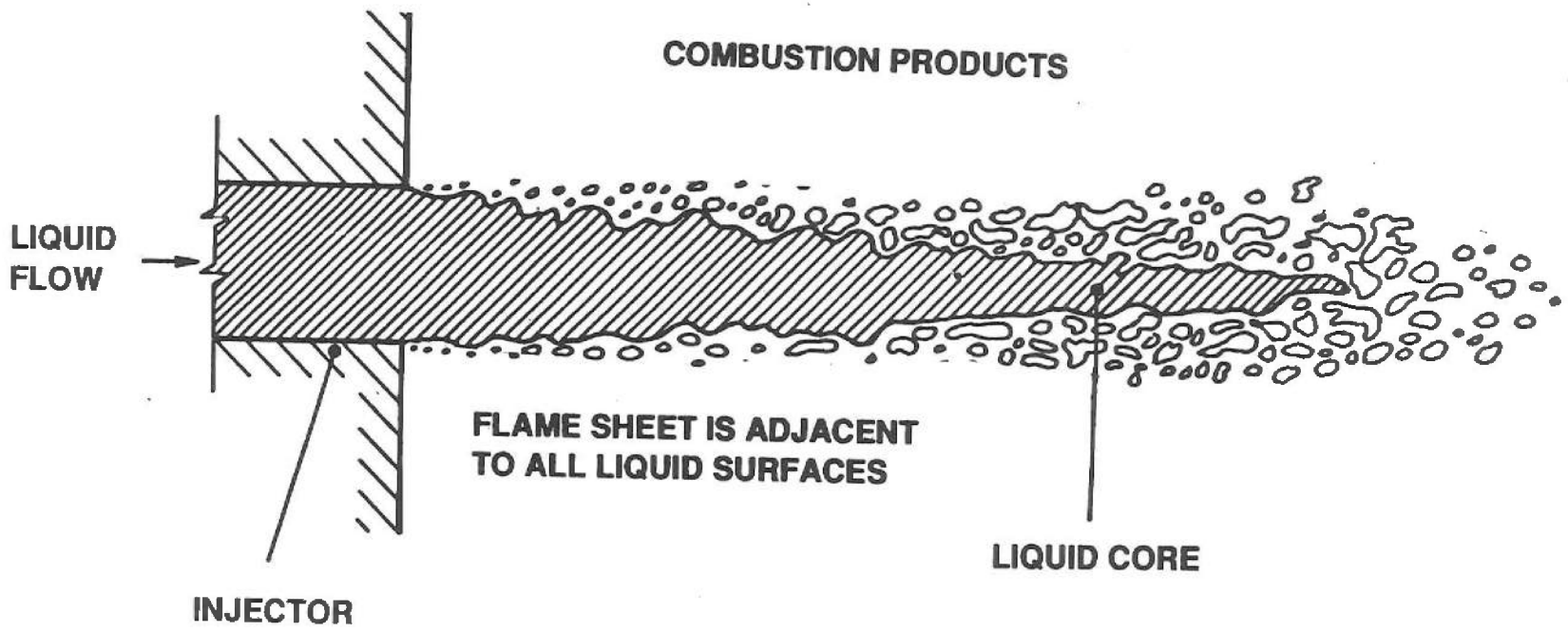

Figure 1. Sketch of a combusting pressure-atomized monopropellant spray.

1. Liquid surface properties and pressures required for the liquid surface to exceed the thermodynamic critical point (the critical combustion pressure) were investigated theoretically.

2. The combustion of individual drops in combustion gas environments was observed at pressures of 0.2-7 MPa, yielding drop burning rates over this range of conditions.

3. The combustion of pressure-atomized sprays in combustion gas environments was observed at pressures of 3-9 MPa, yielding measurements of liquid volume fractions, drop size distributions, and liquid mass flow rate and mass flux distributions. Additionally, models of the process were developed, both ignoring and considering effects of separated flow, and evaluated using the new measurements.

Supercritical combustion, drop combustion and spray combustion are discussed in turn in the next chapter, followed by some concluding remarks. Subsequent chapters summarize publications and personnel of the investigation. The present discussion is brief; more information can be found in Kounalakis and Faeth (1988), Lee et al. (1988, 1989) and Lee and Faeth (1990), which appears as Appendices A.1-A.4. Finally, Lee (1990) reports additional details of both measurements and predictions as well as a complete tabulation of data.

2. Summary of Most-Important Results

2.1 Supercritical Combustion

The objective of this portion of the investigation was to find gas and liquid phase properties at the liquid surface for combusting HAN-based monopropellants at various pressures. The pressures required for the surface to reach its thermodynamic critical pressure, the critical combustion pressure, was also of interest since this defines the pressure regime where conventional spray processes must be considered. The details of this work are described by Kounalakis and Faeth (1988), which appears in Appendix A.1.

Hetereogeneous monopropellant flames at high pressures are very thin, ca. 1μm, and will probably never be resolved by measurements. Therefore, liquid surface properties were found theoretically, using methods developed earlier in this laboratory (Faeth, 1972, 1987). This involved considering transport in the gas phase, at the asymptotic limit of infinitely high activation energies of all reactions so that reaction occurs within a thin flame sheet located at a distance from the liquid surface. Transport in the gas phase allowed for real gas effects (but only considering concentration diffusion with equal binary diffusivities of all species) and nonunity Lewis numbers. Phase equilibrium was assumed at the liquid surface with real-gas effects primarily treated using the Soave equation of state.

Combustion product properties were needed for the computations. They were found assuming thermodynamic equilibrium at the downstream end of the flame, and adiabatic combustion, using the Gordon and McBride (1971) algorithm. The resulting properties of the reactants and the combustion products are summarized in Table 1 for LGP1845 and 1846 at various pressures. Adiabatic flame temperatures are relatively low, ca. 2000-2200 K; therefore, effects of dissociation are small and the composition and temperature of the combustion products varies very little over the range 1-100 MPa. The

Table 1. Combustion Properties of HAN-based Monopropellants[a]

Propellant	LGP 1845[b]			LGP 1846[c]		
Pressure (MPa)	1	10	100	1	10	100
Reactant Density (kg/m^3)	1452	1454	1476	1430	1432	1454
Combustion Product Properties:						
Density (kg/m^3)	1.30	12.9	129	1.36	13.5	135
Temperature (K)	2133	2152	2163	2027	2039	2045
Composition (% by volume)[d]						
Water Vapor	68.8	69.2	69.3	70.6	70.8	70.9
Carbon Dioxide	12.7	12.9	13.0	12.2	12.3	12.3
Nitrogen	17.3	17.4	17.4	16.5	16.5	16.6

[a]Adiabatic constant pressure combustion with the reactant at 298.15 K.
[b]Reactant composition (% by mass): (HAN), 63.2; (TEAN), 20; and H_2O, 16.8.
[c]Reactant composition (% by mass): (HAN), 60.8; (TEAN), 19.2; and H_2O, 20.0.
[d]Major species only. Minor species include CO, H_2, NO, OH and O_2.

combustion products involve unusually large concentrations of water vapor, with the remainder being split about equally between carbon dioxide and nitrogen.

Uncertainties in predictions of liquid surface properties are large due to the uncertainties of the thermochemical and transport properties of the HAN-based monopropellants. Best-estimate predictions of liquid surface properties for LGP1845 are plotted as a function of pressure in Fig. 2 (results for LGP1846 were similar within property uncertainties). Gas-phase compositions are relatively independent of pressure but liquid-phase concentrations vary substantially, due to increased liquid-phase solubilities for combustion products as the thermodynamic critical point is approached. An interesting feature of these results is that the concentration of TEAN at the liquid surface is unusually high at low pressures, due to its low volatility, even though its initial concentration in the propellant is only 20% (see Table 1). This causes liquid surface temperatures to be rather high at low pressures, ca. 1000 K, before decreasing to ca. 800 K as the critical point is approached. Such high temperatures are rarely encountered at the liquid surface for liquid monopropellants and bipropellants; they occur for HAN-based monopropellants since these materials have thermochemical properties like molten salts.

Approach to the thermodynamic critical point is indicated by gas and liquid concentrations approaching one another at high pressures in Fig.2. Predictions ultimately yield a critical combustion pressure of 2500 atm. (250 MPa), with an uncertainty of 50 percent due to property uncertainties. Similar to liquid surface temperatures, the critical combustion pressures of the HAN-based propellants are unusually high in comparison to other monopropellants and bipropellants, which have critical combustion pressures of 100-200 atm. (Faeth, 1971, 1987). Thus, HAN-based monopropellants involve effects of drops and sprays over much of their range of application, except for perhaps the highest-pressure portions of liquid gun cycles. Again, this unusual behavior follows from the molten salt character of the monopropellant.

Examination of the sensitivity of critical pressure predictions to property uncertainties indicated that uncertainties were dominated by the binary interaction parameter of TEAN and water in the Soave equation of state. The effect of this parameter of critical combustion pressure predictions, as well as the effect of using the Redlich-Kwong equation of state, is illustrated in Fig. 3. Use of the Redlich-Kwong equation of state is felt to be less reliable than the Soave equation of state and this approach will not be considered any further (Kounalakis and Faeth, 1988). However, estimates of critical combustion pressures are clearly quite sensitive to binary interaction parameter TEAN and water vapor.

In summary, the present study of liquid surface properties during the combustion of HAN-based monopropellants has shown the following: results for LGP1845 and 1846 are similar; critical combustion pressures are unusually high, 250 MPa with an uncertainty of 50 percent; liquid surface temperatures are unusually high, 800-1000 K; liquid surface properties tend to be dominated by TEAN at low pressures, due to its low volatility; and the uncertainties of the predictions are dominated by the TEAN-water vapor binary interaction parameter. The major conclusion with respect to spray combustion is that combustion occurs by conventional monopropellant spray processes, involving liquid surfaces and drops, at all but the very highest pressures of liquid gun cycles.

2.2 Drop Combustion

With the importance of drop and spray combustion established for the HAN-based monopropellants, the next phase of the investigation considered the combustion properties of individual drops. Drop combustion has been considered earlier by Beyer (1986, 1988), Beyer and Teague (1986) and Zhu and Law (1987), who observed significant subsurface

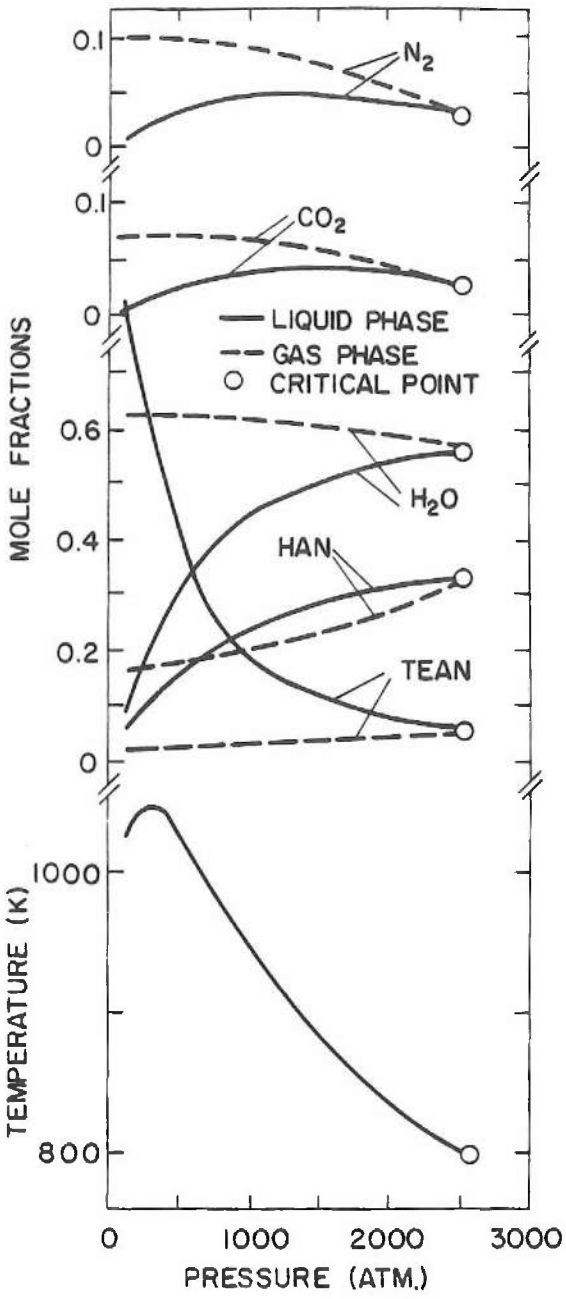

Figure 2. Liquid and gas phase properties at the liquid surface for combusting LGP1845. From Kounalakis and Faeth (1988).

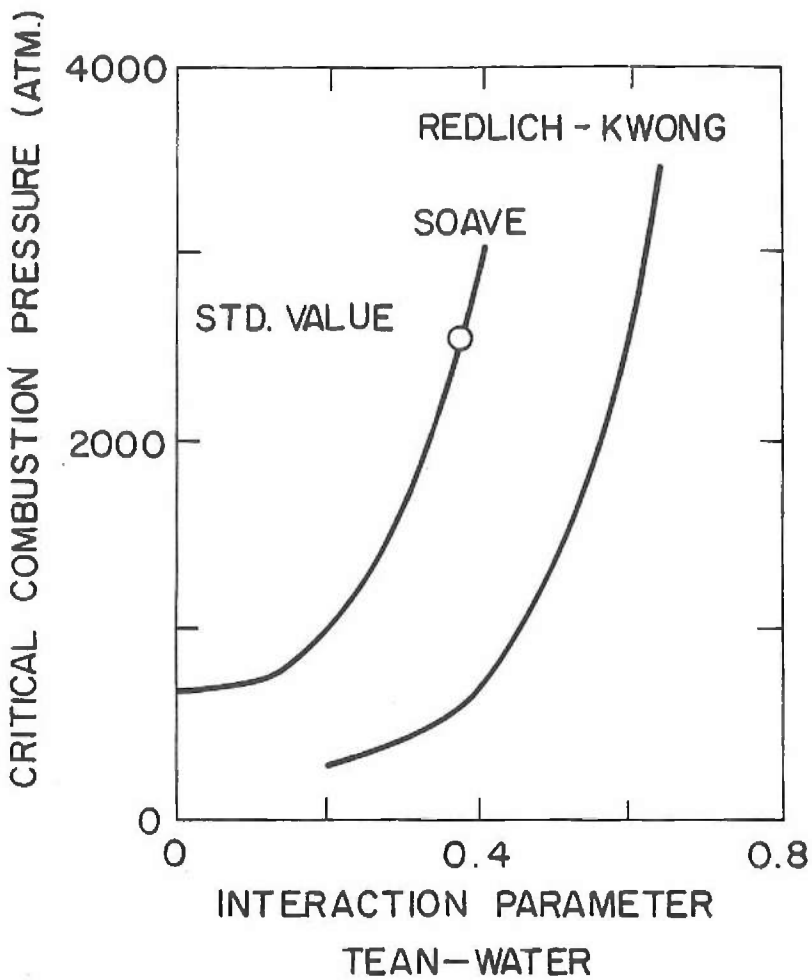

Figure 3. Effect of the TEAN-water binary interaction parameter on the predicted critical combustion pressure of LGP1845. From Kounalakis and Faeth (1988).

reaction leading to bubble formation and growth, and shattering of drops by bursting bubbles. However, these results were either found in low temperature gas environments, Beyer and coworkers, or at atmospheric pressure, Zhu and Law, so that the relevance of the findings to practical combusting monopropellant sprays was uncertain. Additionally, McBratney (1980, 1981) and Vosen (1988) reported measurements of strand burning rates of HAN-based monopropellants, which can be related to drop burning rates. However, McBratney (1980, 1981) used jelled propellants so that the jelling agent could have influenced his measurements; while Vosen (1988) encountered liquid surface instabilities with unjelled propellants which precludes using these data to estimate drop burning rates. Thus, the present investigation considered unjelled drops in high temperature and pressure environments. The details of this work are described by Lee et al. (1989), which can be found in Appendix A.3.

Drop combustion was observed with drops supported in the post-flame region of a premixed flame stabilized within a pressure vessel at pressures of 0.2-7 MPa. The combustion temperature of the premixed flame was generally in the range 2200-2300 K, which is slightly higher than the adiabatic constant pressure flame temperature of the propellants (see Table 1). The drops were supported on quartz fibers (with initial drop diameters in the range 300-1200 μm) within a retractable shield to protect them from disturbances when the premixed flame was ignited. Once the premixed flame had stabilized, the shield was retracted which submerged the drops in the combustion gas. The drops were backlighted and photographed with a high-speed motion picture camera.

Some typical photos of drop diameter as a function of time are illustrated in Fig. 4. The origin of these photos is arbitrary due to uncertainties concerning the time that the drops were actually submerged in the flame, due to disturbances of the flame by the retractable shield. Results at 0.51 MPa are representative of low pressure behavior where subsurface bubble formation and bursting, and mechanical removal of liquid by microexplosions, caused erratic diameter variations. This behavior is consistent with observations of Beyer (1986, 1988) and Beyer and Teague (1986) for lower ambient temperatures and Zhu and Law (1987) for lower ambient temperatures and pressures. This behavior follows from the large liquid surface temperatures discussed in connection with Fig. 2, and the fact that thermal diffusivities are higher than mass diffusivities in liquids. This allows subsurface liquid having high concentrations of HAN to become heated, leading to bubble formation by either vaporization or reaction. Results at higher pressures, e.g. 2.1 MPa in Fig. 4, exhibit more conventional monopropellant behavior with little bubble formation in the liquid and gasification occurring primarily at the drop surface in conjunction with a hetereogeneous flame. This occurs since surface regression rates are high at high pressures, so that the thermal wave cannot propagate very far into the liquid, and liquid residence times at high temperatures become small.

The variation of drop diameter, excluding cases where drops burst completely or fell off the quartz probe between consecutive pictures, was averaged over several tests to give effective drop burning rates. These results are illustrated in Fig. 5, along with the strand burning rate measurements of McBratney (1980, 1981) and Vosen (1988). The combination of drop bursting at low pressures, and conventional hetereogeneous combustion at high pressures, causes present drop burning rates to be relatively independent of pressure. They were relatively independent of diameter as well, which is consistent with a classical linear monopropellant drop burning rate law, e.g. $-dr_p/dt = K_p =$ const. The present results are a crude extension of McBratney's (1980, 1981) measurements with jelled propellants suggesting that use of a jelling agent did not have a strong effect. Vosen's (1988) results are much higher, due to the effects of liquid surface disturbances, noted earlier.

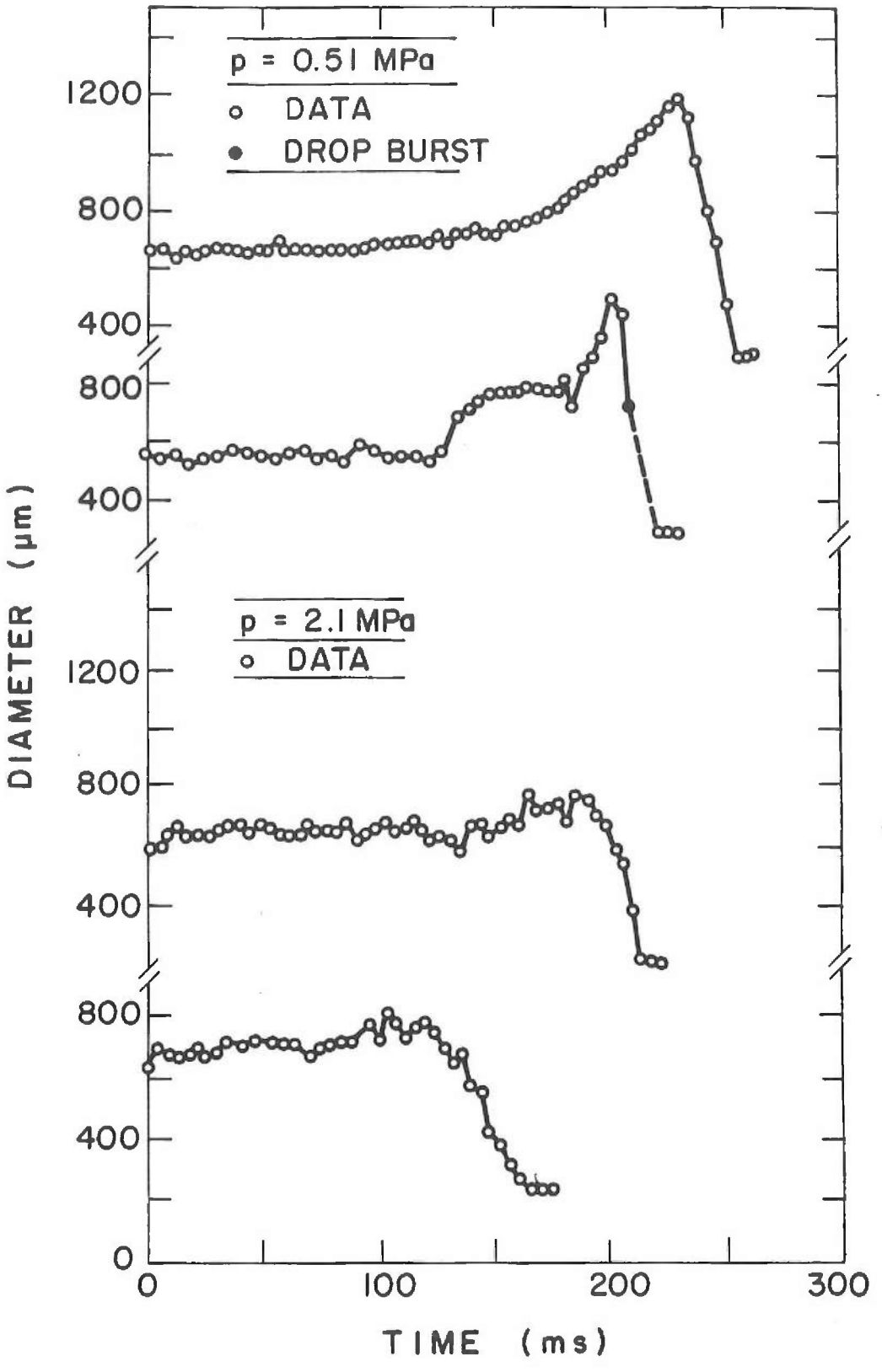

Figure 4. Drop diameter histories at 0.51 and 2.1 MPa. From Lee et al. (1988).

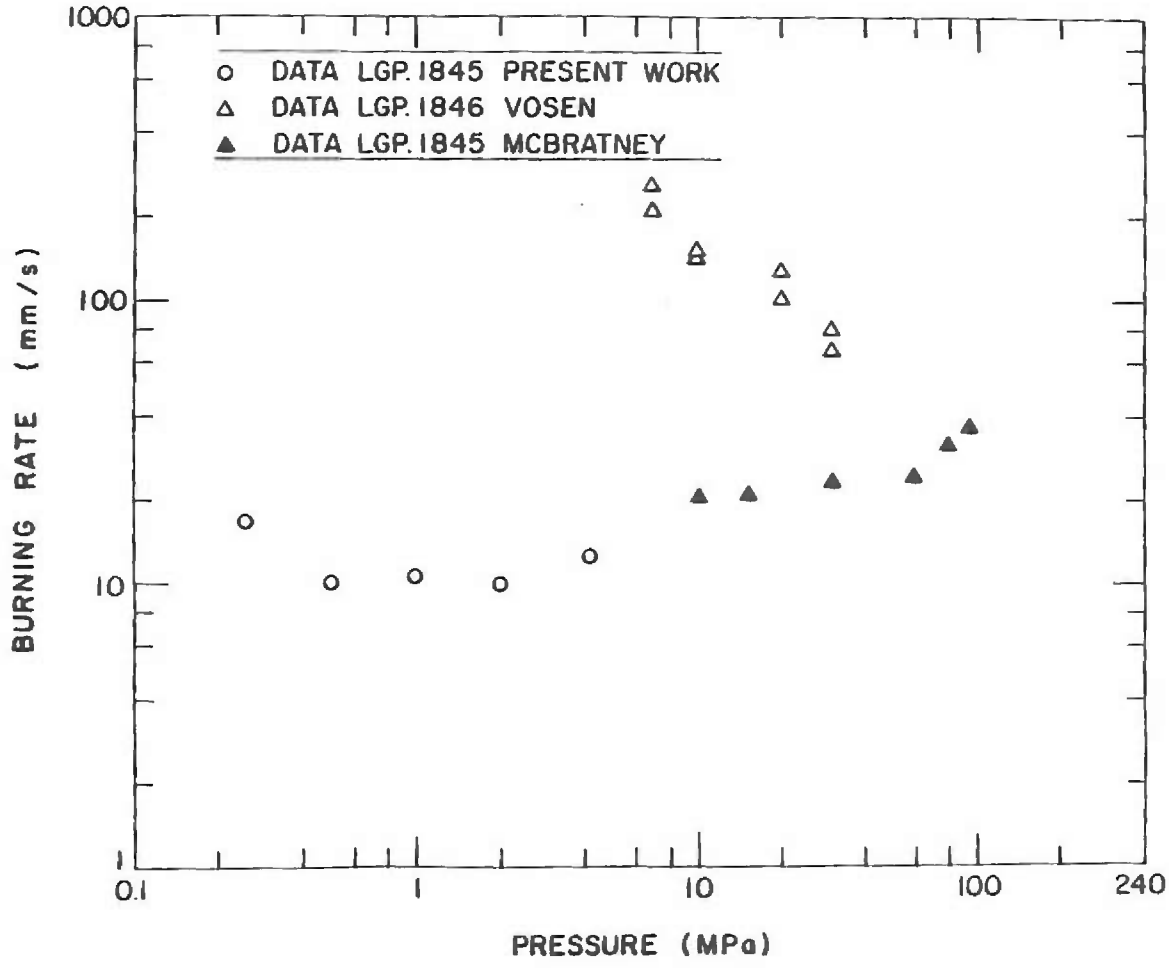

Figure 5. Apparent drop and strand burning rates of LGP1845. From Lee et al. (1988).

In summary, present measurements indicate drop burning rates of ca. 10 mm/s for drop diameters of 300-1200 μm and pressures of 0.2-7 MPa. Present results are consistent with earlier strand burning rate measurements of McBratney (1980, 1981) at pressures greater than 10 MPa. Taken together, these findings suggest a relatively weak effect of pressure on the burning rate, ca. $p^{1/3}$, except at the lowest pressures where subsurface gasification causes bubble formation and microexplosions that mechanically remove liquid from the drop at a relatively high rate. However, these low pressure effects are not very important in practice, since it is difficult to reliably ignite HAN-based monopropellant sprays at pressures below 3 MPa (Lee et al. 1989).

2.3 Spray Combustion

The final phase of the investigation involved consideration of combusting HAN-based pressure-atomized sprays. Birk and Reeves (1987) reported earlier flow visualization results for flows of type. During the present investigation, this information was processed to yield liquid volume fraction distributions. In addition, a spray combustion apparatus was developed and used for measurements of liquid volume fractions, drop size distributions and liquid flow rate and liquid flux distributions. Finally, several models of combusting monopropellant sprays were developed and evaluated using the new measurements, as follows: a locally-homogeneous flow (LHF) model, where interphase transport rates were assumed to be infinitely fast; a deterministic separated flow (DSF) model, where finite interphase transport rates were considered but drop/turbulence interactions were ignored; and a stochastic separated flow (SSF) model where both finite interphase transport rates and drop/turbulence interactions were considered. The details of this work are described by Lee et al. (1988, 1989) and Lee and Faeth (1990), which appear in Appendices A.2-A.4.

The experiments involved observations of combusting sprays in a combustion gas environment at pressures of 3-9 MPa. The test arrangement was similar to Birk and Reeves (1987) but the combustion chamber had a larger internal volume. The combustion gas was produced by filling the chamber with a combustible mixture and then igniting it with a spark to reach the desired final pressure and temperature. The propellant was pressure fed through various injectors into the hot combustion products, where it ignited and burned reliably at pressures greater than 2.7 MPa. Combustion gas temperatures were somewhat greater than the adiabatic flame temperature for constant pressure combustion of the monopropellant (see Table 1). Measurements involved flash shadowgraph motion pictures which were reduced to find liquid volume fractions; and slide impaction measurements of drop size distributions, liquid flow rates and liquid fluxes.

Under the LHF approximation, relative velocities between the phases are assumed to be small and the flow is treated like an equivalent single-phase fluid so that properties that are difficult to estimate, like initial drop size distributions, play no role in the predictions. This type of mixing-limited behavior is expected to work best when ambient pressures and liquid injection velocities are high, which yields relatively small drops after breakup (Ruff and Faeth, 1990). Similarly, a mixing-limited treatment of premixed combustion was used, assuming a thin flame sheet under the laminar flamelet concept of Bray (1980). Turbulent mixing was treated using a Favre-averaged turbulence model that had been calibrated using measurements from a variety of constant and variable density turbulent single and multiphase jets (Bilger, 1976; Faeth, 1987; Jeng and Faeth, 1984; Ruff et al., 1989, 1990).

Initial evaluation of LHF predictions, using measurements of liquid volume fractions obtained from the experiments of Birk and Reeves (1987), was quite promising (Lee et al., 1988). The results are illustrated in Fig. 6. Measured liquid volume fractions have a line of sight bias, however, this effect becomes small near the downstream end of the visible liquid-containing region so the method provides some indication of the penetration of liquid into the flow. Since the degree of flow development at the injector exit was not well known, predictions were carried out for a variety of injector passage lengths ranging from slug flow, $L/d = 0$, to fully-developed turbulent pipe flow, $L/d = \infty$. Predictions and measurements are in fair agreement for L/d in the range 2-10, which was reasonable for the test conditions. Predictions and measurements were also relatively independent pressure. Finally, the predictions are clearly significantly influenced by flow development lengths (L/d) — this behavior was confirmed by independent measurements for nonevaporating sprays at atmospheric pressure (Ruff et al., 1989, 1990).

Subsequently, the LHF predictions were evaluated using the present measurements (Lee et al., 1989). Results analagous to Fig. 6 are illustrated in Fig. 7. The measurements include the results obtained from Birk and Reeves (1987), dark symbols, as well as the present measurement, open symbols, which largely involved nearly fully-developed turbulent flow at the injector exit. Predictions are for fully-developed flow, either ignoring line-of-sight bias effects, dashed line, considering them using a stochastic approach developed by Faeth et al. (1988), solid line. As noted earlier, however, estimates of the downstream end of the liquid-containing region are not strongly effected by line-of-sight bias. Clearly, present measurements yielded a much longer liquid-containing region than Birk and Reeves (1987). This was attributed to potential effects of unstable injector flow or cavitation during the earlier measurements. Comparing LHF predictions with the new measurements yielded more conventional behavior for the predictions based on this approximation; namely, that the LHF method generally overestimates the rate of development of sprays (Faeth, 1987). Single-drop trajectory calculations, using the LHF predictions to define the velocity field, confirmed this behavior and also indicated the presence of significant amounts of liquid beyond the visible end of the liquid-containing region.

The separated flow models were developed motivated by these findings. They also involved use of the thin-flame approximation which implies constant density gas and liquid phases. The approach involved Eulerian calculations for gas-phase properties, with turbulent mixing treated similar to the LHF approach but allowing for drop source terms in the governing equations for conservation of mass and momentum. Lagrangian calculations of drop trajectories were used for the liquid phase, specifying a constant drop burning rate of 10mm/s based on the single drop measurements (this burning rate is sufficiently high that forced convection and curvature have negligible effects on the burning rate). Initial drop size and velocity distributions were specified near the injector exit, based on velocity and liquid flux estimates from the LHF predictions, and drop size distributions extrapolated from the measurements. Notably, initial drop sizes (SMD of 240 μm) were consistent with estimates of aerodynamic breakup (Reitz and Bracco, 1982) or secondary breakup theories, after allowing for effects of turbulent flow at the injector exit (Lee and Faeth, 1990). The DSF approach involved computing drop trajectories based on mean gas velocities. The SSF approach involved random walk calculations with the drops interacting with instantaneous velocities found from random selections satisfying the local moments of velocity fluctuations.

Predicted and measured SMD as a function of distance from the injector are illustrated in Fig. 8 for injector diameters of 0.3 and 0.6 mm. In terms of x/d, the small injector has a much larger liquid-containing region. This is indicative of strong separated

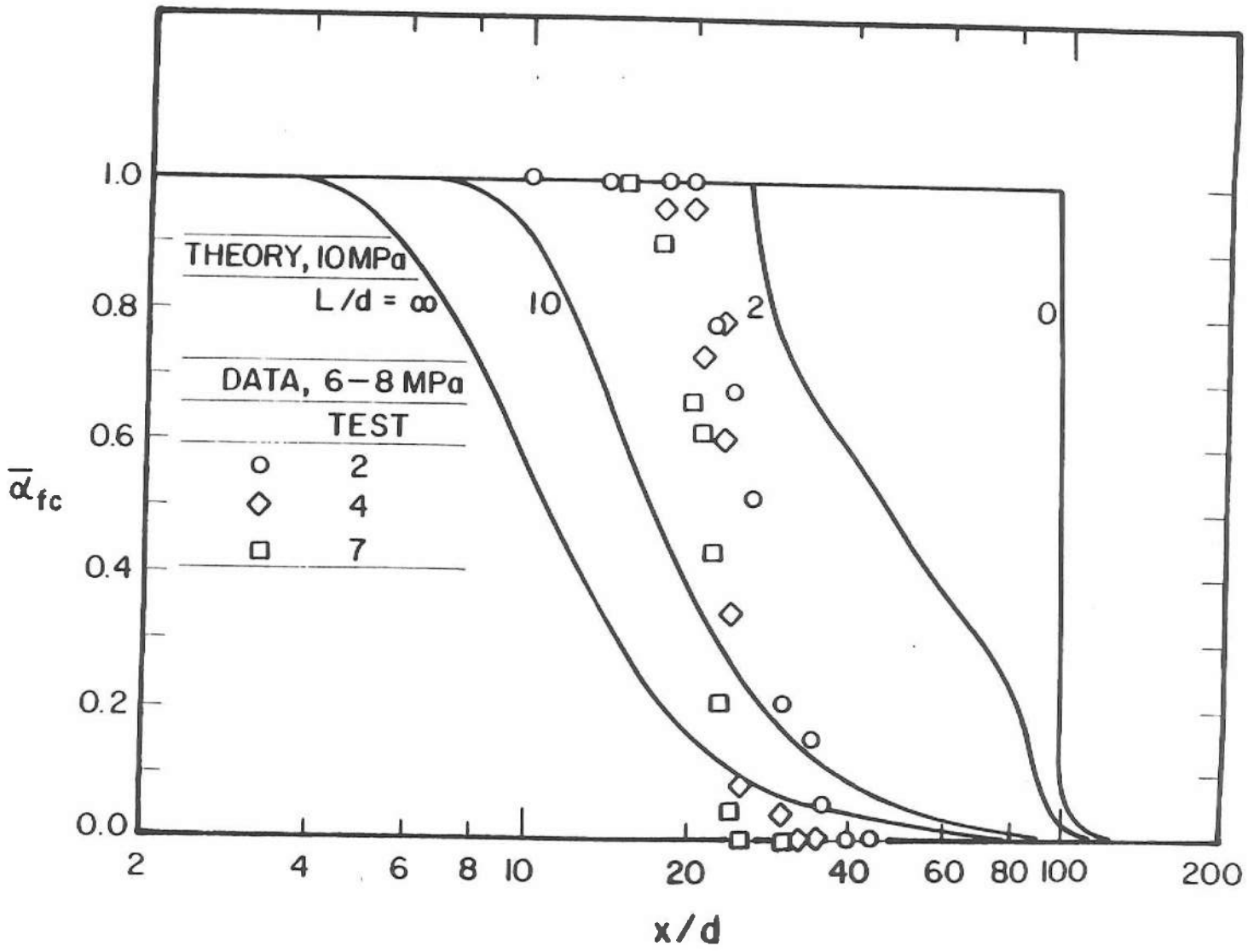

Figure 6. Measured (Birk and Reeves, 1987) and predicted (LHF method) liquid volume fractions along axis of combusting LGP1846 sprays.

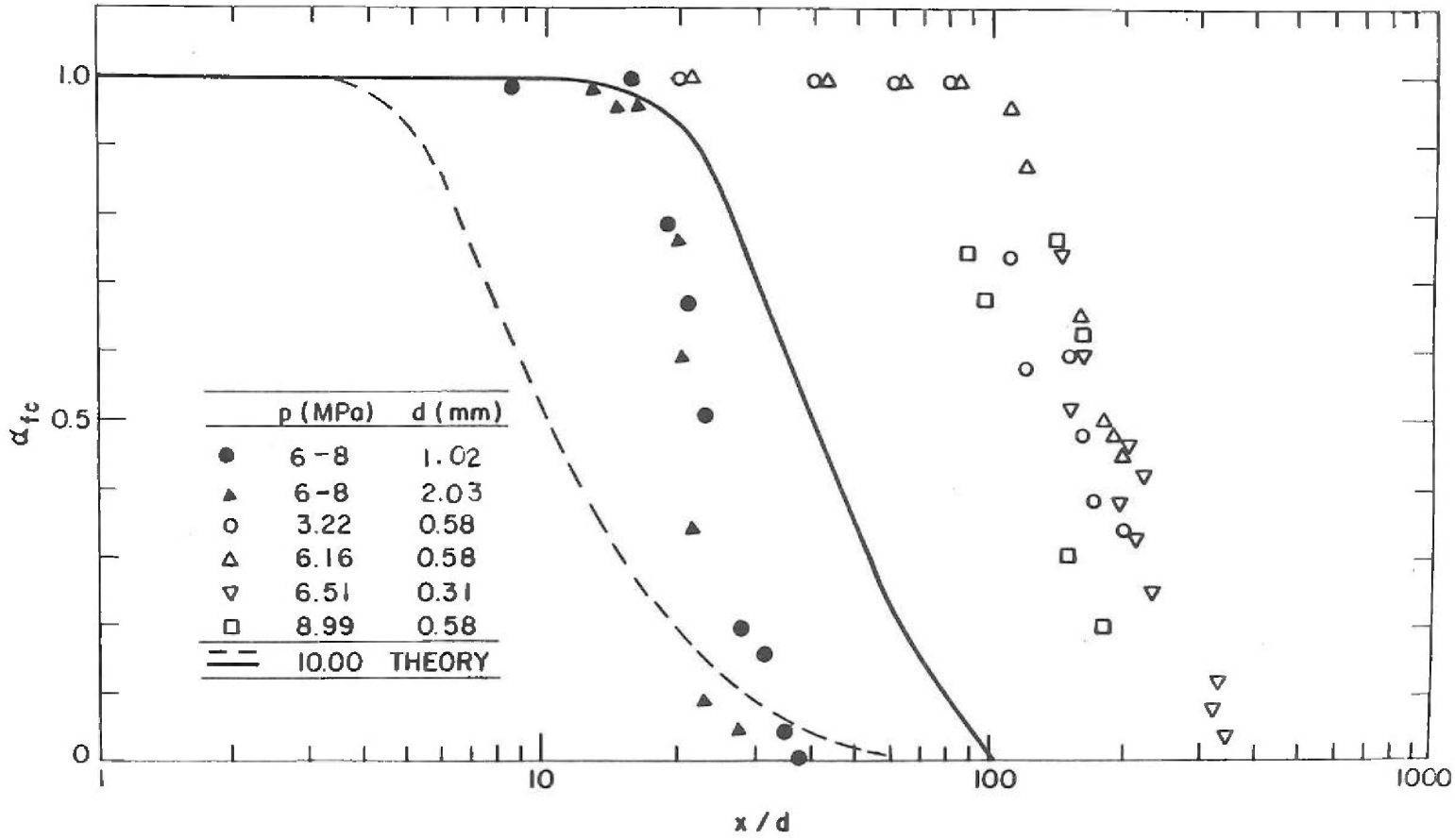

Figure 7. Measured (present study and Birk and Reeves (1987)) and predicted (LHF method) liquid volume fractions along the axis of combusting LGP1845 sprays. From Lee et al. (1989).

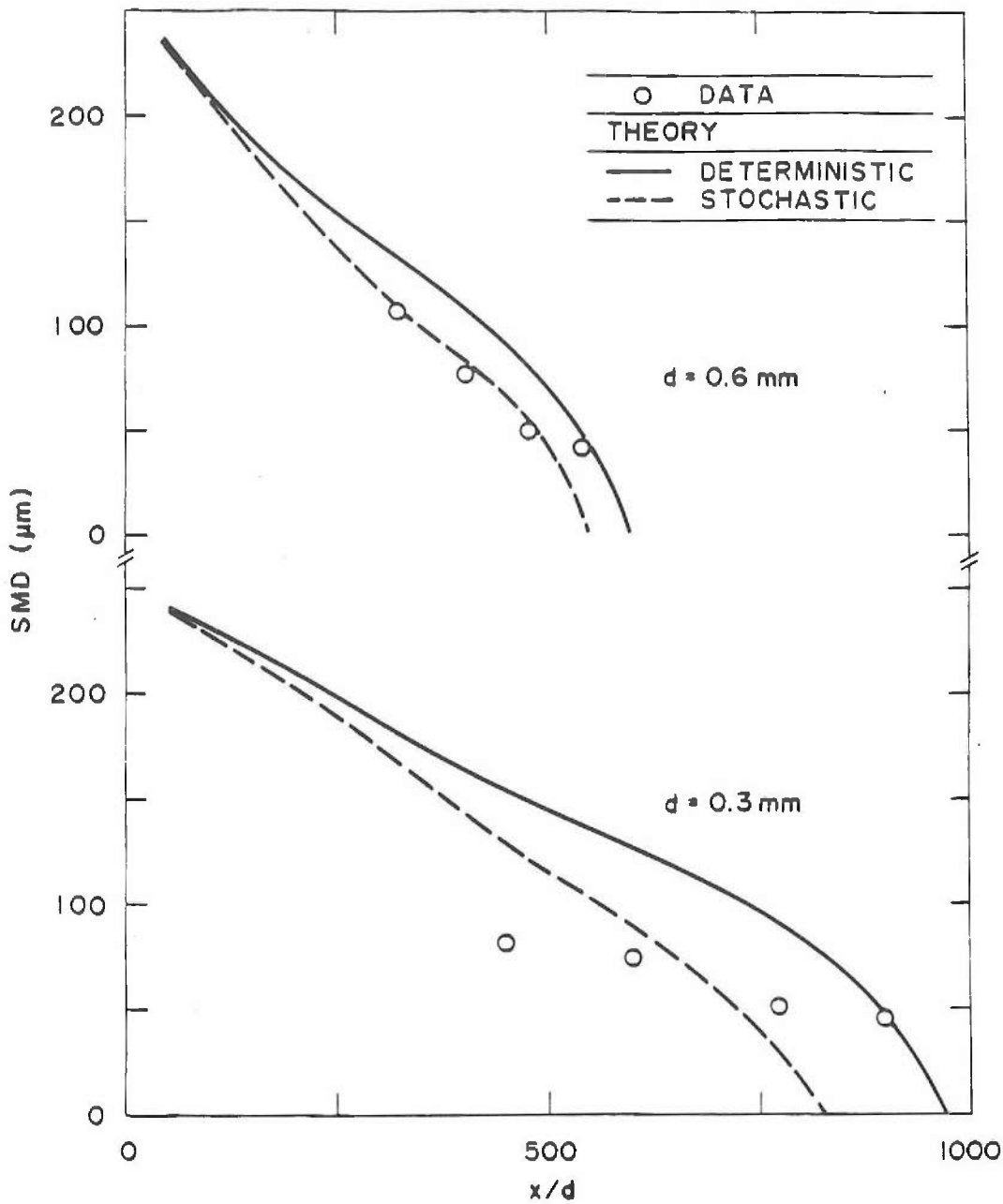

Figure 8. Measured (present study) and predicted (DSF and SSF methods) SMD variation with streamwise distance for combusting LGP1845 sprays. From Lee and Faeth (1990).

flow effects, e.g., drop sizes and velocities were similar for the two injectors and the drops survive for similar distances, implying a larger x/d for the smaller injector. The DSF and SSF predictions are not very different, in view of uncertainties in specifying initial conditions; the DSF method is recommended due to its reduced computational requirements. Finally, predictions are in reasonably good agreement with measurements, implying that the present single drop burning rate measurements are consistent with burning rates in the combusting sprays, since the predictions are very sensitive to this parameter.

The evolution of predicted and measured drop size distributions for the 0.6 mm diameter injector are illustrated in Fig. 9 (results for d = 0.3 mm are similar). Measurements indicate a rather broad distribution of drop sizes at x/d = 320, with the drops becoming progressively concentrated at small sizes as combustion proceeds. Predictions were obtained by extrapolating results at x/d = 320 to the injector exit to specify initial conditions; therefore, agreement at this point is not surprising. However, predictions still treat the subsequent evolution of the drop size distribution reasonably well.

The reason for the importance of separated flow effects can be seen from the predictions illustrated in Fig. 10. Favre-averaged drop velocities and time-averaged gas velocities (which are the same as the Favre averages when the density is constant) are plotted as a function of distance from the injector for d = 0.3 and 0.6mm. Velocity differences between the phases are large, except near the injector exit where the LHF approximation is reasonable (Ruff et al., 1989, 1990) and near the end of the liquid-containing region where drops are small and responsive. Relative velocities are larger for the small injector diameter since it has faster deceleration rates due to its smaller scale. In view of these results, it is not surprising that use of the LHF approximation was not very successful for present test conditions.

Increasing pressures do not improve the response of a particular drop size to gas motion, however, higher ambient pressures reduce drop sizes upon breakup so that the LHF approach becomes more effective (Ruff and Faeth, 1990). Reduced surface tension as the thermodynamic critical point is approached also acts to reduce drop sizes and improve LHF predictions. Thus, it is worthwhile to consider some LHF results relating to high pressure combusting HAN-based monopropellants.

Some typical LHF predictions are illustrated in Figs. 11 and 12. This involves Favre-averaged reaction progress variable (which is 0 in the reactants and 1 in the products) and time-averaged liquid volume fractions along the spray axis for slug and fully-developed turbulent flow at the injector exit. At the LHF limit, effects of Reynolds number are small; thus, pressure is the only parameter on the plots. The results indicate that fully-developed flow yields the fastest mixing rates, but this effect is relatively small at the highest pressures (100 MPa and above) where the LHF approximation is likely to be most correct. For both flows, however, the effect of pressure is quite significant with the liquid containing region becoming smaller at high pressures. This is an effect of increased entrainment due to higher ambient gas densities at high pressures (Faeth, 1987). Since LHF predictions clearly overestimate the length of the liquid-containing region at low pressures (near 10 MPa) the reduction of the length of the liquid containing region with increasing pressure would be even larger, due to combined effects of better atomization and increased entrainment. However, quantitative estimates of spray properties at high pressures using the present LHF model should be approached with caution, pending evaluation of predictions with measurements.

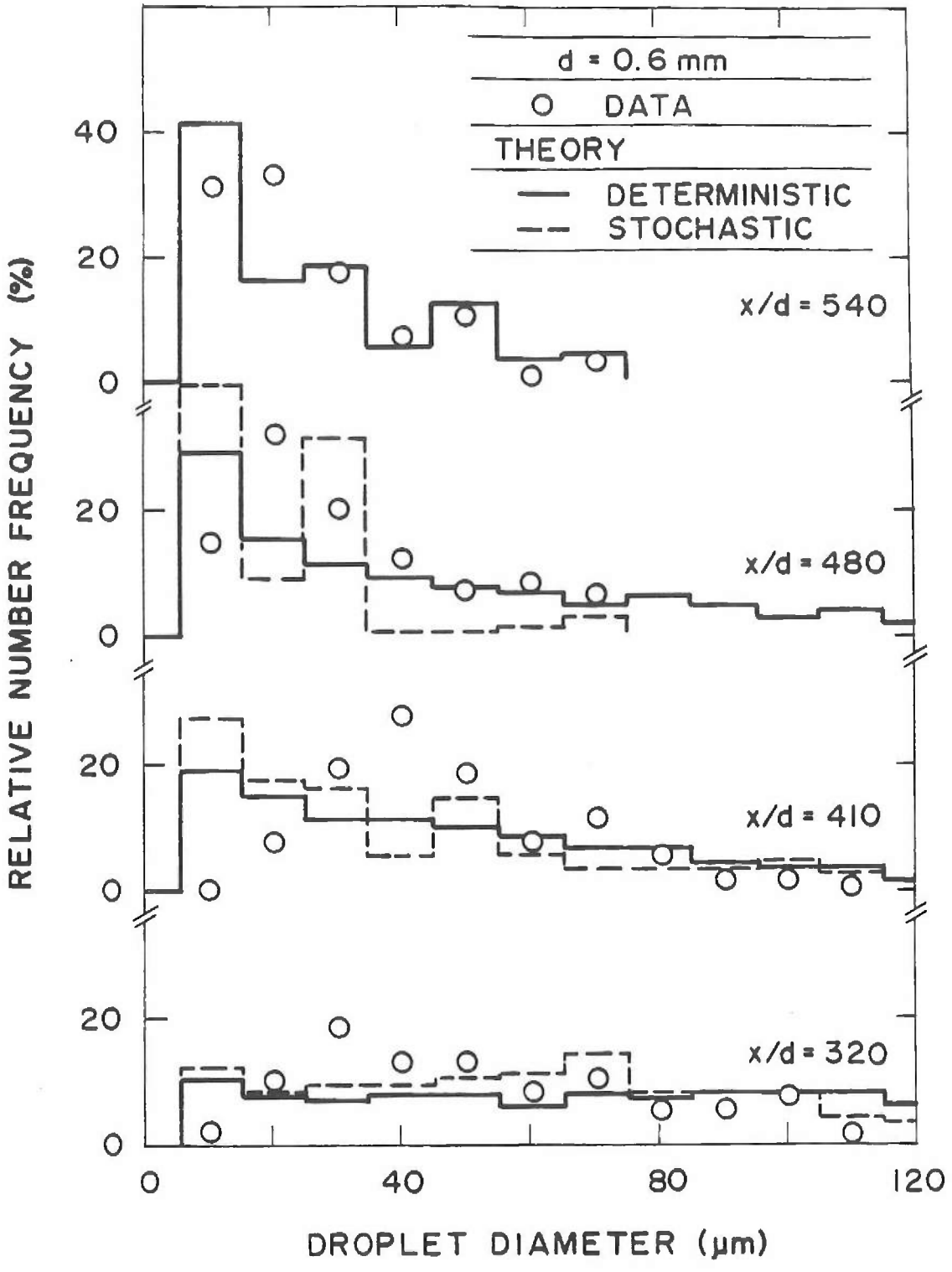

Figure 9. Measured (present study) and predicted (DSF and SSF methods) drop size contributions for combusting LGP1845 sprays. From Lee and Faeth (1990).

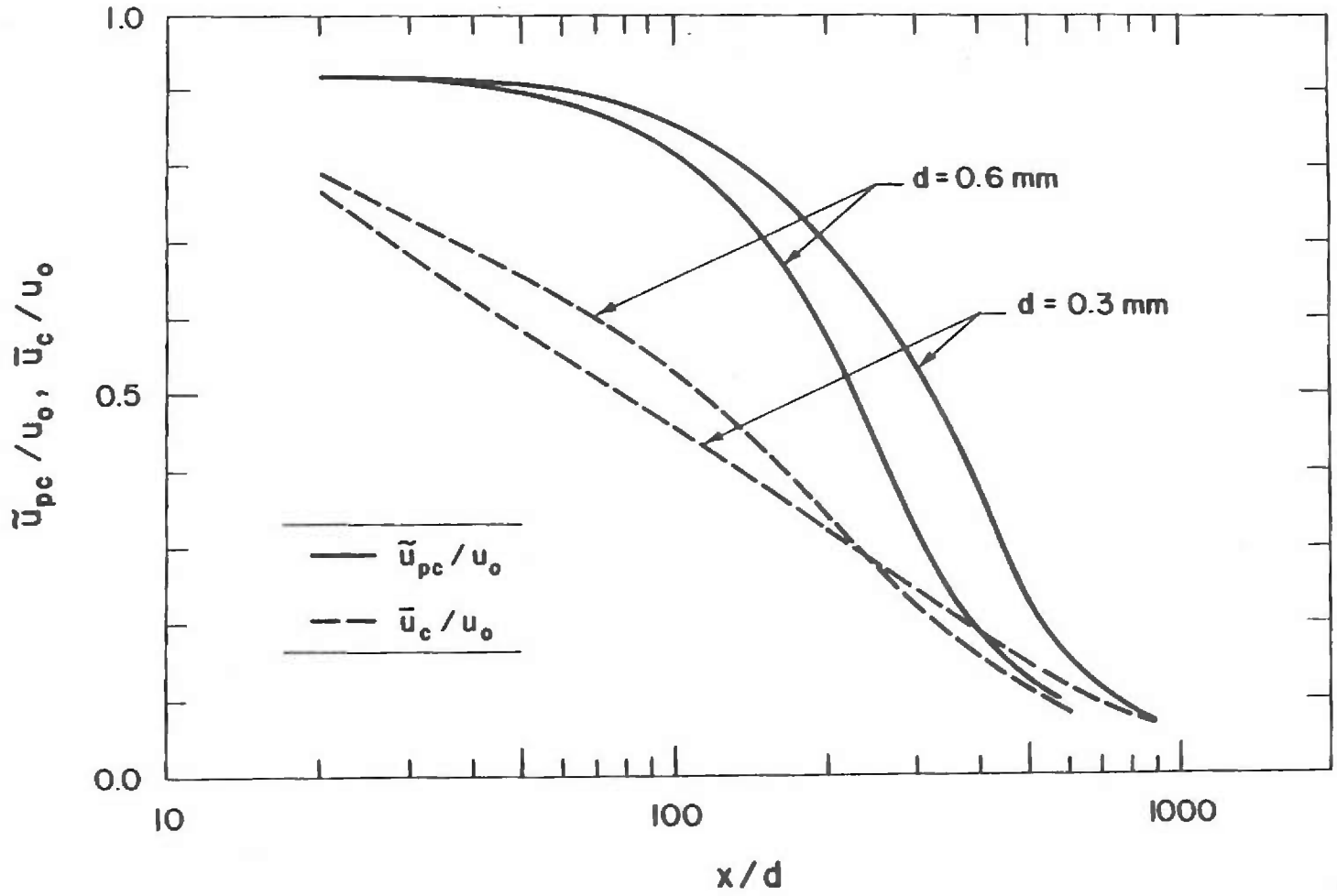

Figure 10. Predicted (DSF method) phase velocity variation along axis of combusting LGP1845 sprays at 10 MPa. From Lee and Faeth (1990).

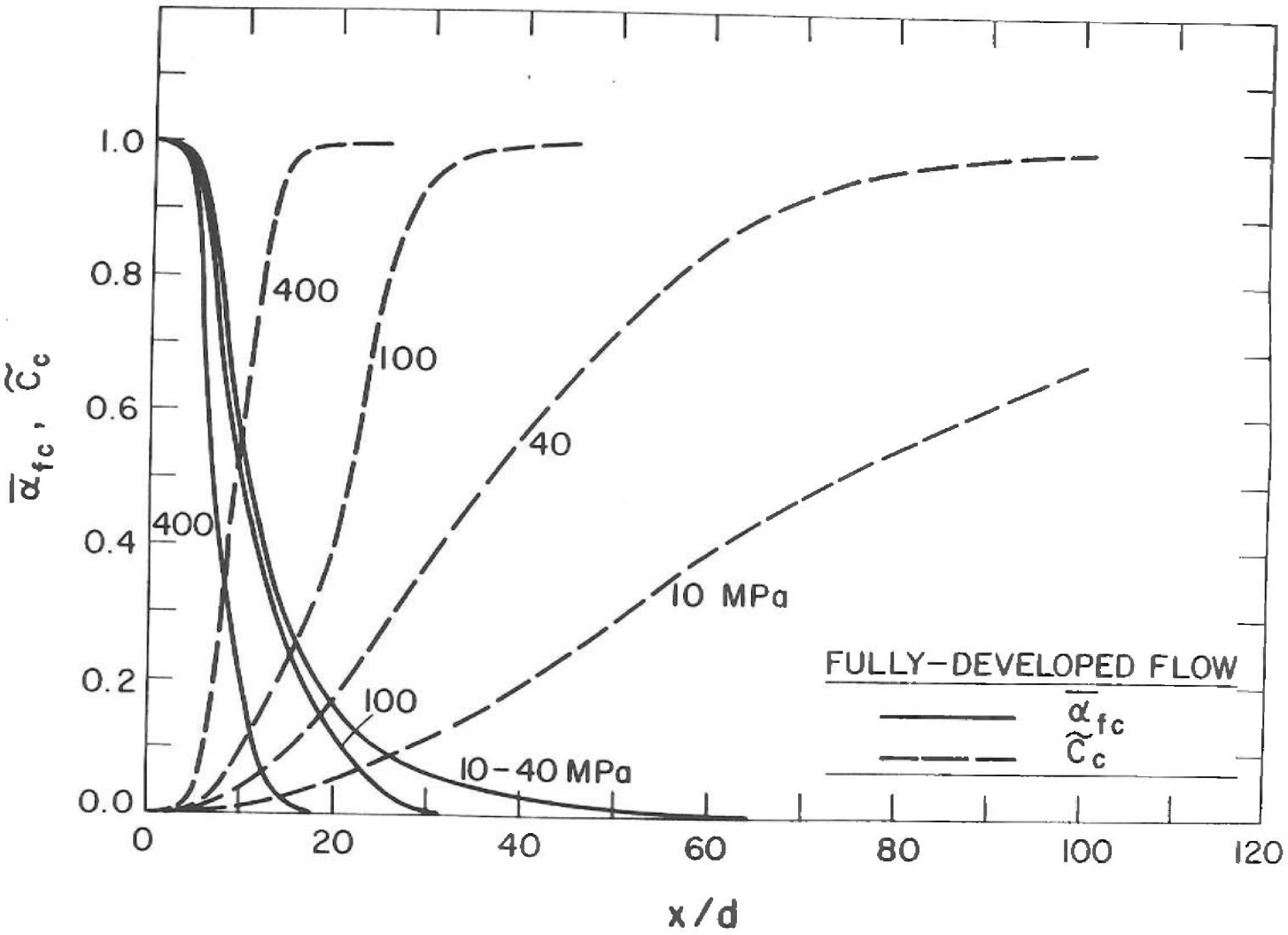

Figure 11. Predicted (LHF method) mean scalar properties along axis of combusting HAN-based monopropellant sprays for fully-developed flow at injector exit. From Lee et al. (1988).

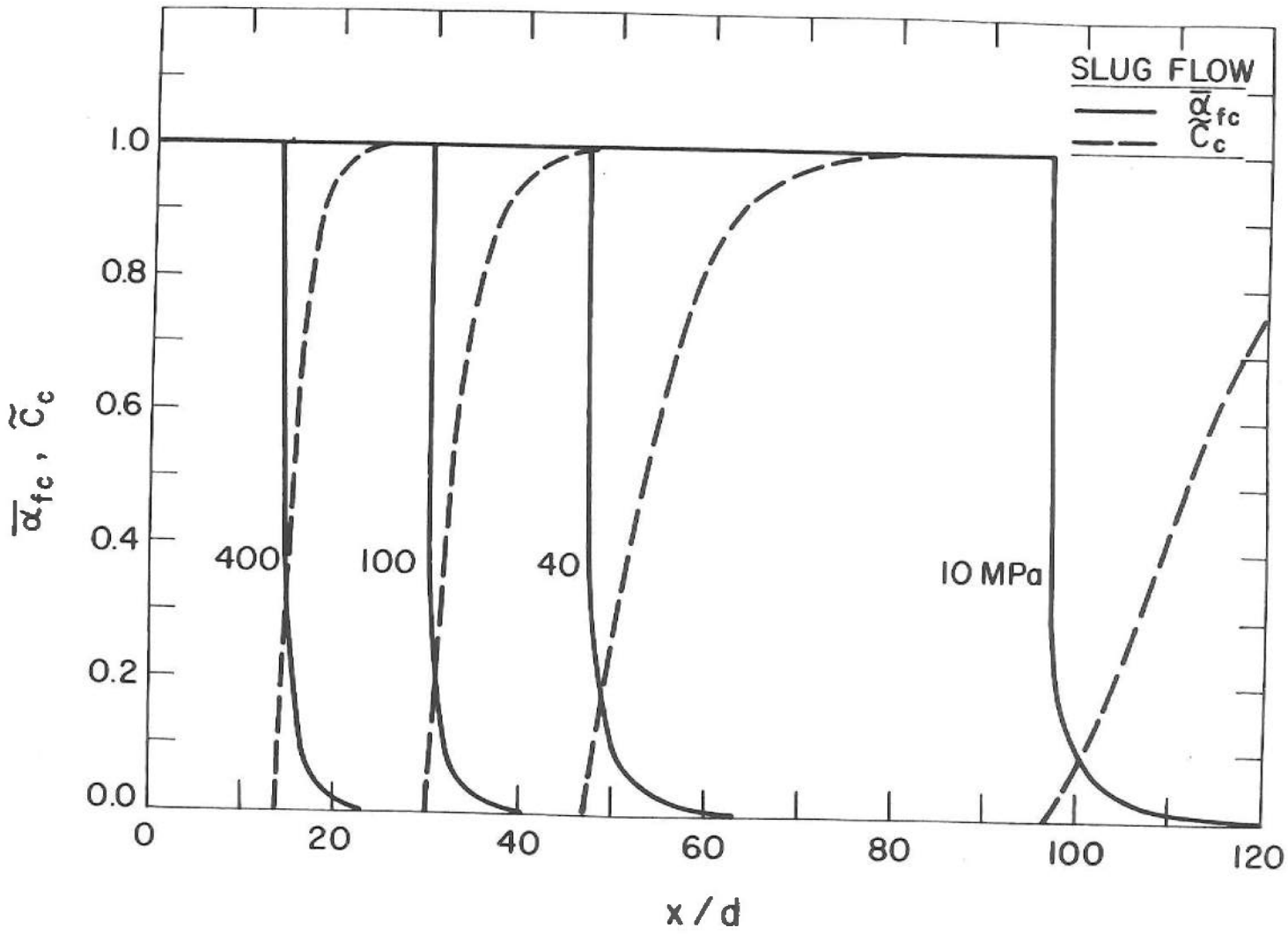

Figure 12. Predicted (LHF method) mean scalar properties along axis of combusting HAN-based monopropellant sprays for slug flow at injector exit. From Lee et al. (1988).

2.4 Conclusions

Major conclusions of the present investigation can be summarized as follows:

1. Critical combustion pressures of the HAN-based monopropellants are unusually high, 250 MPa with an uncertainty of 50 percent. This implies that subcritical combustion and spray processed are relevant for combusting monopropellant sprays, except for the highest-pressure portions of gun cycles.

2. Estimates of liquid surface properties and critical combustion pressures are unusually sensitive to the binary interaction parameter of TEAN and water. Measurements of this and other properties concerning phase equilibrium are needed to reduce uncertainties of critical combustion pressures.

3. Measurements yielded effective drop burning rates of ca. 10mm/s for drop diameters of 300-1200 μm and pressures of 0.2-7 MPa. The effective drop burning rate involved subsurface gas evolution and mechanical removal of liquid by microexplosions, which dominated the process at low pressures (below 2.1 MPa), and conventional hetereogeneous combustion from the liquid surface, which dominated the process at high pressures.

4. Present measurements of drop burning rates at pressures of 0.2-7 MPa were consistent with McBratney's (1980, 1981) strand burning rate measurement for jelled propellants at 10-100 MPa, and present drop combustion rates within combusting sprays.

5. Estimated mean drop sizes near the injector exit were consistent with estimates of aerodynamic or secondary drop breakup theory (Reitz and Bracco, 1982; Ruff and Faeth, 1990), however, this approach is only provisional pending study of effects of liquid turbulence and approach of the flow to the LHF limit.

6. The combusting monopropellant sprays exhibited strong separated flow effects for present test conditions, with the length of the liquid-containing region being nearly the same for injector diameters of 0.3 and 0.6mm when initial SMD and injector velocities were nearly the same.

7. Both separated flow models were in reasonably good agreement with measurements, however, the DSF approach is favored since it requires less extensive computations.

8. The LHF approach overestimated the rate of development of the flow for present test conditions but still could be of value at high pressure conditions approaching and exceeding the critical combustion pressure. The present approach is provisional, however, pending proper calibration of its treatment of turbulent premixed combustion.

3. List of Publications

Kounalakis, M.E. and Faeth, G.M., "Combustion of HAN-Based Liquid Monopropellants near the Thermodynamic Critical Point," Combust. Flame, Vol. 74, No. 2, pp. 179-192, 1988.

Lee, T.-W., Gore, J.P., Faeth, G.M. and Birk, A., "Analysis of Combusting High-Pressure Monopropellant Sprays," Combust. Sci. Tech., Vol. 57, No. 4-6, pp. 95-112, 1988.

Lee, T.-W., Tseng, L.-K. and Faeth, G.M., "Separated-Flow Considerations for Pressure-Atomized Combusting Monopropellant Sprays," AIAA Paper No. 89-0049; also, J. Prop. and Power, in press.

Lee, T.-W. and Faeth, G.M., "Structure and Mixing Properties of Combusting Monopropellant Sprays," AIAA Paper No. 90-0463, 1990; also, J. Prop. and Power, submitted.

Lee, T.-W., Gore, J.P., Faeth, G.M. and Birk, A., "Structure of High-Pressure Monopropellant Sprays," Proceedings of 1987 Spring Technical Meeting, Central States Section of the Combustion Institute, Pittsburgh, PA, pp. 464-469, 1987.

Faeth, G.M., Lee, T.-W. and Kounalakis, M.E., "Mixing and Thermodynamic Critical Phenomena of Combusting Monopropellant Sprays," Proceedings of the 24th JANNAF Combustion Meeting, CPIA, Laurel, MD, 1987.

Lee, T.-W., Tseng, L.-K. and Faeth, G.M., "Structure of Pressure-Atomized Monopropellant Sprays," Proceedings of the 25th JANNAF Combustion Meeting, CPIA, Laurel, MD, 1988.

Lee, T.-W., "Structure of Combusting Monopropellant Sprays at High Pressures," Ph.D. Thesis, The University of Michigan, Ann Arbor, MI, 1990.

4. List of Participating Scientific Personnel

G.M. Faeth, Principal Investigator, Professor, The University of Michigan.

T.-W. Lee, Graduate Assistant, The University of Michigan, Ph.D., June 1990.

L.-K. Tseng, Graduate Assistant, The University of Michigan.

M.E. Kounalakis, Graduate Assistant, The University of Michigan.

References

Beyer, R.A. (1986), "Atmospheric Pressure Studies of Liquid Monopropellant Drops in Hot Flows," Technical Report BRL-TR-2768, Ballistic Research Laboratory, Aberdeen Proving Ground, Maryland.

Beyer, R.A. (1988), "Single Droplet Studies in a Hot, Pressurized Environment," Technical Report BRL-TR-2900, Ballistic Research Laboratory, Aberdeen Proving Ground, Maryland.

Beyer, R.A. and M.W. Teague (1986), "Studies of Single Liquid Propellant Drops in Hot, High-Pressure Environments," 22nd JANNAF Combustion Meeting, CPIA Publication 457, Vol. 2, pp. 429-434.

Birk, A. and P. Reeves (1987), "Annular Liquid Propellant Jets — Injection, Atomization and Ignition," Report No. BRL-TR-2780, Ballistic Research Laboratory, Aberdeen Proving Ground, Maryland.

Bilger, R.W. (1976), "Turbulent Jet Diffusion Flames," *Prog. Energy Combust. Sci.* 1, pp. 98-109.

Bray, K.N.C. (1980), "Turbulent Flows with Premixed Reactants, " Turbulent Reacting Flows, Springer, Berlin, pp. 115-135.

Chen, L.-D. and G.M. Faeth (1981), "Initiation and Properties of Decomposition Waves in Liquid Ethylene Oxide," *Combust. Flame* 40, pp. 13-28.

Faeth, G.M. (1972), "High Pressure Liquid Monopropellant Strand Combustion," *Combust. Flame* 18, pp. 103-113.

Faeth, G.M. (1987), "Mixing, Transport and Combustion in Sprays," *Prog. Energy Combust. Sci.* 13, pp. 293-345.

Faeth, G.M., J.P. Gore, S.G. Chuech and S.M. Jeng (1988), "Radiation from Turbulent Diffusion Flames," *Ann. Rev. Num. Fluid Mech. and Heat Trans.* 2, pp. 1-38.

Gordon, S. and B.J. McBride (1971), "Computer Program for Calculations of Complex Chemical Equilibrium Compositions, Rocket Performance, Incident and Reflected Shocks, and Chapman-Jouguet Detonations," NASA Report SP-273.

Jeng, S.-M. and G.M. Faeth (1984), "Species Concentrations and Turbulence Properties in Buoyant Methane Diffusion Flames," *J. Heat Trans.* 106, pp. 721-727.

Kounalakis, M.E. and G.M. Faeth (1988), "Combustion of HAN-Based Liquid Monopropellants Near the Thermodynamic Critical Point," *Combust. Flame* 74, pp. 179-192.

Lee, T.-W., J.P. Gore, G.M. Faeth and A. Birk (1988), "Analysis of Combusting High-Pressure Monopropellant Sprays," *Combust. Sci. and Tech.* 57, pp. 45-112.

Lee, T.-W., L.-K. Tseng and G.M. Faeth (1989), "Separated-Flow Considerations for Pressure-Atomized Combusting Monopropellant Sprays," AIAA Paper No. 89-0049; also, J. Prop. and Power, in press.

Lee, T.-W. and G.M. Faeth (1990), "Structure and Mixing Properties of Combusting Monopropellant Sprays," AIAA Paper No. 90-0463; also, J. Prop. and Power, submitted.

McBratney, W.F. (1980), "Windowed Chamber Investigation of Burning Rate of Liquid Monopropellants for Guns," Report No. ARBRL-MR-03018, Ballistic Research Laboratory, Aberdeen Proving Ground, Maryland.

McBratney, W.F. (1981), "Burning Rate Data for LGP 1845," Report No. ARBRL-MR-03128, Ballistic Research Laboratory, Aberdeen Proving Ground, Maryland.

Reitz, R.D. and F.V. Bracco (1982), "Mechanism of Atomization of a Liquid Jet," Phys. Fluids 25, pp. 1730-1742.

Ruff, G.A., A.D. Sagar and G.M. Faeth (1989), "Structure and Mixing Properties of Pressure-Atomized Sprays," *AIAA J.* 27, pp. 901-908.

Ruff, G.A., L.P. Bernal and G.M. Faeth (1990), "Structure of Near-Injector Region of Non-Evaporating Pressure-Atomized Sprays," AIAA Paper No. 89-0050; also, J. Prop. Power, in press.

Ruff, G.A. and G.M. Faeth (1990), "Continuous-Phase Properties of the Near-Injector Region of Pressure-Atomized Sprays," AIAA Paper No. 90-0464.

Vosen, S.R. (1988), "The Burning Rate of HAN-Based Liquid Monopropellants," *Twenty-Second Symposium (International) on Combustion*, The Combustion Institute, Pittsburgh, pp. 1817-1825.

Zhu, D.L. and C.K. Law (1987), "Aerothermochemical Studies of Energetic Liquid Materials: 1. Combustion of HAN-Based Liquid Gun Propellants under Atmospheric Pressure," *Combust. Flame* 70, pp. 333-342.

Appendix A. Publications

A.1 "Combustion of HAN-Based Liquid Monopropellants near the Thermodynamic Critical Point" by M.E. Kounalakis and G.M. Faeth; Combust. Flame, Vol. 74, No. 2, pp. 179-192, 1988.

COMBUSTION AND FLAME 74: 179–192 (1988)

Combustion of Han-Based Liquid Monopropellants Near the Thermodynamic Critical Point

M. E. KOUNALAKIS and G. M. FAETH

Department of Aerospace Engineering, The University of Michigan, Ann Arbor, MI 48109-2140

The high-pressure combustion properties of liquid monopropellants involving mixtures of hydroxyl ammonium nitrate (HAN), triethanol ammonium nitrate (TEAN), and water are considered theoretically. Liquid surface properties and the critical combustion pressure (the pressure required for the propellant surface to exceed its thermodynamic critical point) were found allowing for real-gas phenomena and the presence of dissolved combustion product gases in the liquid. Critical combustion pressures for the HAN-based monopropellants were found to be unusually high, ca. 2500 atm, with an estimated uncertainty of 50%. Predictions were unusually sensitive to the critical temperature of TEAN and the binary interaction parameter between TEAN and water; both must be known more accurately for definitive estimates of the liquid-surface properties of HAN-based monopropellants at high pressures.

NOMENCLATURE

c	molar concentration
d	droplet diameter
D	effective binary diffusivity
h_i	partial enthalpy of species i
k_{ij}	binary interaction parameter
$\dot{n}''$	total molar flux
p	pressure
Pr	Prandtl number
R	gas constant
Re	Reynolds number
Sc	Schmidt number
T	temperature
u	streamwise velocity
v	specific volume
x	distance
Y_i	mole fraction of species i
α	thermal diffusivity
δ	characteristic convection thickness
ϵ_i	mole flux fraction of species i
λ	mixture thermal conductivity
ω	acentric factor

Subscripts

c	thermodynamic critical point
f	flame condition
R	reactant
o	far-upstream condition

INTRODUCTION

The combustion of liquid monopropellant sprays involves pressure-atomized injection of the liquid into a high-pressure and high-temperature environment for typical applications, e.g., gas generators and regenerative liquid-propellant guns. After injection, the surfaces of ligaments, drops, etc., become heated, the propellant vaporizes and, finally, reacts to combustion products in the gas phase. At sufficiently high pressures, however, liquid surfaces approach the thermodynamic critical point, causing transition to the supercritical combustion regime at the critical combustion pressure. The process is equivalent to the single-phase premixed combustion of a dense gas within

Published by Elsevier Science Publishing Co., Inc.
655 Avenue of the Americas, New York, NY 10010

0010-2180/88/$03.50

the supercritical combustion regime, and liquid surfaces are no longer observed. Clearly, it is important to know critical combustion pressures and liquid surface properties to define the pressure range where sprays are observed and to find spray properties within this regime. Analysis was undertaken to find these properties for hydroxyl ammonium nitrate-based monopropellants during the present investigation. HAN-based monopropellants are of interest because they are being considered for several high-pressure monopropellant combustion systems [1].

Near-critical phenomena of high-pressure liquid combustion has been studied earlier in this laboratory [2–7]. Various liquid monopropellants, such as nitrate esters [2], ethylene oxide [3], and hydrazine [4] were studied in strand combustion configurations, by analyzing gas phase transport using the thin flame approximation. High-pressure phenomena, such as real-gas effects and the presence of gaseous combustion products dissolved in the liquid phase, were treated using the Redlich–Kwong equation of state [8]. Predictions generally agreed with measured liquid surface temperatures, within uncertainties anticipated due to limitations concerning the high-pressure thermophysical and transport properties of combusting monopropellant systems [2–4]. Critical combustion pressures were in the range 100–200 atm for the nitrate ester monopropellants (normal propyl nitrate, ethyl nitrate, and propylene glycol dinitrate) [2] and ethylene oxide [3], which is typical of other liquid combustion processes that have been studied [5–7]. These predictions were relatively sensitive to values of transport properties and had estimated uncertainties of 30%. Unfortunately, experimental evaluation of predicted critical combustion pressures was not possible, due to the appearance of unstable combustion waves associated with the loss of the stabilizing effect of surface tension near the thermodynamic critical point [2, 3] as the critical combustion pressure was approached.

Similar studies of the liquid surface properties of HAN-based monopropellants have not been reported, although McBratney [9, 10] has measured the strand burning rates of some typical blends. A liquid surface was clearly observed at 290 atm, while jelled samples maintained stable combustion surfaces up to 600 atm. These findings suggest significantly higher critical combustion pressures for HAN-based monopropellants than for other monopropellants studied thus far; however, the presence of a jell complicates the interpretation of these results. The results also indicate that measurements of the liquid surface properties of HAN-based monopropellants would be very difficult. First, the burning rates of HAN-based monopropellants are on the order of 20 mm s^{-1} [9, 10], which is an order of magnitude faster than other propellants that have been studied [2, 3]. Such burning rates imply characteristic flame thicknesses, α/u for each phase, and characteristic flame residence times, α/u^2 for each phase, on the order of 1 μm and 1 μs based on typical transport properties. Thus, adequate resolution and response for surface temperature measurements, or even for distinguishing a liquid surface in such a thin flame zone, is unlikely. Finally, past attempts to measure critical combustion pressures, or liquid surface properties near the thermodynamic critical point, have not been successful [2, 3].

In view of the experimental problems, theory was used to find liquid surface properties and critical combustion pressures during the present investigation. Earlier theoretical methods [2–4] were extended to treat the specific features of some representative HAN-based monopropellants. Predictions require thermophysical and transport properties that must be estimated for monopropellants; therefore, the effects of these uncertainties were evaluated using sensitivity analysis. The study was limited to two HAN-based monopropellants, LGP 1845 and LPG 1846, which are mixtures of HAN, triethanol ammonium nitrate, and water. These choices were made because McBratney studied LGP 1845 [10], because recent spray studies have used LGP 1846 [1], and because similar formulations are candidates for practical applications.

THEORY

General Description

The theory is an extension of the approach used in [3]. Phase equilibrium considerations were im-

proved by considering the more highly developed modified Redlich-Kwong equation of state due to Soave [11, 12], as well as the basic Redlich-Kwong equation of state [7] used by this laboratory in earlier work [2, 3]. The earlier methods were developed for the analysis of monopropellant strand combustion [2, 3]; the relevance of this approach for estimating liquid surface properties and critical combustion pressures in sprays was also considered.

As in past work [2–4], the combustion process was assumed to be a steady, laminar one-dimensional deflagration wave. Typical combusting spray conditions involve pressures greater than 10 MPa and drops or other liquid elements having diameters or radii of curvature greater than 10 μm, because smaller liquid elements approximate the dynamics of the gas phase in any event [13]. Under these conditions, pressure drops across the wave are less than 100 Pa even for the high burning rates of the HAN-based propellants; therefore the approximation of a constant-pressure deflagration wave can be adopted with little error. Based on the burning rate measurements of McBratney [9, 10], combustion lifetimes of the liquid elements of interest are greater than 1 ms, which is much greater than the estimated characteristic residence time (1 μs) in the wave; therefore, the steady (quasisteady) wave approximation is appropriate as well.

Forced convection and turbulence in sprays can cause departures from one-dimensional waves near liquid surfaces. Multidimensional effects due to forced convection are small when the characteristic convection thickness is greater than the characteristic flame thickness [14]. The convection thickness for drops can be estimated with sufficient accuracy for present purposes as follows [13]

$$\delta = d/(2 + 0.556\ \mathrm{Re}^{\frac{1}{2}}(\mathrm{Pr}\ \text{or}\ \mathrm{Sc})^{\frac{1}{3}}). \qquad (1)$$

Maximum drop Reynolds numbers in sprays are on the order of 10^2 [13]; therefore, Eq. 1 implies that characteristic convection thicknesses are greater than the 1-μm characteristic flame thickness of present propellants for drop diameters greater than 10 μm. Existing information on the length microscales of turbulence in spray flames is very limited; however, one estimate for the fully developed portion of sprays having a typical Reynolds number of 10^4 suggests that the microscales are on the order of 10^{-3} times the distance from the injector [13]. This implies that microscales are greater than the characteristic flame thickness for distances greater than 1 mm from the injector exit; therefore, turbulence should have little effect on the one-dimensionality of flame properties for most portions of monopropellant spray flames. Based on these considerations, the assumption of one-dimensional laminar flow appears to be relevant for spray combustion of the present monopropellants.

Combustion was assumed to be adiabatic with thermodynamic equilibrium reached at the downstream edge of the reaction zone, which are reasonable assumptions for high-intensity spray combustion at high pressures. The properties of the combustion products were computed under these assumptions using the Gordon and McBride code [15]; results for LGP 1845 and LPG 1846 are summarized in Table 1 for pressures of 1 MPa, 10 MPa, and 100 MPa. Both reactant mixtures are stoichiometric and have virtually identical combustion product compositions; the main difference between the two is that the flame temperature of LGP 1845 is roughly 100 K higher than that of LGP 1846. The combustion products are nearly 70% water vapor. Due to the relatively low combustion temperatures and high pressures, dissociation effects are small, and combustion product concentrations are nearly independent of pressure.

The propellants have relatively low flame temperatures; therefore, effects of radiation can be neglected. For example, if we conservatively assume that the emissivity of the combustion products is unity and that reabsorption between the flame and the liquid surface is negligible, the burning rate measurements of McBratney [9, 10] imply that radiation contributes less than 4% to the enthalpy rise of gasification of the liquid.

Precise treatment of combustion chemistry is not possible, because the mechanisms and rate constants are not known for the high-pressure decomposition of HAN-based monopropellants;

TABLE 1

Combustion Properties of HAN-Based Monopropellants[a]

Propellant	LGP 1845[b]			LGP 1846[c]		
Pressure (MPa)	1	10	100	1	10	100
Reactant density (kg m^{-3})	1452	1454	1476	1430	1432	1454
Combustion product properties						
Density (kg m^{-3})	1.30	12.9	129	1.36	13.5	135
Temperature (K)	2133	2152	2163	2027	2039	2045
Composition (% by volume)[d]						
Water vapor	68.8	69.2	69.3	70.6	70.8	70.9
Carbon dioxide	12.7	12.9	13.0	12.2	12.3	12.3
Nitrogen	17.3	17.4	17.4	16.5	16.5	16.6

[a] Adiabatic, constant pressure combustion, with the liquid reactant at 298.15 K.
[b] Reactant composition (% by mass): HAN, 63.2; TEAN, 20; and H_2O, 16.8.
[c] Reactant composition (% by mass): HAN, 60.8; TEAN, 19.2; and H_2O, 20.0.
[d] Major species only. Minor species include: CO, H_2, NO, OH, and O_2.

therefore, the limiting approximation of an infinitely thin gas phase reaction zone located at some distance from the liquid surface was made, as in past work [2–4]. This large activation energy limit is favored for the present monopropellants due to their relatively low flame temperatures.

Consistent with the thin flame approximation, liquid phase reactions were also ignored. This is favored by the very short residence times in the high-temperature portions of the liquid phase, ca. 100 ns. Typical unimolecular decomposition reactions, which are at least representative of the first stage of reaction in the liquid, have characteristic reaction times two or more orders of magnitude longer than the liquid residence time for present conditions, providing some justification for this assumption.

Phase equilibrium was assumed at the liquid surface, as in past work [2–4]. This is a good approximation for drop diffusion flames at pressures greater than 0.1 MPa [12]; however, the assumption was reexamined due to the high burning rates of the HAN propellants. Following Dunn and Reay [16], the burning rate measurements of McBratney [9, 10] imply differences between actual and saturated vapor pressures at the liquid surface less than 0.3 MPa due to finite rates of evaporation. This is clearly small in comparison to the combustion pressures of interest, which were greater than 10 MPa. The corresponding temperature jumps at the surface, due to finite evaporation rates, were found using the present phase equilibrium analysis. The resulting temperature jumps were less than 0.3 K, which is also small in comparison to the temperature rise in the liquid phase. Thus, phase equilibrium at the surface can be adopted with little error.

Gas phase transport was treated similar to earlier analyses of liquid combustion processes at high pressures [2–7]. Only concentration diffusion was considered, taking the binary diffusivities of all species to be equal, and neglecting the Dufour energy flux. The assumption of an effective binary diffusion coefficient is more questionable for blends like the HAN-based propellants than for blends studied in earlier work where only a single species was diffusing and the approximation was exact. However, the present approach seems reasonable in view of the other approximations of the analysis; the effect of the approximation was examined by sensitivity calculations. The specific treatment of thermophysical and transport properties will be discussed later. Effects of compressibility and varying Lewis numbers were consid-

ered, particularly because variations in the Lewis number are known to influence predictions of critical combustion pressures [2–7].

Monopropellants typically have negligible dissolved gas concentrations prior to injection; therefore, carbon dioxide and nitrogen are not present in the bulk liquid and have negligible mass fluxes upstream of the flame. However, the propellant components HAN, TEAN, and water, all have finite mass fluxes upstream of the flame, the last being both a propellant component and a combustion product.

Transport Analysis

Because only liquid surface properties are of interest (not burning rates), the equations to be solved are identical in all one-dimensional coordinate systems: Cartesian for large liquid elements, cylindrical for ligaments, and spherical for drops. A Cartesian formulation, sketched in Fig. 1, is used to simplify the notation. The analysis is confined to the region between the flame and liquid surface, corresponding to the outer region of asymptotic analysis of monopropellant flames at the high activation energy limit. Effects of multicomponent diffusion and the presence of dissolved gases cause reactant (HAN and TEAN) concentrations to vary in the liquid phase. There is a concentration jump at the liquid surface, dictated by phase equilibrium requirements. The corresponding temperature jump is small, however, as noted earlier. Properties at the flame surface are given by the adiabatic flame calculations discussed earlier, see Table 1.

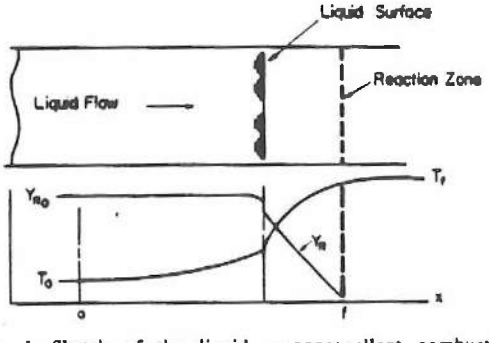

Fig. 1. Sketch of the liquid monopropellant combustion process.

Gas phase transport was formulated in terms of molal quantities to simplify matching with the phase equilibrium analysis. Under present assumptions, the equations governing conservation of energy and species between the liquid surface and the flame sheet are as follows [2–4]

$$\dot{n}'' \sum_{i=1}^{N} \epsilon_i (h_i - h_{i0}) = \lambda \frac{dT}{dx} \tag{2}$$

$$\dot{n}'' (Y_i - \epsilon_i) = cD \frac{dY_i}{dx}, \quad i = 1, \cdots, N. \tag{3}$$

Initial conditions for Eqs. 2 and 3 can be specified in terms of known flame properties as follows

$$x = x_f, \; T = T_f, \; Y_i = Y_{if}, \; i = 1, \cdots, N. \tag{4}$$

Denote the species present in the original monopropellant as $i = 1, \cdots, R < N$. Then, eliminating spatial derivatives among Eq. 3, integrating, and applying the concentration boundary conditions of Eq. 4 yields

$$Y_i = \epsilon_i + \frac{(Y_{if} - \epsilon_i)(Y_j - \epsilon_j)}{(Y_{jf} - \epsilon_j)} \tag{5}$$

where $i \neq j$, and j can be any species $j = 1, \cdots R$.

Eliminating spatial derivatives between Eq. 2 and Eq. 3 for $i = j$ yields

$$\frac{dY_j}{dT} = -\frac{(\lambda/cD)(\epsilon_j - Y_j)}{\sum_{i=1}^{N} \epsilon_i (h_i - h_{i0})} \tag{6}$$

where j is selected in the same manner as Eq. 5. The initial condition for Eq. 6 is

$$T = T_f, \; Y_j = Y_{jf}. \tag{7}$$

As noted earlier, the effects of pressure on flame properties were small; therefore, a single flame condition was used for each propellant. These properties, as well as the ϵ_i that are fixed by the propellant composition, are summarized in Table 2 for each propellant.

TABLE 2

Mole Flux Fractions and Flame Properties for Calculations

Fuel	LGP 1845	LGP 1846
Mole Flux Fractions (%)		
HAN	39.1	34.5
TEAN	5.6	4.9
H_2O	55.3	60.6
Flame Properties:		
Temperature (K)	2146	2040
Composition (% by volume):		
H_2O	69	71
CO_2	13	12
N_2	18	17

Given Eq. 5 and mixture properties as a function of temperature and pressure, Eq. 6 can be integrated from the flame toward the liquid surface, providing the transport locus of the variation of species mole fractions with temperature. Liquid surface conditions are reached when the properties along the transport locus reach a dew point of the phase equilibrium analysis. Dew-point computations are considered next.

Phase Equilibrium Analysis

Two methods were used to compute phase equilibrium at the liquid surface: the Redlich–Kwong equation of state with mixing rules developed by Prausnitz and Chueh [8], which was used during earlier studies of high-pressure liquid combustion [2–7]; and the more highly developed modified Redlich–Kwong equation of state due to Soave [11, 12]. The use of these equations of state for polar compounds like HAN, TEAN, and water is tentative, for lack of a viable alternative. Prausnitz et al. [17] found, however, that polar corrections of the equation of state are small when reduced temperatures are greater than 0.95; this condition was generally satisfied for the most polar compounds during present computations.

Phase equilibrium at the liquid surface requires that the temperature, pressure, and fugacity of each species is the same in both phases. Given the pressure and the gas phase composition along the transport locus, the corresponding liquid phase composition and equilibrium temperature can be computed from the equation of state. This corresponds to a dew-point calculation, using the computer codes found in [11] and [7] for the Soave and Relich–Kwong equations of state. Liquid surface conditions are reached when the transport and phase equilibrium temperatures are the same.

Thermophysical Properties

The equations of state require critical properties and acentric factors, while computations of flame properties require enthalpies of formation. The values of these properties used during the calculations are summarized in Table 3. The properties of H_2O, CO_2, and N_2 listed in this table are drawn from standard references [18, 19], and present no problems.

HAN and TEAN decompose at high temperatures; therefore, their thermophysical properties must be estimated. The Lyderson method [20, 21]

TABLE 3

Thermophysical Properties

Species	HAN	TEAN	H_2O	CO_2	N_2
Critical Properties					
Temperature (K)	763	1294	647.3	304.2	126.2
Pressure (atm.)	76	36	217.6	72.8	33.5
Volume (cm^3/gmol)	196	528	56	94	89.5
Acentric factor	0.68	1.41	0.344	0.225	0.040
Enthalpy of formation at 298.15 K (kcal $gmol^{-1}$)	−95.3	−185.5	−57.8	−94.0	0.0

was used to estimate the critical pressure, the critical volume, and the ratio of the normal boiling and critical temperatures. Acentric factors were computed from their definition, using the Lee and Kesler generalized vapor-pressure relationship [22]. The critical temperature was then computed from the Lee and Kesler expression [22] for the compressibility factor, applied at the critical point, as follows

$$T_c = (p_c v_c / R)/(0.291 - 0.080\omega) \quad (8)$$

These methods are routinely used for hydrocarbons, but they have not been tested for compounds like HAN and TEAN. Thus, the approach was evaluated by applying it to a variety of organic and inorganic compounds whose critical properties and acentric factors were known: NH_3, CO_2, H_2O, SO_2, NO_2, *n*-hexanol, benzyl alcohol, *n*, *n*-dimethylaniline, *n*-hexadecane, *n*-eicosane, and *n*-butanol. The average errors were as follows: critical temperature, −5%; critical pressure, −2.5%; critical volume, −9.6%; and the acentric factor, 0.6%. Based on these findings, the approach appears to be reasonable for present purposes.

The enthalpies of formation of HAN and TEAN listed in Table 3 were found using the Verma and Doraiswamy group contribution method [23]. Uncertainties in these properties are not very important, however, because flame properties are dominated by the enthalpies of formation of H_2O, CO_2, and N_2, which are well known [18, 19].

Ideal-gas enthalphy changes with temperature were found from standard sources for H_2O, CO_2, and N_2 [18, 19]. The group contribution specific heat correlation of Rihani and Doraiswamy [24] was used to compute ideal-gas enthalpy changes for HAN and TEAN. Enthalpy deviations and *c* were found directly from the equations of state.

Binary interaction parameters k_{ij} are used in the equations of state. Present values of the k_{ij} are summarized in Table 4. These estimates were found from [11, 12] for the Soave equation of state, and from [5, 8] for the Redlich–Kwong equation of state. Measurements of k_{ij} are not available for binary pairs involving HAN and TEAN; therefore, the values for the hydrocarbon homomorphs of these species were used, as in past work [2–7].

TABLE 4

Binary Interaction Parameters (k_{ij})[a]

Substance	H_2O	CO_2	N_2
Soave equation of state			
HAN	0.381	0.136	0.140
TEAN	0.368	0.138	0.164
H_2O	0.000	0.102	0.140
CO_2	0.102	0.000	−0.022
Redlich–Kwong equation of state			
HAN	0.385	0.285	0.335
TEAN	0.790	0.650	0.745

[a] $k_{ii} = 0$; $k_{ij} = k_{ji}$; other interaction parameters not shown were taken to be zero. The systems were modeled by homomorphs.

Transport Properties

Mixture thermal conductivities and effective binary diffusivities are needed to integrate Eq. 6. Correlations of mixture thermal conductivities require the viscosities of all species as well. Ideal-gas thermal conductivities and viscosities were taken from Svehla [25] for H_2O, CO_2, and N_2, while the Eucken model [25] and the Reichenberg method [26] were used to estimate these properties for HAN and TEAN. Ideal gas mixture thermal conductivities were then found from the Wassiljewa equation [27], following Lindsay and Bromley [26]. The effect of compressibility on the mixture's thermal conductivity was determined by the Stiel and Thodos method [29], using the Prausnitz and Gunn rules for mixture pseudocritical properties [18].

Low-pressure binary diffusivities were found for all binary pairs in the system using the method of Fuller, Schettler and Giddings [30, 31] based on the average of these values at each temperature. The effect of compressibility on the effective binary diffusivity was computed following Dawson et al. [32], using the Prausnitz and Gunn modified rules for mixture pseudocritical properties [18], as before.

RESULTS AND DISCUSSION

Critical Combustion Conditions

Results for LGP 1845 and LPG 1846 were very similar, in view of property uncertainties; therefore, findings for LGP 1845 will be taken as representative in the following.

The nature of the solution for liquid surface properties, in the vicinity of the thermodynamic critical point, can be seen by reference to Fig. 2. Transport and phase equilibrium loci are plotted as functions of the gas phase mole fraction of HAN and the temperature at various pressures. The phase equilibrium locus was found using the Soave equation of state with all $k_{ij} = 0$; however, the properties of the plots are similar to findings for the range of k_{ij} considered during the investigation. Both loci satisfy Eq. 5, which relates the mole fractions of TEAN, H_2O, CO_2, and N_2 to the mole fraction of HAN in the gas phase. In addition, the transport locus satisfies the conservation of energy requirements of Eq. 6, while the phase equilibrium locus satisfies the requirements of thermodynamic equilibrium at the liquid surface. The intersection of these two loci, at a given pressure, is a solution for the gas phase properties at the liquid surface, where Eqs. 5 and 6 and the requirements for phase equilibrium are all satisfied.

At the lowest pressure illustrated in Fig. 2, 500 atm, the transport and phase equilibrium loci intersect, yielding a liquid-surface solution point. This behavior persists for all pressures below 640 atm. However, the transport locus becomes tangent to the phase equilibrium locus at 640 atm; this is the highest pressure where a liquid surface is present for the conditions illustrated in Fig. 2, and it corresponds to the critical combustion pressure. Pressures greater than 640 atm are within the supercritical combustion regime where the transport and phase equilibrium loci no longer intersect, see the results illustrated in Fig. 2 for 650 atm. In this regime, flow properties simply vary along the transport locus until the initial conditions in the bulk liquid are reached, and a liquid surface is never observed.

Liquid Surface Properties

The properties of the liquid surface for the subcritical regime, using the same solution parameters as Fig. 2 (the Soave equation of state with all $k_{ij} = 0$), are illustrated in Fig. 3. The surface temperature and species mole fractions in the gas and liquid phases are plotted as a function of pressure up to the critical combustion pressure.

Gas phase concentrations are relatively independent of pressure in Fig. 3; however, liquid phase concentrations vary substantially due to the presence of dissolved gases in the liquid at higher pressures. Other liquid combustion systems behave in a similar manner [2–7]. At low pressures, concentrations of dissolved combustion product gases (CO_2 and N_2) are quite small, and the more

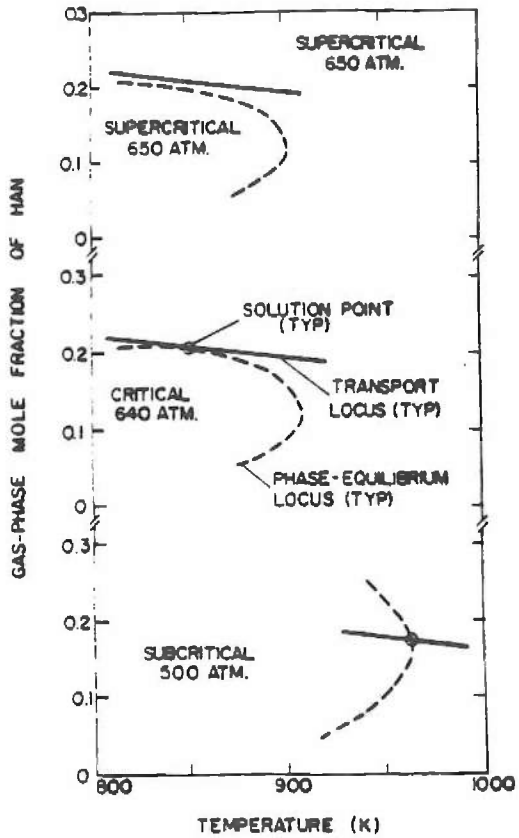

Fig. 2. Transport- and phase-equilibrium loci for subcritical, critical, and supercritical conditions; Soave equation of state, $k_{ij} = 0$.

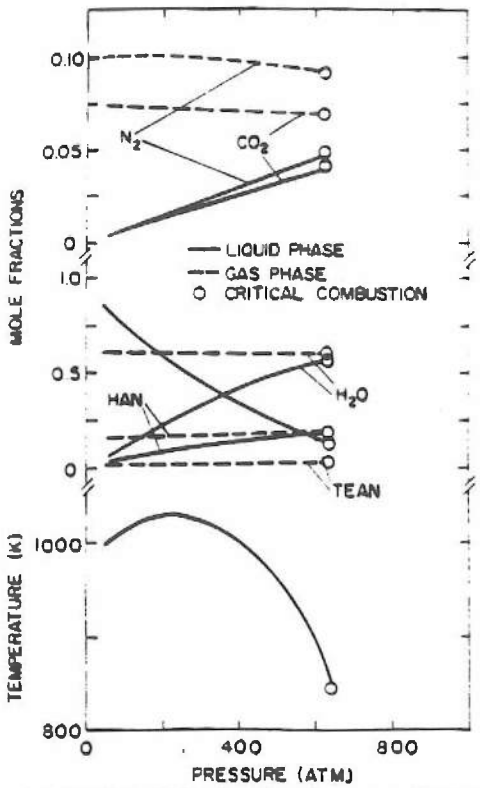

Fig. 3. Properties of the liquid surface as a function of pressure; Soave equation of state, $k_{ij} = 0$.

volatile propellant components (HAN and H_2O) are depleted in the liquid phase, leaving a high concentration (a mole fraction near 0.9) of the relatively nonvolatile TEAN. As the pressure is increased, however, concentrations of the more volatile components increase in the liquid, with water having the highest concentrations in the liquid for pressures greater than 400 atm. Concentrations of the gas and liquid are not the same at the critical combustion condition, and neither are the enthalpies; therefore, the critical combustion condition does not correspond to a thermodynamic critical point in this case. Thus, while the critical combustion condition often is a thermodynamic critical point [2–7], such behavior is not always observed.

At low pressures, the surface temperatures plotted in Fig. 3 increase with increasing pressure, which is typical of the behavior of other monopropellants that have been studied [2–4]. However, the surface temperature reaches a maximum, and then declines as the critical combustion pressure is approached. Similar behavior has been observed for ethylene oxide [3]. The effect is due to the greater concentrations of more volatile species, which have relatively low critical temperatures, in the liquid phase at high pressures. Due to the relatively low volatility of HAN and TEAN, however, liquid surface temperatures are unusually high; e.g., peak temperatures approach 1000 K in Fig. 3, as opposed to 500 K for the nitrate esters and ethylene oxide [2, 3].

The best estimate of liquid surface properties for LGP 1845, using the Soave equation of state and the standard k_{ij} values, is illustrated in Fig. 4.

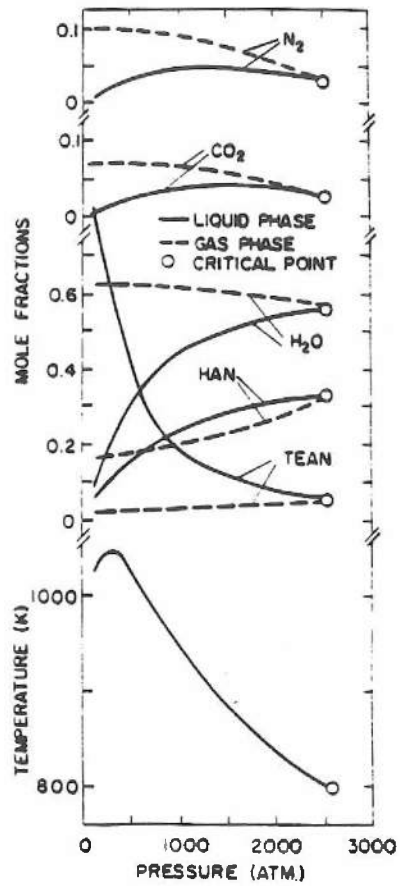

Fig. 4. Properties of the liquid surface as a function of pressure; Soave equation of state, standard k_{ij}.

The change in the k_{ij} causes a substantial increase in the predicted critical combustion pressure, from 640 atm for $k_{ij} = 0$, to 2600 atm for the standard k_{ij}. Such strong effects of the k_{ij} on liquid surface properties were not observed during earlier studies of liquid monopropellants [1-3]. For the results illustrated in Fig. 4, the critical combustion condition coincides with a thermodynamic critical point; this is indicated by the equality of gas and liquid compositions at the critical combustion pressure. Other differences when the standard k_{ij} are used included a greater variation of gas phase compositions and higher concentrations of HAN in the liquid phase, cf., Figs. 3 and 4. However, the range of liquid surface temperatures and the presence of a peak temperature at low pressures are similar in Figs. 3 and 4.

The Soave equation of state was felt to be the most reliable, because the k_{ij} values for the Redlich-Kwong equation of state were unusually high, and solutions with this approach were numerically very stiff. Nevertheless, results were obtained using the Redlich-Kwong equation of state, because it has been used for monopropellants in the past [2, 3]. Liquid surface properties computed in this manner for LGP 1845 are illustrated in Fig. 5 using standard values of the k_{ij}. The main difference between the results using the Soave and Redlich-Kwong equations of state, cf. Figs. 3 and 4, is that the latter yields a much higher critical combustion pressure, higher than the 4000-atm pressure range considered in Fig. 5. Thus, the results in Fig. 5 are similar to the low-pressure region of Fig. 4: the gas phase compositions are relatively independent of pressure; the liquid phase concentrations of the more volatile components (CO_2, N_2, and H_2O) increase with pressure; and the surface temperature increases with pressure. Predicted liquid surface temperatures become quite high as the pressure is increased, which, if true, raises concerns about potentially significant effects of reaction near the liquid surface.

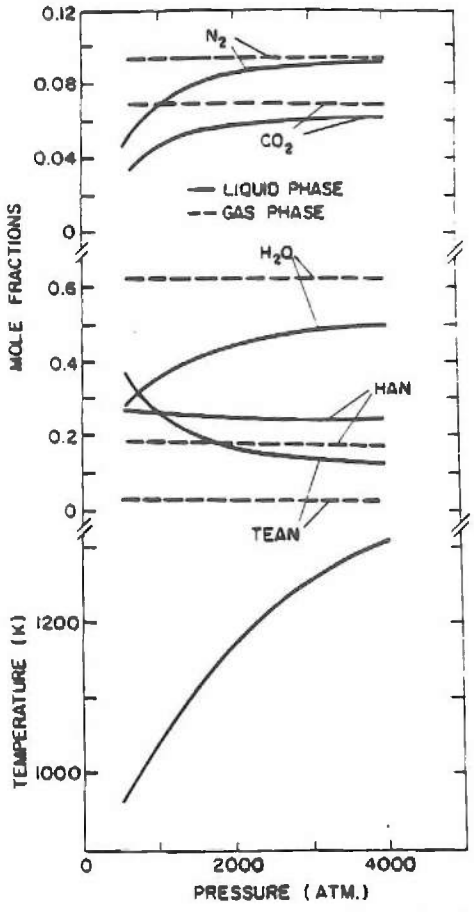

Fig. 5. Properties of the liquid surface as a function of pressure; Redlich-Kwong equation of state, standard k_{ij}.

Sensitivity Analysis

The equation of state and the values of the k_{ij} clearly have a significant effect on predictions of liquid surface conditions and the critical combustion pressure. Sensitivity analysis was undertaken to more precisely identify parameters that have a strong influence on predictions. The baseline for the sensitivity calculations was the Soave equation of state with all $k_{ij} = 0$. An exhaustive search procedure was used, where the effect of each parameter was evaluated independently.

Table 5 is a summary of the results of the sensitivity analysis, considering only the most sensitive parameters. The percent change in the critical combustion pressure, the critical combustion temperature, the pressure where the surface temperature is maximum, and the maximum surface temperature are given as a function of the percent change of the parameters (or the change in

TABLE 5

Sensitivity Analysis (LGP 1845)

Output variable		Critical combustion pressure (atm)	Critical combustion temperature (K)	Pressure at maximum temperature (atm)	Maximum temperature (K)
Standard Value[a]		640	840	200	1030
Parameter[b]	Variation	Percent change			
Thermal conductivity	+25%	−18	10	0	−0
	−25%	6	2	0	−0
Diffusion coefficient	+25%	6	2	0	−0
	−25%	−18	10	−14	−0
Critical temperature of TEAN	+10%	44	5	0	11
	−10%	−34	−4	−25	−18
Acentric factor of TEAN	+20%	13	2	0	2
	−20%	−18	2	0	2
k_{ij}[c] TEAN–H_2O	0.25	80	−11	25	0

[a] Standard property values except all $k_{ij} = 0$, Soave equation of state.
[b] Results for the most sensitive parameters are listed.
[c] All other $k_{ij} = 0$.

value of the k_{ij}). The most sensitive parameters include the mixture thermal conductivity, the effective diffusion coefficient, the critical temperature and acentric factor of TEAN, and the binary interaction parameter between TEAN and water. For continuous variables, such as the mixture thermal conductivity or the effective diffusion coefficient, the parameter variations involved changing the parameter from the standard value, by the percentage shown, at every point in the calculation. Except for the k_{ij}, which will be considered subsequently, the variations are representative of anticipated uncertainties [18, 25], similar to past work [2, 3].

Uncertainties in the critical combustion pressure due to uncertainties in the thermal conductivity, the diffusion coefficient, and the acentric factor of TEAN, are comparable to the uncertainties in the parameter itself, which is similar to findings for other monopropellants [2, 3]. The effect of changes in these parameters on other output variables, however, is relatively small. On the other hand, except for the critical combustion temperature, all output variables exhibit unusually strong sensitivity to uncertainties in the critical temperature of TEAN. This effect appears to be related to the vapor pressure of TEAN, with the reduced volatilities of TEAN at higher critical temperatures driving the system toward higher critical combustion pressures. The importance of TEAN for critical combustion phenomena, in spite of its relatively low concentration in the propellant, is probably due to its low volatility, which causes it to have relatively high concentrations at the liquid surface, see Fig. 3.

The high concentrations of both TEAN and water at the liquid surface are also responsible for the strong sensitivity of the critical combustion pressure to variations in the value of the binary interaction parameter between TEAN and water. Higher values of this binary interaction parameter tend to increase concentrations of TEAN in the

liquid at the surface, acting in a manner similar to the critical temperature of TEAN. Comparable changes of all other k_{ij} had a small effect, influencing output parameters less than 10%, similar to past findings concerning effects of uncertainties in the k_{ij} [2, 3]. Thus, the large increase in critical combustion pressure between Fig. 3 for all $k_{ij} = 0$, and Fig. 4 for the standard k_{ij}, is largely due to change of the binary interaction parameter between TEAN and water.

Findings were similar using the Redlich-Kwong equation of state. Predictions were most sensitive to the binary interaction parameter between TEAN and water, and to a lesser degree to the critical temperature of TEAN.

The direct effect of the binary interaction parameter between TEAN and water on critical combustion pressure predictions is illustrated in Fig. 6. Results are illustrated for both the Soave and Redlich-Kwong equations of state. All parameters are at their standard values, except for the TEAN-water binary interaction parameter which varies as shown. The solution at the standard value of the interaction parameter is marked for the Soave equation of state: the standard critical combustion condition for the Redlich-Kwong equation of state is outside the pressure range illustrated in Fig. 6. The critical combustion pressure is relatively insensitive to the binary

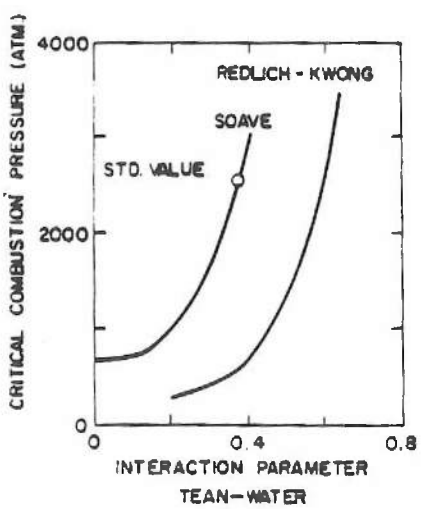

Fig. 6. Effect of the TEAN-water binary interaction parameter on the predicted critical combustion pressure.

interaction parameter between TEAN and water at low values of this parameter, but becomes very sensitive in the range of the standard values. For the Soave equation of state, a 25% variation of the TEAN-water interaction parameter about the standard value would result in a 50% variation in the critical combustion pressure. This sensitivity is smaller than the sensitivity to the critical temperature of TEAN shown in Table 5; however, uncertainties in the binary interaction parameter between TEAN and water are larger than those for the critical temperature of TEAN. Thus, this interaction parameter will have to be known more accurately for definitive estimates of liquid surface temperatures and critical combustion pressures of LGP 1845 and LPG 1846.

Based on these considerations, the best estimate of the critical combustion pressure for LGP 1845 and LPG 1846 is 2500 atm, with an uncertainty of 50%. This follows from predictions using the Soave equation of state with an uncertainty of 10% for the critical temperature of TEAN, which is reasonable in view of the assessment of estimates of this property discussed earlier; and uncertainties of all other properties of 25%, which is typical of past practice [2-7]. A low estimate of the critical combustion pressure would be 600 atm, based on the asymptotic of the critical combustion pressure plot for the Soave equation of state illustrated in Fig. 6. The low estimate is in the region where McBratney [9, 10] observed the onset of unsteady combustion waves, which often been associated with near-critical phenomena; however, the use of jelled propellants during these tests, and the absence of direct evidence concerning the onset of supercritical combustion, raises questions concerning the interpretation of these findings. The Redlich-Kwong equation of state yields critical combustion pressures greater than 4000 atm; however, estimated binary interaction parameters for this approach are unusually high. Therefore, this finding is felt to be less reliable than results using the Soave equation of state.

In spite of the uncertainties, it seems clear that the critical combustion pressures of the HAN-based monopropellants LGP 1845 and LPG 1846 are unusually high, roughly an order of magnitude higher than other liquid monopropellant and bipro-

pellant combustion processes that have been studied [2–7]. Present uncertainties in estimates of liquid surface properties and critical combustion pressures could be reduced if liquid surface temperatures were measured; however, this is a very challenging experimental problem due to the unusually high burning rates of these monopropellants.

CONCLUSIONS

The main conclusions of the present investigation are as follows:

1. Present findings suggest unusually high critical combustion pressures for typical HAN-based monopropellants (LGP 1845 and LPG 1846), on the order of 2500 atm with an uncertainty of 50%. This suggests that subcritical combustion and spray processes are relevant to the combustion of these monopropellants for most applications.
2. Estimates of the liquid surface properties of the present HAN-based monopropellants are unusually sensitive to the binary interaction parameter between TEAN and water, and to a lesser degree, to the critical temperature of TEAN.
3. Depending on the thermophysical and transport properties of the system, conditions at the liquid surface at the highest pressure where a liquid surface is observed (the critical combustion condition) may or may not correspond to a thermodynamic critical point.
4. The present HAN-based monopropellants exhibited relatively high liquid surface temperatures, 800–1000 K, in the pressure range of interest (pressures greater than 100 atm). This reduces polar liquid effects, which complicate the thermodynamics at lower temperatures, but increases the potential for significant liquid phase reaction near the surface, although the short residence times found under these conditions (ca. 100 ns) mitigate the potential reaction effects to some degree).

It should be noted that McBratney [9, 10] has observed unstable combustion, which is often associated with critical combustion conditions [2, 3], at pressures of 600–1000 atm; therefore, present estimates may be high. New measurements are needed to reduce the uncertainties of present findings and to definitively establish the range of pressures where spray phenomena must be considered for these monopropellants.

This research was supported, in part, by the Army Research office, Contract No. DAAL03-86-K-0154, under the Technical Management of D. M. Mann, and by the U.S. Army Armament Research, Development and Engineering Center, under the Technical Management of A. Bracuti and P.-L. Lu. The authors also wish to acknowledge useful discussions with A. Birk, E. Freedman, and W. F. McBratney of the Ballistic Research Laboratory, Aberdeen Proving Ground, Maryland.

REFERENCES

1. Lee, T.-W., Gore, J. P., Faeth, G. M., and Birk, A. *Combust. Sci. Tech.*, 57:95–112 (1988).
2. Faeth, G. M. *Combust. Flame* 18:103–113 (1972).
3. Chen, L.-D., and Faeth, G. M. *Combust. Flame* 40:13–28 (1981).
4. Allison, C. B., and Faeth, G. M. *AIAA J.* 13:1287–1294 (1975).
5. Lazar, R. S., and Faeth, G. M., in *Thirteenth Symposium (International) on Combustion*. The Combustion Institute, Pittsburgh, 1971, p. 743.
6. Canada, G. S., and Faeth, G. M., in *Fourteenth Symposium (International) on Combustion*. The Combustion Institute, Pittsburgh, 1973, p. 1345.
7. Canada, G. S., and Faeth, G. M., in *Fifteenth Symposium (International) on Combustion*. The Combustion Institute, Pittsburgh, 1975, p. 419.
8. Prausnitz, J. M., and Chueh, P. L. *Computer Calculations for High-Pressure Vapor-Liquid Equilibria*. Prentice-Hall, Englewood Cliffs, 1968.
9. McBratney, W. F., "Windowed Chamber Investigation of the Burning Rate of Liquid Monopropellants for Guns," report no. ARBRL-MR-03018, Ballistic Research Laboratory, Aberdeen Proving Ground, 1980.
10. McBratney, W. F., "Burning Rate Data, LGP 1845," report no. ARBRL-MR-03128, Ballistic Research Laboratory, Aberdeen Proving Ground, 1981.
11. Starling, K. *Fluid Thermodynamic Properties of Light Petroleum Systems*. Gulf Publishing Co., Houston, 1973.
12. *Technical Data Book - Petroleum Refining* American Petroleum Institute, Washington, Third Ed., Vol. 2, p. 8–55, 1976.

13. Faeth, G. M. *Prog. Energy Combust. Sci.* 3:191–224 (1977); 9:1–76 (1983).
14. Faeth, G. M. *Combust. Flame* 8:167–174 (1967); 12:411–416 (1968).
15. Gordon, S., and McBride, B. J., "Computer Program for Calculation of Complex Chemical Equilibrium Compositions, Rocket Performance, Incident and Reflected Shocks, and Chapman-Jouguet Detonations," report no. NASA SP-273, NASA, Washington, 1971.
16. Dunn, P. D., and Reay, D. A. *Heat Pipes*. Pergamon Press, Oxford, 1976, p. 72.
17. Prausnitz, J. M., Eckert, C. A., Orye, R. V., and O'Connell, J. P. *Computer Calculations for Multi-Component Vapor-Liquid Equilibria*. Prentice-Hall, Englewood Cliffs, 1967, p. 18.
18. Reid, R. C., Prausnitz, J. M., and Sherwood, T. K. *The Properties of Gases and Liquids*. McGraw-Hill, New York, third ed., 1977.
19. Stull, D. R., and Prophet, H. *JANAF Thermochemical Tables*, National Bureau of Standards, Vol. NSRDS-NBS 37, second ed., Washington, 1971.
20. Lyderson, A. L., Greenkorn, R. A., and Hougen, O. A. "Generalized Thermodynamic Properties of Pure Liquids," College of Engineering report no. 4, University of Wisconsin, Madison, 1955.
21. Lyderson, A. L. "Estimation of Critical Properties of Organic Compounds," College of Engineering report no. 3, University of Wisconsin, Madison, 1955.
22. Lee, B. T., and Kesler, M. G. *AIChE J.* 21:510–527 (1975).
23. Verma, K. K., and Doraiswamy, L. K. *Ind. Engr. Chem. Fund.* 4:389–396 (1965).
24. Rihani, D. N. and Doraiswamy, L. K. *Ind. Engr. Chem. Fund.* 4:17–21 (1965).
25. Svehla, R. A. "Estimated Viscosities and Thermal Conductivities of Gases at High Temperatures," technical report no. R-132, NASA, Washington, 1962.
26. Reichenberg, D., DSC report no. 11, National Physical Laboratory, Teddington, England, 1971; *AIChE J.* 19:854–865 (1973); *AIChE J.* 21:181–183 (1975).
27. Wassiljewa, A. *Physik Z.* 5:737–742 (1904).
28. Lindsay, A. L., and Bromley, L. A. *Ind. Engr. Chem.* 42:1508–1511 (1950).
29. Stiel, L. I., and Thodos, G. *AIChE J.* 10:26–30 (1964).
30. Fuller, E. N., and Giddings, J. C. *J. Gas Chromatogr.* 3:222–227 (1965).
31. Fuller, E. N., Schettler, P. D., and Giddings, J. C. *Ind. Engr. Chem.* 58:18–27 (1966).
32. Dawson, R., Khovny, F., and Kobayashi, R. *AIChE J.* 16:725–729 (1970).

Received 21 September 1987; revised 18 February 1988

A.2 "Analysis of Combusting High-Pressure Monopropellant Sprays," by T.-W. Lee, J.P. Gore, G.M. Faeth and A. Birk; Combust. Sci. Tech., Vol. 57, No. 4-6, pp. 95-112, 1988.

Combust. Sci. and Tech., 1988, Vol. 57, pp. 95–112
Reprints available directly from the publisher
Photocopying permitted by license only

Analysis of Combusting High-Pressure Monopropellant Sprays

T. -W. LEE, J. P. GORE and G. M. FAETH *Department of Aerospace Engineering, The University of Michigan, Ann Arbor, MI 48109-2140*

A. BIRK *U.S. Army Ballistic Research Laboratory, Aberdeen Proving Ground, MD 21005-5066*

(Received May 1, 1987; in final form August 3, 1987)

Abstract—A simplified analysis of monopropellant spray combustion was developed, based on the locally-homogeneous-flow approximation of multiphase flow theory and the thin-flame approximation of turbulent premixed flame theory. The performance of the analysis was evaluated using shadowgraphs of spray flames for a hydroxyl ammonium nitrate (HAN)-based liquid monopropellant at ambient pressures of 6–8 MPa. Predictions showed that these spray flames are very sensitive to the degree of flow development at the injector exit, with fully-developed turbulent flows requiring significantly smaller combustion volumes than slug flows having low initial turbulence levels. There was encouraging agreement between predictions and measurements; however, uncertainties concerning injector exit conditions for the experiments precluded definitive assessment of the analysis

INTRODUCTION

Combusting monopropellant sprays have applications for throttlable thrustors, underwater propulsion systems, and regenerative liquid-propellant guns. Monopropellant spray flames are also an important fundamental problem of combustion science, as the premixed counterpart of the spray diffusion flame. Motivated by these considerations, the structure of combusting monopropellant sprays was examined during the present investigation. The main objective was to develop a simplified analysis of the process, and to evaluate predictions by comparison with measurements.

Theories of combusting monopropellant sprays are not highly developed; therefore, the present analysis was simplified. Multiphase effects were treated using the locally-homogeneous-flow (LHF) approximation of multiphase flow theory. The LHF approximation implies that relative velocities between the phases are negligible (negligible slip), yielding a single-fluid formulation which is independent of the specifics of spray breakup and initial drop-size distributions. The LHF approach generally provides useful qualitative information concerning spray structure (Faeth, 1983, 1987; Mao *et al.*, 1980, 1981; Shearer *et al.*, 1979). Additionally, Wu *et al.* (1983, 1984) report encouraging quantitative performance of LHF analysis for pressure-atomized injection at elevated pressures—conditions which are most often encountered for combusting monopropellant sprays. Finally, recent work in this laboratory (Ruff *et al.*, 1988), suggests that LHF analysis is effective for near-injector conditions in the atomization breakup regime, based on predictions and measurements of the properties of pressure-atomized water sprays in still air at normal temperature and pressure.

Address correspondence to: G. M. Faeth, 217 Aerospace Engineering Building, The University of Michigan, Ann Arbor, MI 48109-2140. Telephone: (313) 764-7202.

A second major assumption of the analysis involved use of the laminar flamelet concept of premixed turbulent single-phase combustion, proposed by Bray (1978, 1980). Liquid monopropellants generally have relatively high burning rates at elevated pressure (McBratney, 1980, 1981), which implies relatively thin reaction zones; therefore, the limit of an infinitely-thin flame was used to provide a simple formulation with minimal empiricism (Bray, 1978, 1980).

The performance of the analysis was evaluated using measurements of pressure atomized sprays from a round injector passage, obtained with an apparatus developed by Birk and Reeves (1987). The measurements consisted of shadowgraphs of spray flames produced by a hydroxl-ammonium-nitrate (HAN)-based liquid monopropellant at ambient pressures of 6–8 MPa. The data was reduced to yield mean and fluctuating liquid volume fractions as a function of position, for comparison with predictions.

Experimental and theoretical methods are described in the next two sections of the paper. Predictions of spray structure are then compared with measurements. The paper concludes with discussion of additional theoretical findings for conditions where test results are not available.

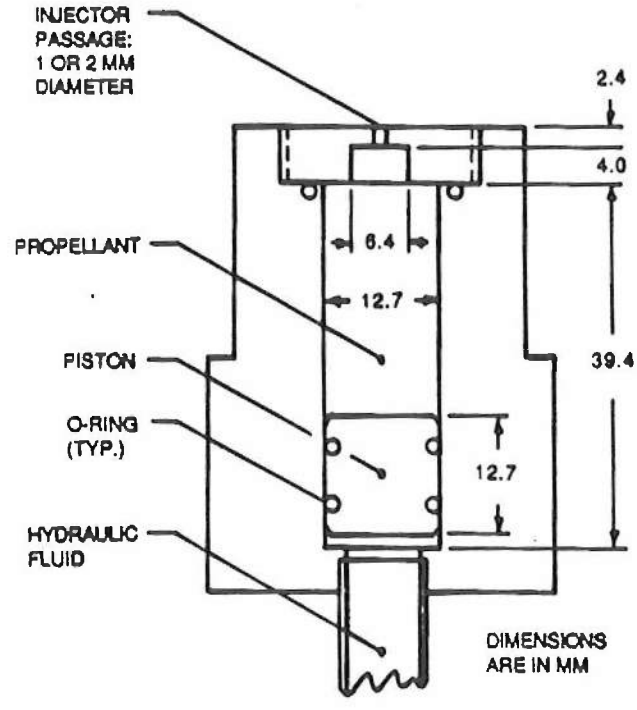

FIGURE 1 Injector assembly.

EXPERIMENTAL METHODS

Experimental methods will be only briefly described, more details are provided by Birk and Reeves (1987). The experiments were carried out within a windowed cylindrical test chamber having an inside diameter of 57 mm and an interior length of 406 mm, yielding a volume of roughly 1050 cc. The axis of the chamber was vertical, with the pressure-atomized spray injected vertically upward along the axis. The propellant was injected into a hot precombusted gas mixture, in order to simulate injection into an adiabatic combustion environment.

The arrangement of the injector assembly is illustrated in Figure 1. The propellant was pressurized and fed through the injector passage using a hydraulically driven piston arrangement, with the hydraulic system ultimately actuated by a pneumatic system (Birk and Reeves, 1987). The injector passages were round (1 and 2 mm diameter), and were 2.4 mm long, yielding passage length-to-diameter ratios of 1.2 and 2.4. Due to steps in the propellant feed system and effects of the vena-contracta at the passage inlet, however, it is likely that the effective length-to-diameter ratios, as a measure of flow development at the passage exit, are not very well defined and are probably somewhat larger: they are taken to be in the range 2–10 in the following. The outputs of pressure transducers (Kistler 601B) were recorded to provide the test chamber pressure and the pressure differential across the injector passage.

The experiments were limited to the HAN-based monopropellant, LGP 1846, see Table I for propellant properties. The hot gas within the chamber, used to simulate an adiabatic combustion environment, was produced by spark igniting a combustible gas mixture, initially at 1 MPa, having the following composition (by volume): hydrogen, 20 percent; oxygen, 10 percent; and argon, 70 percent. Argon served as a diluent to prevent detonation of the gas mixture. Due to the relatively large surface-to-volume ratio of the test chamber, heat losses from the burning gas mixture were significant, yielding gas temperatures and pressures of roughly 1800 K and 5.5 MPa after combustion. The temperature level was roughly 10 percent below estimated adiabatic flame temperatures for the propellant (see Table I), providing a resonable approximation adiabatic combustion conditions. The

TABLE I
Properties of LGP 1846[a]

Pressure (MPa)	1	10	100
Reactant Properties			
Density (kg/m^3)	1430	1432	1454
Product Properties			
Density (kg/m^3)	1.36	13.5	134.7
Temperature (K)	2027	2039	2045
Mass Fractions (%)[b]			
Water Vapor	53.8	53.9	54.0
Carbon Dioxide	24.3	24.6	24.7
Nitrogen	21.0	21.0	21.1

[a]Adiabatic constant pressure combustion with the reactant at 298.15 K. Reactant composition (% by mass): hydroxyl-ammonium nitrate (HAN), 60.8; triethanol-ammonium nitrate (TEAN), 19.2; and water, 20.0.

[b]Major species only. Minor species include CO, H_2, NO, OH and O_2.

chamber pressure increased as the propellant burned: present measurements were obtained at chamber pressures of 6–8 MPa. The density of the burned gas mixture is greater than the density of the adiabatic combustion products of the propellant, due to the lower temperature and the presence of argon; therefore, the ambient density of the experiments at 6–8 MPa, approximates ambient densities for adiabatic propellant combustion at pressures of 10–13 MPa.

The combusting spray was observed using motion picture shadowgraphs. A Photec camera was used, with Kodak VNF 7240 film. Typical film speeds were 5000 frames per second. Backlighting was provided by flash sources synchronized with the camera. Maximum flash durations were less than 2 μs; therefore, the image of the spray was effectively stopped on the films.

A typical spray shadowgraph is illustrated in Figure 2. The spray or liquid-containing region appears as the dark irregular zone near the center of the photograph. The boundaries of the spray are reasonably well-defined. The shadowgraphs were unusually clear in comparison to combusting hydrocarbon sprays at comparable pressures (Mao *et al.*, 1981). Factors responsible for this behavior include the absence of particulates, like soot, in the monopropellant combustion products; and the relatively uniform temperature of the combustion products, which minimizes sharp density gradients that cause irregular shadowgraph patterns. The dark zones are wispy, suggesting that the liquid behaves somewhat like tracer particles in the outer region of the liquid-containing region that can be seen on the photographs. This appearance tends to support use of the LHF approximation as a point of departure for analysis.

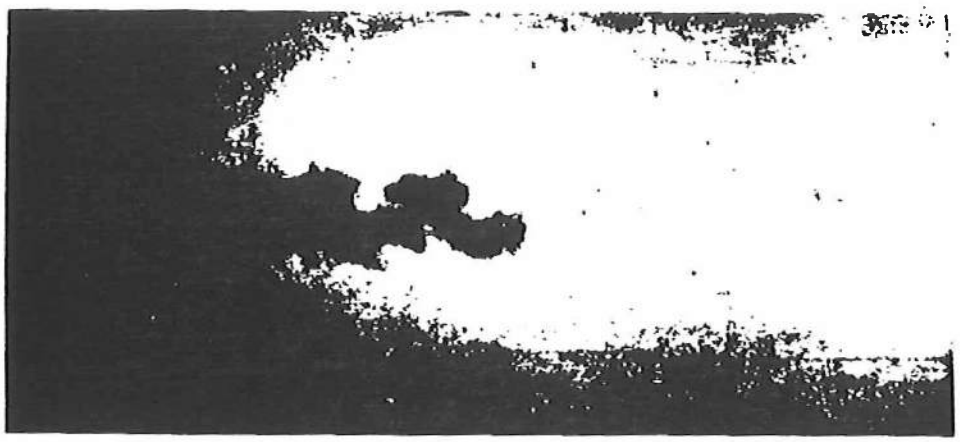

FIGURE 2 Photograph of combusting monopropellant spray (1 mm diameter injector, 6–8 MPa).

The motion picture films were analyzed to yield time-averaged mean and fluctuating liquid volume fractions. Maintaining the thin-flame concept, each picture frame was analyzed, assigning dark zones to unburned liquid reactant and light zones to gaseous combustion products. For each test, 15–25 frames were available for analysis during the steady flow portion of the spray combustion process. Separating dark and light zones on the film was somewhat subjective; and since the measurements correspond to line-of-sight projections, they are biased downstream and radially outward from correct point measurements of mean and

fluctuating liquid volume fractions. These effects were not quantified, but are not felt to be large in comparison to other experimental uncertainties, as will be seen subsequently.

Measurements to be considered were obtained from three tests, denoted tests 2, 4 and 7 in the following. A 1.0 mm diameter injector was used during test 2, while a 2.0 mm diameter injector was used during tests 4 and 7. In the portions of the films that were analyzed, liquid velocities were in the range 45–55 m/s for both injectors. Based on liquid properties summarized by Birk and Reeves (1987), this yields injector Reynolds numbers in the range $1-2\times10^4$ and Ohnesorge numbers of 0.023 (test 2) and 0.016 (tests 4 and 7). The Reynolds numbers are sufficiently high to insure reasonably turbulent flow, while the Reynolds number/Ohnesorge number combinations suggest that operation for all tests was well within the atomization breakup regime (Miesse, 1955; Ranz, 1958; Ruff *et al.*, 1988).

THEORETICAL METHODS

The analysis involves the LHF and thin-flame approximations, with turbulent mixing treated using a Favre-average turbulence model along the lines of Bray (1978, 1980) and Bilger (1976). This approach provides a useful limit and is consistent in the sense that both multiphase and chemical reaction phenomena are assumed to be controlled by turbulent mixing, vastly reducing the empiricism and amount of input data, *e.g.*, initial drop size and velocity distributions, chemical kinetic properties,. etc., needed to define the problem (Bray, 1978, 1980; Faeth, 1983, 1987). As noted earlier, the LHF approach has proven to be effective for providing at least qualitative information on the structure of pressure-atomized sprays at high pressures (Faeth, 1983, 1987; Mao *et al.*, 1980, 1981; Shearer *et al.*, 1979; and Wu *et al.*, 1983, 1984); while more recent work (Ruff *et al.*, 1988) suggests that LHF analysis, similar to the approach used here, has potential for useful quantitative predictions for the near-injector region of turbulent pressure-atomized sprays in the atomization breakup regime—conditions which are met for present tests. Furthermore, the approach does not seem unreasonable in view of the wispy, gas-like, appearance of the spray-containing region seen on the spray shadowgraphs, see Figure 2.

High pressure conditions, which are generally of interest for monopropellant sprays, are favorable for application of the thin-flame approximation. Strand burning rate measurements reported by McBratney (1980, 1981) for HAN-based monopropellants suggest liquid regression rates of 20 mm/s at pressures on the order of 10 MPa. Using typical transport properties, this implies a characteristic flame thickness on the order of 1 μm (representative of both the liquid-phase preheat zone and the distance from the liquid surface to the reaction zone in the gas phase). The liquid-containing regions of the sprays had characteristic dimensions on the order of 10–100 mm, see Figure 2; therefore, the probability of a typical spatial position being within the reaction zone is quite small, justifying the thin-flame approximation. As noted earlier, the rather sharp distinction between liquid and gas, and the absence of refractive index variations in the gas-containing regions, based on photographs like Figure 2, are also supportive of this hypothesis.

It seems probable that the main structural features of turbulent pressure-atomized sprays in the atomization breakup regime are generally similar for both noncombusting and combusting monopropellant sprays. Based on what is known about noncombusting sprays, the flow should involve an all-liquid core which can

extend an appreciable distance from the injector, surrounded by a growing two-phase shear layer which originates very close to the exit of the injector (Chehroudi *et al.*, 1985; Hiroyasu *et al.*, 1982; Ruff *et al.*, 1988; Wu *et al.*, 1983, 1984). The shear layer contains irregularly-shaped liquid elements, ligaments, and drops. Upon merging the LHF and thin-flame approximations, a thin flame is assumed to cover all these surfaces: the all-liquid core, the irregularly-shaped elements, the ligaments, and the drops. Except for very near the liquid surface, the liquid is at the same state as in the injector: while beyond the outer edge of the thin flame, the gas has uniform properties equivalent to adiabatic flame conditions. Locally, the relative velocities of the phases (slip) is small.

This picture is analogous in many ways to a gaseous premixed flame in the multiple reaction sheet regime defined by Williams (1985), except that breakup of the liquid yields well-defined islands of the reactant, rather than high localized values of flame stretch in a single-phase flow. Effects of flame curvature and high flame stretch, analogous to gaseous flames, are still present in the spray, *e.g.*, reaction in the immediate vicinity of small drops and drops having very high relative velocities may be extinguished. However, due to the small flame thickness for present conditions, drops having no slip will be very small (*ca.* 1 μm in diameter) when they extinguish and will not have much effect on the mixing properties of the flow, while large slip velocities are precluded under the LHF approximation.

Other major assumptions of the analysis are as follows: (1) steady (in the mean) axisymmetric flow with no swirl; (2) low Mach number flow with negligible potential and kinetic energy changes, and negligible viscous dissipation, in the mean; (3) boundary-layer approximations apply; (4) negligible effects of radiant energy exchange; (5) equal exchange coefficients of all species and heat; and (6) high Reynolds numbers, so that laminar transport is negligible in comparison to turbulent transport. Most of these assumptions are satisfied by the conditions of present experiments. In particular, the boundary layer approximations are justified in view of the large aspect ratio of the liquid-containing region, see Figure 2. The small dimensions of the liquid-containing region and high near-injector velocities imply low radiation numbers and thus negligible effects of radiant energy exchange. The assumption of equal exchange coefficients of all species and heat is always suspect under the LHF approximation, since rates of diffusion of even small drops are small (Faeth, 1983, 1987). However, laminar exchange is not likely to be very important at Reynolds numbers on the order of 10^4 and this approximation seems no worse than other aspects of the LHF and thin-flame limits.

Under these assumptions, Bray (1978, 1980) shows that flow properties can be found by solving governing equations for conservation of mass, momentum and the reaction progress variable, in conjunction with second order turbulence model equations for turbulence kinetic energy and its rate of dissipation. The governing equations then take the following general form (Bray, 1980; Bilger, 1976; Jeng and Faeth, 1984):

$$\frac{\partial}{\partial x}(\bar{\rho}\tilde{u}\tilde{\phi}) + \frac{1}{r}\frac{\partial}{\partial r}(r\bar{\rho}\tilde{v}\tilde{\phi}) = \frac{1}{r}\frac{\partial}{\partial r}\left(r\frac{\mu_t}{\sigma_\phi}\frac{\partial\tilde{\phi}}{\partial r}\right) + S_\phi, \tag{1}$$

where $\phi = 1$ (for conservation of mass), $\tilde{u}$, $\tilde{c}$, k and ε. The source terms, S_ϕ, appearing in Eq. (1) are summarized in Table II, along with the empirical constants used during present computations. The turbulent visosity was calculated as usual:

$$\mu_t = C_\mu \bar{\rho} k^2/\varepsilon. \tag{2}$$

The boundary conditions for Eq. (1) involve symmetry at the axis, and a constant-property ambient environment, *e.g.*:

$$r = 0, \frac{\partial \phi}{\partial r} = 0; \quad r \to \infty, \quad \phi = 0 (\text{for } \phi \neq \tilde{c}); \quad \tilde{c} = 1. \tag{3}$$

Except for C_μ, the empirical constants appearing in Table II are the same as past analysis of single- and multi-phase round jets in this laboratory (Faeth, 1983, 1987; Jeng and Faeth, 1984). These values were selected to match measurements for a variety of constant and variable density noncombusting single-phase round jets (Faeth, 1983; Jeng and Faeth, 1984). Values used, however, are not very different from those used during early work with k-ε turbulence models (Lockwood and Naguib, 1975).

TABLE II
Source terms in the governing equations

ϕ	S_ϕ					
1	0					
$\tilde{u}$	0					
$\tilde{c}$	$C_r \bar{\rho} \tilde{c}(1 - \tilde{c})\varepsilon/k$					
k	$\mu_t (\partial \tilde{w}/\partial r)^2 - \bar{\rho}\varepsilon$					
ε	$(C_{\varepsilon 1}\mu_t (\partial \tilde{w}/\partial r)^2 - C_{\varepsilon 2}\bar{\rho}\varepsilon)\varepsilon/k$					
C_μ	$C_{\varepsilon 1}$	$C_{\varepsilon 2}$	C_r	σ_k	σ_ε	σ_c
0.09	1.44	1.87	1.87	1.0	1.3	0.7

Values of C_r depend on the shape assumed for the reacting-mode probability density function and several turbulence modeling constants, as discussed by Bray (1980). Considering various probability density functions and estimates of empirical constants from Bray (1980), Spalding (1971), Lockwood and Naguib (1975) and Jeng and Faeth (1984), yielded values of C_r of roughly two. Thus, $C_r = C_{\varepsilon 2} = 1.87$ was adopted during present calculations, as a baseline. The influence of the value of C_r on predictions was evaluated by parameter sensitivity calculations, to be discussed later.

It was pointed out earlier that injector exit conditions were not measured and that the flow involved complicated internal injector passages which precluded accurate estimates of exit conditions. Furthermore, computations indicated that spray properties were strongly inflenced by injector exit conditions. In order to highlight this effect, a range of initial conditions was studied. This included limiting conditions of slug flow, with a uniform exit velocity and low turbulence intensities, and fully-developed pipe flow. In addition, calculations were carried out for a range of length-to-diameter ratios of the injector passage, assuming a clean entry with no vena contracta. Except for slug flow, profiles of mean velocities and turbulence quantities for these conditions were obtained from Hinze (1959) and

Schlichting (1979), given the flow rate and the diameter of the passage. The initial shear layer for the slug flow calculations was assumed to have a thickness of 0.1 percent of the passage diameter, while properties in this layer were specified similar to past work (Faeth, 1983).

Under the thin-flame approximation, the process only has two scalar states, namely, unburned reactant liquid and completely reacted gaseous products of adiabatic combustion. The properties of these states are summarized in Table I for a range of pressures. Density is the only liquid (reactant) property needed for the calculations: the values given in Table I allow for liquid compressibility and were provided by Friedman (1986). Combustion-product properties were found by assuming thermodynamic equilibrium for an adiabatic constant-pressure combustion process at the stated pressure, using the Gordon and McBride (1971) computer code.

The thin-flame approximation only admits a double-delta function probability density function for the reaction progress variable. Then, mean and fluctuating scalar properties are functions of $\tilde{c}$, which is known from the solution of Eq. (1). The functions for various scalar properties are as follows (Bray, 1978, 1980):

$$\tilde{\phi} = \phi_0(1-\tilde{c}) + \phi_\infty \tilde{c}, \tag{4}$$

$$\tilde{\phi} = (\phi_0 \rho_\infty (1-\tilde{c}) + \phi_\infty \rho_0 \tilde{c})/(\rho_\infty (1-\tilde{c}) + \rho_0 \tilde{c}), \tag{5}$$

$$\widetilde{\phi''^2} = (\phi_0 - \phi_\infty)^2 \tilde{c}(1-\tilde{c}), \tag{6}$$

$$\widetilde{\phi''^2} = \tilde{\rho}^2 (\phi_0 - \phi_\infty)^2 \tilde{c}(1-\tilde{c})/(\rho_0 \rho_\infty), \tag{7}$$

where $\tilde{\rho}$, needed to solve Eq. (1), can be found by setting $\phi = \rho$ in Eq. (5). Time-averaged mean and fluctuating liquid volume fractions are of particular interest, since these quantities were provided by the experiments. The equations for these properties are as follows:

$$\tilde{\alpha}_f = \tilde{\rho}(1-\tilde{c})/\rho_0, \tag{8}$$

$$\widetilde{\alpha_f''^2} = \tilde{\rho}^2 \tilde{c}(1-\tilde{c})/(\rho_0 \rho_\infty). \tag{9}$$

The calculations were performed using a GENMIX algorithm due to Spalding (1978). The large density variations in the flow created problems of stability and numerical accuracy, requiring a much finer grid than is usually needed for single-phase flows. Results reported here involved 360 crosstream grid nodes; with streamwise step sizes limited to 0.3 percent of the current flow width. Doubling the number of grid nodes, in both the crosstream and streamwise directions, changed the predictions by less than 0.7 percent; therefore, the numerical accuracy far exceeds expected uncertainties of other aspects of the analysis.

RESULTS AND DISCUSSION

Evaluation of Predictions

Predictions and measurements of time-averaged liquid volume fractions along the spray axis are plotted as a function of normalized distance from the injector exit in

Figure 3. The measurements for both injector diameters are very similar when plotted in this manner. By itself, this finding suggests a mixing-controlled process for the conditions of the experiments. Similarly, predictions are also relatively insensitive to changes of injector diameters and Reynolds numbers over the range of the tests; therefore, only a single line is shown for each injector exit condition. As noted earlier, predictions were carried out for a pressure of 10 MPa, in order to match the ambient density of the experiments at 6–8 MPa. However, later results will show that the effect of pressure on the predicitions for this range of conditions is small; therefore, using pressures of 6–8 MPa for the calculations would not materially influence the results.

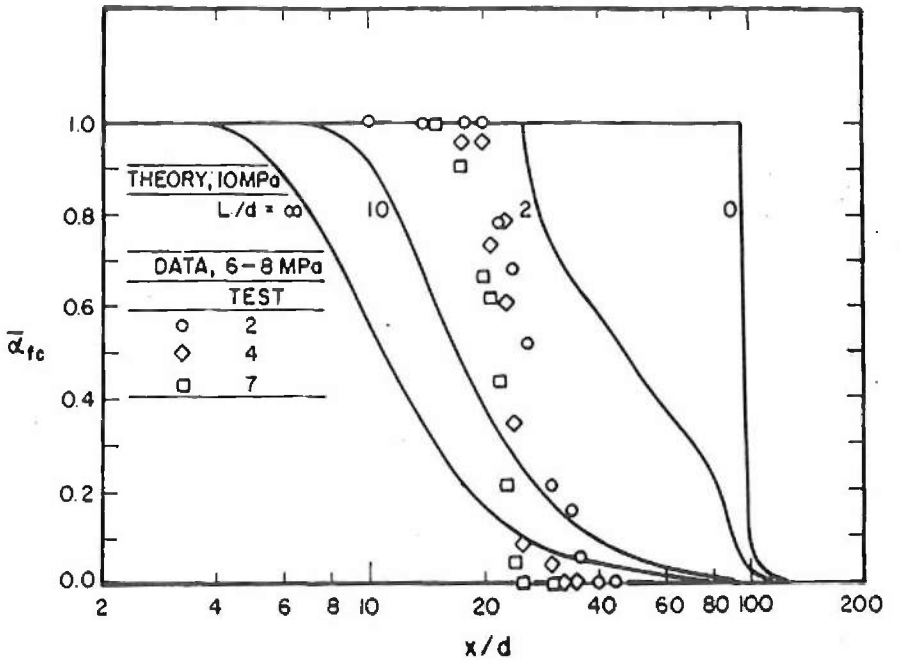

FIGURE 3 Predicted and measured variation of $\bar{\alpha}$, along axis.

In contrast to other variables, the degree of flow development at the injector exit has a strong influence on the predictions illustrated in Figure 3. For example, if the characteristic length of the combustion process is represented by the condition where $\bar{\alpha}_{fc} = 0.1$, this length is roughly five times longer for slug flow ($L/d = 0$) than for fully-developed flow ($L/d = \infty$). Due to uncertainties concerning experimental injector exit conditions, this large effect precludes definitive assessment of predictions, or any attempt to optimize C_r. Nevertheless, estimates of the properties of the test injectors suggest an effective L/d in the range 2–10; therefore, it is encouraging that predictions at these limits generally bound the measurements. The slopes of predictions and measurements are somewhat different, however, in the region where $\bar{\alpha}_{fc}$ decreases most prominently. This may be due to line-of-sight biasing and difficulties in distinguishing low concentrations of gas or liquid from

the other phase on the photographs. Effects of initial flow properties may also be a factor. Further study, and tests with better-defined injector flow conditions, required to quantify these effects.

The strong effect of initial conditions on the predicted flow properties illustrated in Figure 3 is perhaps not surprising. It is widely recognized that changes in initial conditions for single-phase turbulent jets can significantly influence the development of the flow near the injector (typically, $x/d < 20$–30). The large density of the liquid, in comparison to the gas, in a pressure-atomized spray, clearly provides the potential for carrying effects of conditions at the injector exit farther into the flow field.

Present findings concerning the strong effect of initial flow development on the properties of combusting monopropellant sprays are also supported by recent measurements and analysis of noncombusting pressure-atomized sprays due to Ruff *et al.* (1987). Their measurements show that fully-developed flow at the injector exit causes much faster mixing than slug flow, similar to the predicted trends illustrated in Figure 3. Furthermore, LHF analysis, similar to the present approach but naturally not considering premixed combustion, provided reasonably-good estimates of the effect of flow development in the injector exit for operation in the atomization breakup regime—the regime of interest here.

Direct experimental proof of effects of initial flow development on the mixing properties of combusting monopropellant sprays is clearly needed, but the preceding discussion indicates that there is some evidence that the predicted behavior is illustrated in Figure 3 is real. This has important practical implications, since the findings suggest that fully-developed injector flows can substantially reduce combustion volumes. This can be used to provide either a more-compact combustion chamber, or to reduce tendencies for combustion instabilities by minimizing the amount of unreacted propellant within the combustion chamber at any instant.

Predicted and measured time-averaged fluctuating liquid volume fractions along the axis of the sprays are illustrated in Figure 4. Both predictions and measurements reach a maximum value of $\overline{\alpha}'_{fc} = 0.5$ at $\bar{\alpha}_{fc} = 0.5$, which is a fundamental requirement of an intermittent (on/off) property at the thin-flame limit. Predictions and measurements were not influenced significantly by different injector sizes and Reynolds numbers, similar to findings discussed in connection with Figure 3. As before, predictions for $L/d = 2$ and 10 tend to bound the measurements. However, the measured lengths of the $\overline{\alpha}'_{fc}$ profiles in the streamwise direction are narrower than predicted, possibly due to line-of-sight and photographic-contrast biasing, as discussed earlier.

Radial profiles of predicted and measured time-averaged mean and fluctuating liquid volume fractions are illustrated in Figures 5 and 6. The results are plotted as a function of r/x, the similarity variable for turbulent jets, at various distance (x/d) from the injector. The experimental scatter of the tests is greater for the radial profiles than the results plotted in Figures 3 and 4 for properties along the axis, particularly near the end of the liquid-containing region ($x/d = 20$) where the streamwise variation of flow properties is quite large, see Figure 3. Nevertheless, effects of injector diameter and Reynolds number are seen to crudely scale as a mixing-controlled process.

Predictions are illustrated in Figures 5 and 6 for the fully-developed and slug flow limits. The predictions scale in the same way as the measurements; however, the measured profiles are broader than either of the limiting predictions, even though LHF predictions generally overestimate the width of the liquid-containing

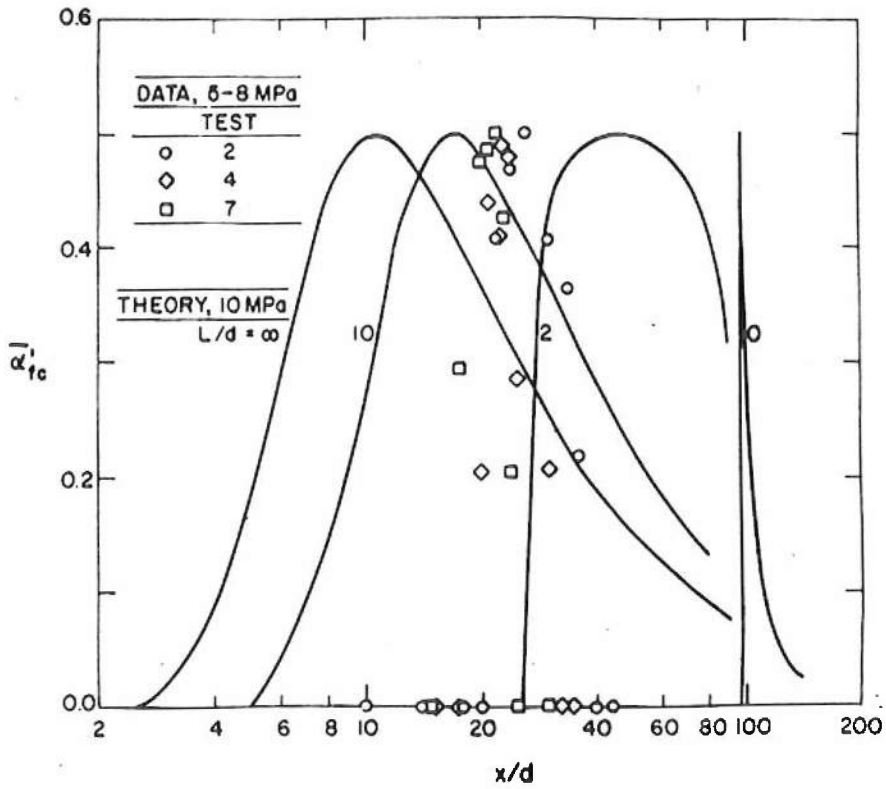

FIGURE 4 Predicted and measured variation of $\overline{\alpha'}$ along axis.

region (Faeth, 1983, 1987; Mao *et al.*, 1980, 1981; Ruff *et al.*, 1988). There are several possible explanations for this behavior. First of all, the predictions shown are not expected to properly bound measurements in the radial direction, based on the results illustrated in Figure 3. Slug flow mixes much more slowly than measured, accounting for its relatively small spread in the radial direction in comparison to measurements. Fully-developed flow mixes much more rapidly than measured, and volume fractions predicted for fully-developed flow are much lower than measured values everywhere, particularly for the results illustrated in Figure 5. Thus use of intermediate flow development conditions, *e.g.*, $L/d = 2$ or 10, yields better quantitative agreement with measurements, although such matching was not pursued since injector exit conditions were uncertain in any event. Next, there was evidence of unstable flapping of the jet as a whole. Such flapping does not have a significant effect on properties in the streamwise direction, but does increase the apparent radial spread of the flow through a mechanism that is not a direct effect of turbulence. Finally, somewhat broadened measured profiles are expected, due to line-of-sight and photographic-contrast biasing, as noted earlier. In view of these considerations, the order-of-magnitude and the trends of the predictions are reasonable. However, a wider range of experimental conditions with improved control of initial conditions are needed for a more definitive evaluation of the present analysis

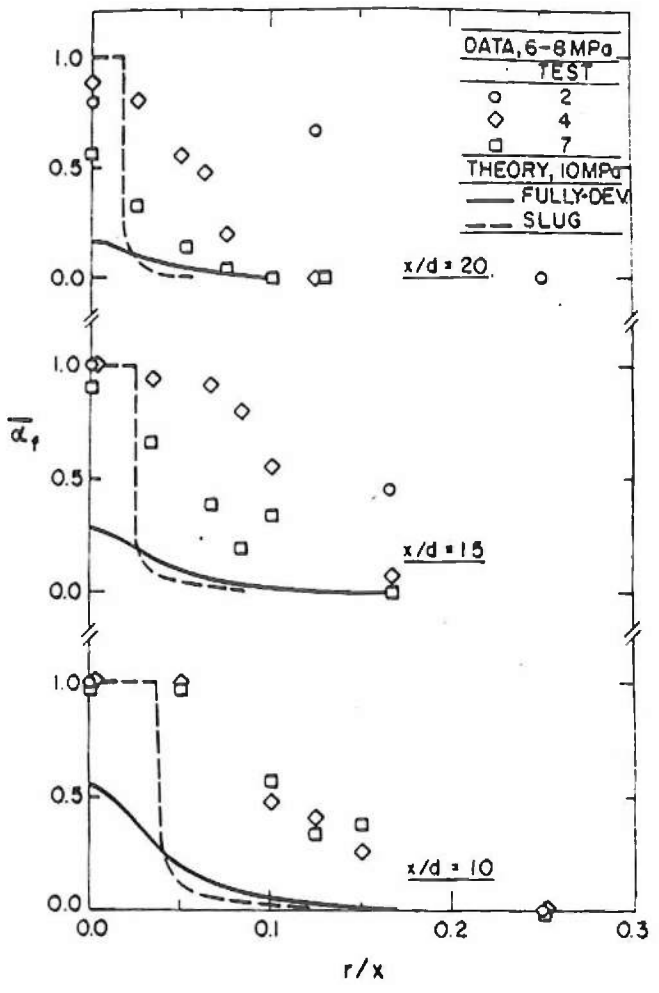

FIGURE 5 Predicted and measured radial variation of $\bar{\alpha}_f$.

Additional Predictions

Since predictions were at least in qualitative agreement with the measurements, the analysis was exploited to examine some of the general properties of monopropellant sprays using the HAN-based propellant. The influence of ambient pressure and the state of flow development at the injector exit can be seen from the results illustrated in Figures 7 and 8. Predictions of $\overline{\alpha}_{fc}$ and $\dot{c}_c$ for combusting sprays are plotted at ambient pressures ranging from 10–400 MPa, which covers the range of pressures encountered for most applications of monopropellant spray flames.

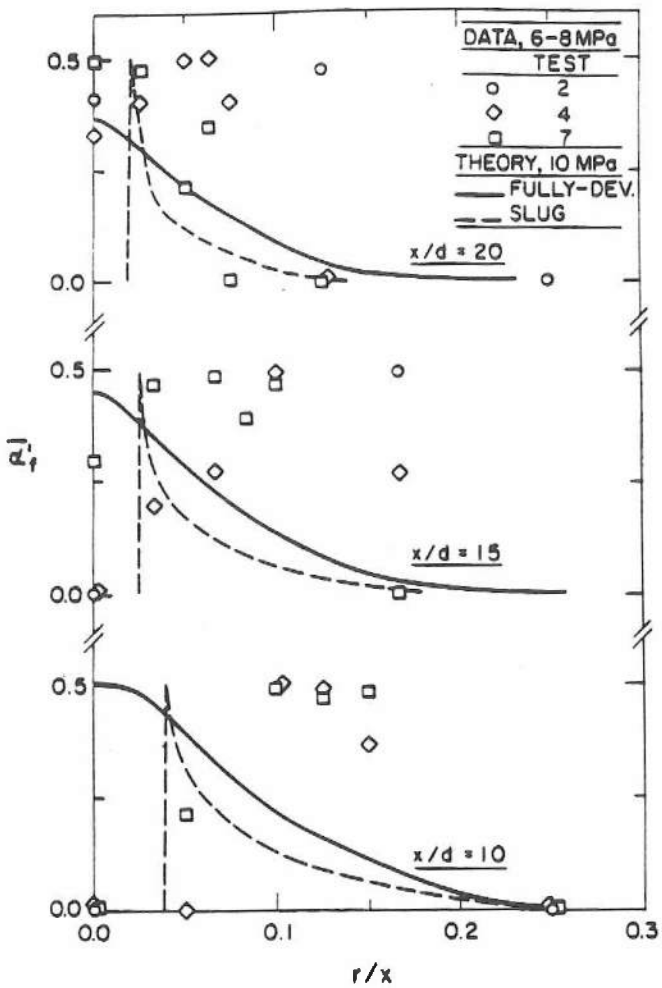

FIGURE 6 Predicted and measured radial variation of $\bar{\alpha}'_f$.

The findings for fully-developed injector exit conditions are illustrated in Figure 7. The Favre-averaged reaction progress variable, $\tilde{c}_c$, is a measure of the mass of propellant reacted in the flow. Pressure clearly has a strong influence on $\tilde{c}_c$, with the reaction nearing completion much closer to the injector at high pressures. This behaviour is caused by higher entrainment rates of the jet at higher pressures, which increases the rate of reaction at the turbulent mixing-controlled limit considered during the analysis. Existing measurements suggest that the relative entrainment rates of turbulent jets are proportional to $(\rho_{\infty}/\rho_{\infty})^{1/2}$ in the similarity region of the flow see Ricou and Spalding (1961) for single-phase jets, and Faeth (1983, 1987) for multiphase jets under the LHF approximation. Jet development in the near-injector region tends to modify this behavior for the results illustrated in Figure 7; however, the trend is crudely followed, *e.g.*, $\tilde{c}_c$ tends to approach unity at

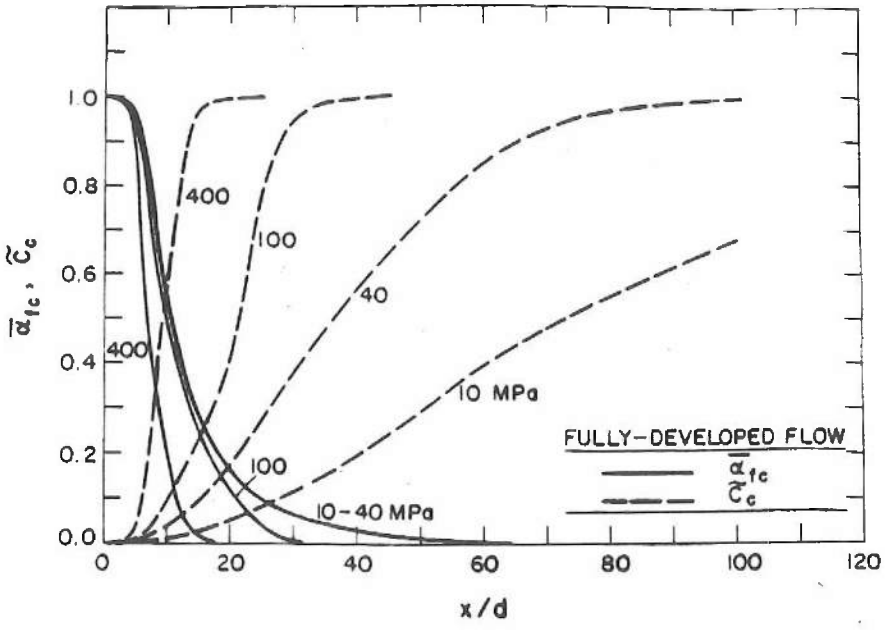

FIGURE 7 Mean scalar properties along axis at various pressures for fully-developed flow at injector exit.

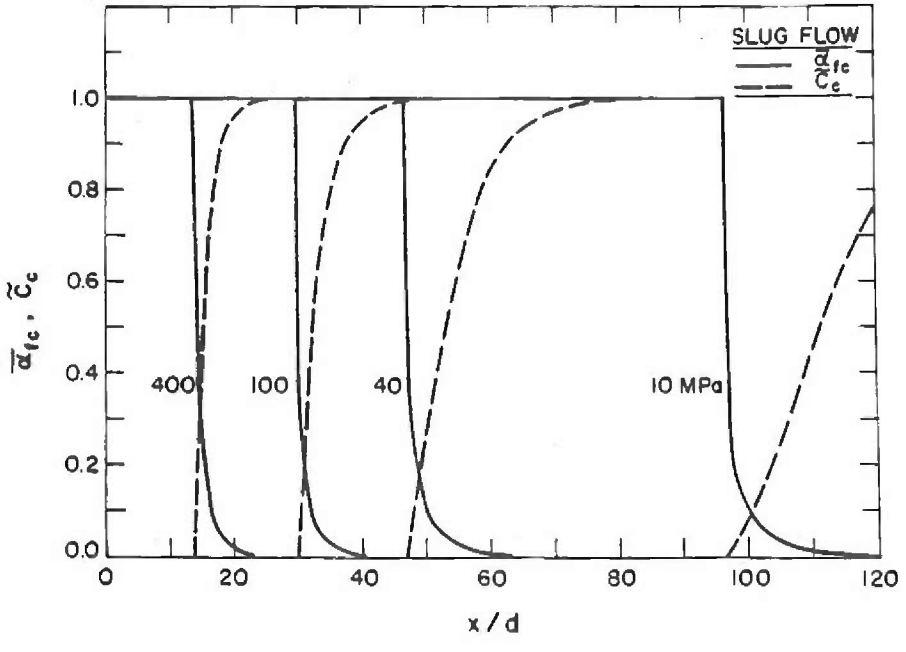

FIGURE 8 Mean scalar properties along axis at various pressures for slug flow at injector exit.

$x/d = 15$ and 60 for ambient pressures of 400 and 40 MPa. In contrast, the effect of pressure on $\bar{\alpha}_{fc}$ distributions is relatively small for pressures in the range 10–40 MPa. This is due to compensation of increased entrainment rates by reduced phase-density ratios as the pressure is increased.

The most obvious difference between the results for slug flow in Figure 8 and for fully-developed flow in Figure 7 is the dominating effect of an extended all-liquid potential core for slug flow. Such all-liquid cores have been observed for pressure-atomized sprays by Hiroyasu *et al.* (1982), Chehroudi *et al.* (1985) and Ruff *et al.* (1988); therefore, this behavior is not unexpected. The presence of the core tends to delay the development of the flow, particularly at low pressures. However, in spite of the core, the penetration of the sprays, represented by $\bar{c}_c$ approaching unity, still tends to scale according to $(\rho_{lv}/\rho_\infty)^{1/2}$, similar to the entrainment properties of fully-developed jets. In contrast, the effect of pressure on $\bar{\alpha}_{fc}$ differs from results for fully developed flow, since the presence of the all-liquid core causes $\bar{\alpha}_{fc}$ to vary significantly with pressure over the whole range considered in Figure 8.

Predicted isochors (for $\bar{\alpha}_f = 0.01$, which is representative of minimum liquid volume fractions generally resolvable from photographs) are illustrated in Figure 9. Results are shown for fully-developed and slug flow initial conditions at pressures in the range 10–400 MPa. The plots are distorted to improve their readability, *e.g.*, the radial scale is expanded by a factor of ten in comparison to the streamwise scale. The liquid-containing region is relatively narrow in comparison to its length at all pressures, suggesting that use of the boundary-layer approximations is adequate for these flows. This is very helpful, since the turbulent premixed flame analysis has been most successful for boundary-layer flows (Bray, 1978, 1980). Increasing pressure acts to reduce the size of the region bounded by the $\bar{\alpha}_f = 0.01$ isochor; for both boundary conditions and all pressures. However, the effect of pressure on the variation of $\bar{\alpha}_{fc}$, at higher values of this parameter, is relatively small for fully-developed flow at pressures in the range of 10–40 MPa, as noted earlier, see Figure 7.

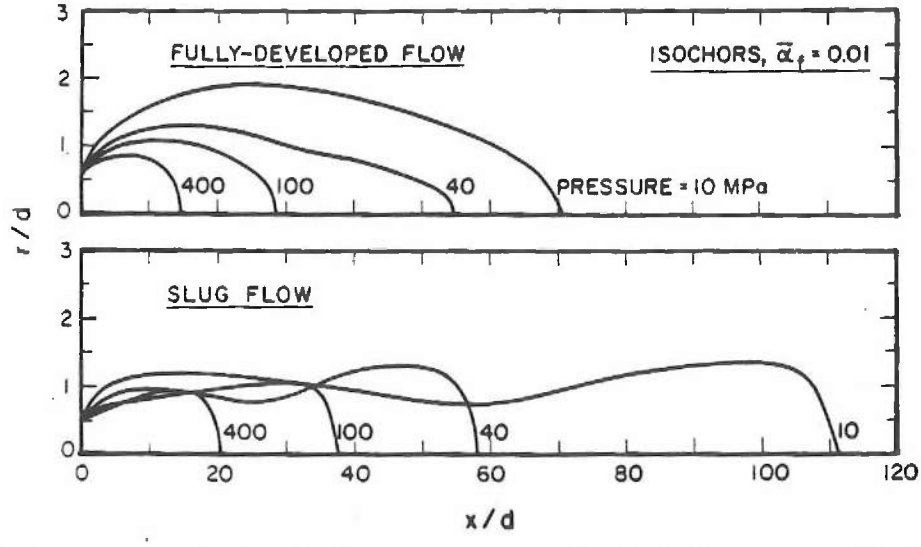

FIGURE 9 Predicted isochors ($\bar{\alpha}_f = 0.01$) at various pressures for fully-developed and slug flows at the injector exit.

Parameter Sensivitity

In addition to the extent of flow development at the injector exit, uncertainties concerning turbulence properties at the injector exit, and for other parameters of the analysis, contribute to uncertainties of predictions. This was evaluated by parametrically varying these quantities in order to observe their effect.

Table III is a summary of a portion of the parameter sensitivity results. The percent change of a given output parameter is tabulated for either a 50 percent reduction or a 100 percent increase of various input parameters, as indicated in the table. These results are for fully-developed flow at 10 MPa and $x/d = 20$. This position corresponds to conditions near the end of the liquid-containing region, see Figure 3. The most sensitive output parameter is $\tilde{\alpha}_{fc}$, with mean concentrations of unreacted liquid, $(1-\tilde{c})_c$, and the mean velocity ratio, $\tilde{u}_c/\tilde{u}_{c0}$, being relatively insensitive to the parameter variations. The effect of pressure is not very significant for any of the output variables at this pressure; however, this would not be the case at higher pressure levels, see Figures 7 and 8. The initial turbulence kinetic energy has the strongest influence on $\tilde{\alpha}_{fc}$, with a 50 percent reduction of k_0 causing almost a 300 percent increase of $\tilde{\alpha}_{fc}$. This highlights the importance of turbulent mixing, which increases with increasing k_0 in the near-injector region, for the mixing-controlled turbulent reaction limit considered in the calculations. Predictably, a factor-of-two reduction of C_τ causes roughly a 100 percent increase in $\tilde{\alpha}_{fc}$, implying that this constant can be calibrated using measurements, if the fundamental approximations of the analysis, like the effect of slip, are appropriate. The other parameters considered, ε_0 and Re, exhibit relatively small effects on output properties for these conditions.

TABLE III
Effect of parameter variations[a]

Input parameter	Output parameter (% increase)		
	$\tilde{\alpha}_{fc}$	$(1-\tilde{c})_c$	$\tilde{u}_c/\tilde{u}_{c0}$
C_τ	110	2	−2
k_0	290	4	5
ε_0	−37	−3	−4
p_∞	−2	−5	−0
Re	17	1	1

[a]For fully-developed injector exit conditions at 10 MPa. Output parameter evaluated at x/d = 20
[b]Parameter variations as follows: $C_\tau = C_\tau/2$, $k_0 = k_0/2$, $\varepsilon_0 = \varepsilon_0/2$, $p_\infty = 2p_\infty$ and $Re_0 = 2Re_0$.

CONCLUSIONS

The major conclusions of the investigation are as follows:

1) Use of the locally-homogenous flow and thin laminar flamelet approximations yielded encouraging agreement with measurements; however, uncertainties concerning injector exit conditions for the experiments precluded definitive assessment of the analysis.

2) Pressure-atomized monopropellant spray flames appear to be unusually sensitive to the degree of flow development and the turbulence levels at the injector exit; fully-developed flows with enhanced turbulence intensities require significantly smaller combustion volumes than slug flows with low initial turbulence intensities.

3) Predictions indicate that pressure-atomized monopropellant spray flames generally satisfy the boundary-layer approximations, except at very high pressures where phase densities become comparable. This is helpful since premixed turbulent flame analysis has been most successful for flows of this type, and the degree of empiricism needed for predictions is minimized (Bray, 1978, 1980).

4) Present predictions at the mixing-controlled limit suggest that combustion volumes decrease with increasing pressure due to increased entrainment rates; however, this effect is modified appreciably by the degree of flow development at the injector exit.

ACKNOWLEDGEMENT

This research was supported, in part, by the Army Research Office, Contract No. DAAL03-86-K-0154, under the Technical Management of D. M. Mann, and by the U.S. Army Armament of Research, Development and Engineering Center, under the Technical Management of P.-L. Lu.

REFERENCES

Birk, A., and Reeves, P. (1987). Annular liquid propellant jets. Technical Report BRL-TR-2780, Ballistic Research Laboratory, Aberdeen Proving Ground, Maryland.

Bilger, R. W. (1976). Turbulent jet diffusion flames. *Prog. Energy Combust. Sci.* **1**, 87.

Bray, K. N. C. (1978). Interaction between turbulence and combustion. *Seventeenth Symposium (International) on Combustion*, The Combustion Institute, Pittsburgh, pp. 223–233.

Bray, K. N. C. (1980). Turbulent flows with premixed reactants. In P. A. Libby and F. A. Williams (Eds.), *Turbulent Reacting Flows*, Springer, Berlin, pp. 115–183.

Chehroudi, B., Onuma, Y., Chen, S.-H., and Bracco, F. V. (1985). On the intact core of full-cone sprays. SAE Paper 850126.

Faeth, G. M. (1983). Evaporation and combustion in sprays. *Prog. Energy Combust. Sci.* **9**, 1.

Faeth, G. M. (1987). Mixing, transport and combustion in sprays. *Prog. Energy Combust. Sci.*, in press.

Friedman, E. (1986). Personal communication, Ballistic Research Laboratory, Aberdeen Proving Ground, Maryland.

Gordon, S., and McBride, B. J. (1971). Computer program for calculations of complex chemical equilibrium compositions, rocket performance, incident and reflected shocks, and Chapman–Jouguet detonations. NASA Report SP-273, Washington.

Hinze, J. O. (1959). *Turbulence*, McGraw-Hill, New York, pp. 491–528.

Hiroyasu, H., Shimizu, M., and Arai, M. (1982). The breakup of high speed jet in a high pressure gaseous atmosphere, *Proceedings of the 2nd International Conference on Liquid Atomization and Spray Systems*, Madison, Wisconsin.

Jeng, S.-M., and Faeth, G. M. (1984). Species concentrations and turbulence properties in buoyant methane diffusion flames. *J. Heat Trans.* **106**, 721.

Lockwood, F. C., and Naguib, A. S. (1975). The prediction of the fluctuations in the properties of free, round jet, turbulent diffusion flames. *Comb. Flame*, **24**, 109.

Mao, C.-P., Szekely, G. A., Jr., and Faeth, G. M. (1980). Evaluation of a locally homogenous model of spray combustion. *J. Energy* **4**, 78.

Mao, C.-P., Wakamatsu, Y., and Faeth, G. M. (1981). A simplified model of high pressure spray combustion *Eighteenth Symposium (International) on Combustion*, The Combustion Institute, Pittsburgh, pp. 337–347.

McBratney, W. F. (1980). Windowed chamber investigation of the burning rate of liquid monopropellants for guns. Report No. ARBRL-MR-03018, Ballistic Research Laboratory, Aberdeen Proving Ground, Maryland.

McBratney, W. F. (1981). Burning rate data, LGP 1845. Report No. ARBRL-MR-03128, Ballistic Research Laboratory, Aberdeen Proving Ground, Maryland.

Miesse, C. C. (1955). Correlation of experimental data on the disintegration of liquid jets. *Ind. Engr. Chem.* **470**, 1690.
Ranz, W. E. (1958). Some experiments on orifice sprays. *Can. J. Chem. Engr.* **36**, 175.
Ricou, F. P., and Spalding, D. B. (1961). Measurements of entrainment by axisymmetric turbulent jets. *J. Fluid Mech.* **11**, 21.
Ruff, G. A., Sagar, A. D., and Faeth, G. M. (1988). Structure and mixing properties of pressure-atomized sprays. AIAA Paper No. 88-0237.
Schlichting, H. (1979). *Boundary-Layer Theory*, 7th ed., McGraw-Hill, New York, pp. 599-600 and 636-638.
Shearer, A. J., Tamura, H., and Faeth, G. M. (1979). Evaluation of a locally homogeneous flow model of spray evaporation. *J. Energy*, **3**, 271.
Spalding, D. B. (1971). Concentration fluctuations in a round turbulent free jet. *Chem. Engr. Sci.* **26**, 95.
Spalding, D. B. (1978). GENMIX: *A General Computer Program for Two-Dimensional Parabolic Phenomena*. Pergamon Press, Oxford.
Williams, F. A. (1985). *Combustion Theory*, 2nd Ed., Benjamin/Cummings, Menlo Park, CA, pp. 411-423.
Wu, K. -J., Su, C. -C., Steinberger, R. L., Santavicca, D. A., and Bracco, F. V. (1983). Measurements of the spray angle of atomizing jets. *J. Fluids Engr.* **105**, 406.
Wu, K. -J., Coghe, A., Santavicca, D. A., and Bracco, F. V. (1984). LDV Measurements of drop velocity in diesel-type sprays. *AIAA J.* **22**, 1263.

NOMENCLATURE

c	reaction progress variable
C_i	constants in turbulence model, Table II
d	injector exit diameter
k	turbulence kinetic energy
L	length of injector passage
p	pressure
r	radial distance
Re	injector exit Reynolds number
S_ϕ	source source term, Table II
u	streamwise velocity
v	radial velocity
x	streamwise distance

Greek Letters

α	phase volume fraction
ε	rate of dissipation of turbulence kinetic energy
μ_t	turbulent viscosity
ρ	density
σ_i	turbulent Prandtl/Schmidt number
ϕ	generic property

Subscripts

c	centerline value
f	liquid-phase property
g	gas-phase property
0	injector-exit condition

Superscripts

$(-), (-')$	time-averaged mean and root-mean-squared fluctuating properties
$(\sim), (\sim'')$	Favre-averaged mean and root-mean-squared fluctuating properties.

A.3 "Separated-Flow Considerations for Pressure-Atomized Combusting Monopropellant Sprays," by T.-W. Lee, L.-K. Tseng and G.M. Faeth; AIAA Paper No. 89-0049, 1989; also, J. Prop. and Power, in press.

AIAA '89

AIAA 89-0049
Separated Flow Considerations for Pressure Atomized Combusting Monopropellant Sprays

T. Lee, L. Tseng and G. Faeth, Univ. of Michigan, Ann Arbor, MI

27th Aerospace Sciences Meeting
January 9–12, 1989/Reno, Nevada

SEPARATED-FLOW CONSIDERATIONS FOR PRESSURE-ATOMIZED COMBUSTING MONOPROPELLANT SPRAYS

AIAA-89-0049

T.-W. Lee,* L.-K. Tseng,* and G.M. Faeth†
The University of Michigan, Ann Arbor, Michigan

Abstract

The drop and spray combustion properties of the HAN-based monopropellant LGP 1845 were studied. Drop burning rates were measured with drops supported in a combustion gas environment at pressures of 0.2-7.0 MPa. Some internal gasification of drops -- causing swelling, partial bursting, and microexplosions -- was observed throughout this region but these disturbances decreased with increasing pressure. Effective drop burning rates (including effects of both surface gasification and bursting) were relatively constant, ca. 10 mm/s, and were consistent with earlier strand burning rate measurements of gelled propellant. Pressure-atomized combusting sprays were studied in combustion gas environments at pressures of 3-9 MPa. The liquid-containing region was significantly larger than earlier measurements of Birk and Reeves, as well as predictions based on the locally-homogeneous-flow approximation of multiphase flow theory. In conjunction with drop trajectory calculations, based on present measurements of drop burning rates, these findings suggest significant effects of separated flow in combusting HAN-based monopropellant sprays.

Nomenclature

C_D	= drop drag coefficient
d	= injector diameter
d_p	= drop diameter
k	= turbulence kinetic energy
K_p	= drop burning rate
L	= length of injector passage
Oh	= Ohnesorge number
p	= pressure
r	= radial distance
r_p	= drop radius
Re	= Reynolds number
t	= time
u	= streamwise velocity
We	= Weber number
x	= streamwise distance
α_f	= liquid volume fraction
ε	= rate of dissipation of turbulence kinetic energy
μ	= viscosity
ρ	= density
σ	= surface tension

Subscripts

c	= centerline value
f	= liquid-phase property
g	= gas-phase property
p	= drop property
o	= injector exit condition
∞	= ambient condition

Superscripts

$(\bar{\ })$	= time-averaged property
$(\tilde{\ })$	= Favre-averaged property

Introduction

Combusting monopropellant sprays have applications to regenerative liquid-propellant guns, throttable thrustors, and underwater propulsion systems. The objective of the present study was to experimentally investigate aspects of monopropellant spray combustion, seeking to extend earlier theoretical results obtained in this laboratory.[1-3] Two spray processes were considered, as follows: (1) the combustion properties of individual drops supported in combustion gas environments at pressures of 0.2-7.0 MPa; and (2) the structure of pressure-atomized combusting sprays in combustion gas environments at pressures of 3-9 MPa. The new measurements were used to assess the importance of separated-flow phenomena within pressure-atomized combusting monopropellant sprays, i.e., effects of finite relative velocities and transport rates between the phases. Similar to our earlier work,[1-3] the investigation was limited to a hydroxyl-ammonium nitrate (HAN)-based monopropellant (LGP 1845) which is of interest for several high-pressure monopropellant combustion systems.

Individual drop burning rates are needed for fundamental consideration of the properties of combusting monopropellant sprays. Earlier studies relevant to drop burning rates of HAN-based monopropellants have included measurements of strand burning rates[4-6] and the burning rates of individual drops in heated environments.[7-11] McBratney[4,5] measured strand burning rates of HAN-based monopropellants at pressures of 7-100 MPa. The propellant liquid was gelled with 2 weight percent Kelzan in order to stabilize turbulent-like disturbances of the liquid surface that are normally encountered during strand combustion tests at high pressures. The strand burning rates of gelled LGP 1845 were high (ca. 20 mm/s) and the pressure dependence was relatively weak (ca. $p^{0.1}$). A frothy region was observed at low pressures, where the thermal disturbance of the combustion wave extends an appreciable distance into the unburned propellant, suggesting significant reaction in the condensed phase for these conditions. While these results are valuable, however, the use of a gelling agent raises questions concerning its influence on the process. Vosen[6] measured strand burning rates of two ungelled HAN-based monopropellants, LGP 1846 and a 9.1 molar solution of HAN and water, at pressures of 7-30 MPa. The burning rates of both propellants were very high, 100-250 mm/s, and liquid surfaces were clearly disturbed, indicative of turbulent-like instability of burning liquid strands normally seen at high pressures; therefore, these results are difficult to interpret to find the fundamental combustion properties of the propellants.

Zhu and Law[7] studied the drop combustion properties of LGP 1845 and other HAN-based propellants, in combustion gases at 1170 K and 1 atm. The drops were observed to heat up with no radius change at first, then gasify from the surface for a time (with surface regression rates of ca. 0.2 mm/s), and finally burst when the drop diameter had decreased by roughly 15 percent. Beyer[8,9] and Beyer and Teague[10] studied the combustion of LGP 1846 drops supported in nitrogen at temperatures of 570-920 K and pressures of 0.1-8.2 MPa. These observations yielded results similar to Zhu and Law:[7] after a heat-up time and a period of relatively slow surface gasification (0.2 mm/s at 730 K and 1 MPa) the drops often burst -- particularly the larger drops. Both sets of drop experiments suggest that bulk liquid reaction and microexplosions may be important for combustion of HAN-based monopropellants but drop environment tempera-

* Graduate Assistant, Aerospace Engineering
† Professor, Aerospace Engineering, Fellow, AIAA

tures were low in comparison to the adiabatic combustion temperature of the monopropellant, (ca. 2150 K); therefore, the drops may not have ignited in a manner representative of spray combustion.

Earlier theoretical work in this laboratory addressed liquid surface and spray properties of combusting HAN-based monopropellants.[1-3] Analysis of liquid surface properties,[1,2] indicated relatively high liquid surface temperatures (in the range 800 - 1050 K for pressures greater than 10 MPa) and unusually high pressures for the liquid surface to reach its thermodynamic critical point (250 MPa with an estimated uncertainty of 50 percent). The high surface temperatures of the liquid surface provides greater potential for significant effects of chemical reaction in the bulk liquid than most monopropellants, helping to explain observations of microexplosions reported in Refs. 7-10. Furthermore, the high critical combustion pressure suggests that spray combustion of HAN-based monopropellants involves subcritical combustion with a drop-containing combusting spray for most applications.

The earlier analysis of combusting HAN-based monopropellant sprays,[1,3] was based on the locally-homogeneous-flow (LHF) approximation of multiphase flow theory, i.e., the assumption that velocity differences between the phases are negligible at each point in the flow;[11-13] and the thin laminar flamelet approximation of turbulent premixed flame theory, proposed by Bray.[14,15] Turbulent mixing was estimated using a Favre-averaged k-ε turbulence model, with empirical constants established from measurements in noncombusting variable-density round jets,[16,17] however, the constants used are very similar to early proposals based on constant-density turbulent flows.[18] The performance of the analysis was evaluated using the measurements of Birk and Reeves[19] for pressure atomized combusting LGP 1846 sprays at pressures of 6-8 MPa. There was encouraging agreement between predictions and measurements, however, predictions were very sensitive to the degree of flow development at the injector exit which was not known very well; therefore, this assessment was not definitive. Later measurements of noncombusting pressure-atomized sprays by Ruff et al.[13] established the strong sensitivity of spray properties to the degree of flow development at the jet exit and observed reasonably good performance of LHF analysis in the dense-spray region (liquid volume fractions greater than 0.2) near the injector exit for atomization breakup. However, these measurements also disclosed significant deficiencies of LHF analysis for other breakup regimes and in the dilute portion of the spray -- the last being in general agreement with other recent evaluations of the LHF approach for dilute sprays.[11,12]

The present investigation sought to extend past work concerning both drop and spray combustion of HAN-based monopropellants. Drop combustion was observed using an approach similar to Beyer[10] for pressures of 0.2-7 MPa, however, the drop environment more closely matched the gas temperature of a combusting monopropellant spray. Measurements of spray properties were undertaken seeking to confirm the measurements of Birk and Reeves,[19] while considering a broader range of experimental conditions at pressures of 3-9 MPa. The new spray measurements, in conjunction with both LHF analysis and drop trajectory calculations based on the present drop burning rate measurements, were used to assess the importance of separated-flow phenomena for these flows.

Drop Combustion

Experimental Methods

Apparatus. Figure 1 is a sketch of the drop combustion test apparatus. The supported-drop technique was used with the drops exposed to gases in the post-flame region of a premixed burner which was operated within a pressure vessel. The pressure vessel had an inside diameter and length of 130 and 430 mm and was fitted with two 25 mm diameter quartz windows so that the drops could be observed.

The premixed burner had a diameter of 10 mm with a stainless steel screen (0.17 mm diameter wires, 2000 wires/m, square pattern) to help stabilize the flame. The gas flow rates of the premixed burner were metered and controlled with critical flow orifices and pressure regulators. Burner operating times were short, just sufficient to stabilize the premixed flame and complete the drop combustion test. Burner gas flows were initiated and terminated with solenoid valves while the burner was ignited with an exploding wire. The pressure rise of the chamber (measured with a pressure transducer) was small in the period when the burner was operating, ca. 5 percent; therefore, the chamber pressure was set by backfilling it with air. The properties of the post-flame region of the premixed burner roughly approximated the temperatures of adiabatic combustion of the monopropellant, but contained significantly lower concentrations of water vapor, see Table 1 for the combustion product properties of LGP 1845 and the burner gases (denoted burner 1 and 2).

The drop support assembly is illustrated in Fig. 2. The drops were mounted on quartz fibers, 50-150 μm in diameter, with the bottom end of the fiber flame polished to a bead of somewhat larger diameter to help support the drop. The drop was surrounded with a retractable shield to protect it from transients when the premixed flame was ignited. Once the premixed

Table 1. Combustion Product Properties[a]

Mixture	LGP 1845[b]	Simulent Gases		
		Burner 1[d]	Burner 2[d]	Spray
Temperature (K)	2150	2295	2230	2790
Composition (% by volume)[c]				
H_2O	69.2	18.8	18.0	19.8
CO_2	12.9	9.1	8.9	--
N_2	17.4	71.2	72.6	38.3
Ar	--	--	--	40.9

[a] Computed for 10 MPa using the Gordon and McBride[20] algorithm, but effects of dissociation are small.
[b] Reactant composition (% by mass): HAN, 63.2, TEAN, 20; and H_2O, 16.8.
[c] Major species only. Minor species include CO, H_2, NO, OH and O_2.
[d] Volume flow rate of burner gases (cold) of 6.28×10^{-5} m^3/s.

flame was stabilized the shield was rapidly retracted by fusing its wire retainer so that the unbalanced pressure force on the shield forced it to one side of the pressure vessel where it was stopped by a rubber cushion.

Instrumentation. Drop diameter was measured as a function of time using backlighted high-speed motion picture photographs. The arrangement of the illuminating and camera system is illustrated in Fig. 1. The drops were backlighted by a continuous arc source, using a condensing lens to direct the light to a diffusion screen located at one of the windows. The photographs were obtained using a high-speed motion picture camera operating at roughly 1000 pictures per second which incorporated an internal timing marker.

Results and Discussion

Drop combustion at low pressures yielded very irregular variations of drop diameter as a function of time due to bubble formation and bursting within the drops. Some typical results at low pressures are illustrated in Fig. 3. Drop diameters are plotted as a function of time for five tests at 0.51 MPa with initial drop diameters in the range 580-770 μm and a 300 μm diameter bead on the quartz fiber to help support the drop. The origin of these plots is somewhat arbitrary since the motion of the retractable shield disturbed the premixed flame causing it to flap for a time; therefore, the time when the drop was finally submerged in the post flame gases was uncontrolled and variable. The results in Fig. 3 show swelling of the drop due to bubbles in the liquid in every case. The bubbles would periodically burst, carrying off some of the liquid, and occasionally the bursting of a bubble was sufficiently severe to carry off all of the liquid. At these low pressure conditions, internal reaction and bursting, with some mechanical removal of liquid caused by the bursts, appears to be the main mechanism for the reduction of the drop diameter.

The degree of drop swelling due to the presence of bubbles in the bulk liquid, and the severity of drop bursting, decreased as the pressure was increased. Some typical results at higher pressures are illustrated in Fig. 4. Drop diameter is plotted as a function of time for five representative tests at 2.1 MPa with initial drop diameters in the range 520-680 μm and a 200 μm diameter bead on the quartz fiber. As before, the time origin is arbitrary due to effects of initial disturbances on the premixed flame. All these conditions exhibited some degree of internal bubble formation, however, effects of bubbles bursting were relatively mild and complete bursting of drops was not observed at pressures of 2.1 MPa and higher.

Reduced effects of internal bubbles at high pressures appears to be largely caused by increased gas density so that a given degree of bulk liquid reaction yields a lower volume of gas: this reduces bubble sizes and growth rates which tends to reduce the severity of bursting phenomena. Counter to this is the fact that liquid surface temperatures tend to increase with increasing pressure for the present range of conditions (reaching a maximum at roughly 25 MPa):[1,2] this is expected to increase rates of bulk liquid reaction.

The time period of drop swelling, or relatively constant drop diameters, was irregular due to uncertainties concerning the time when the drop was submerged in the combustion gas environment. However, the period when the drop diameter decreased was analyzed to obtain effective drop burning rates. Plots of drop diameter as a function of time in the period where the drop diameter is decreasing are illustrated for the present test conditions in Fig. 5. The origins of these plots are arbitrary since the data has been plotted to overlap in the region where the drop diameter is decreasing. In addition, conditions where the drops burst completely at low pressures have been excluded. Results at low pressures show wide variations due to significant effects of bubble swelling and bursting but the diameter traces become more regular and repeatable at high pressures. These data were fitted to determine effective burning rates for the drops, $K_p = -dr_p/dt$: the fits are also illustrated in Fig. 5.

Present effective burning rates are plotted as a function of pressure in Fig. 6. These results are for drop diameters in the range 300-1200 μm and include effects of both internal reaction forming bubbles which burst, mechanically removing some liquid, as well as conventional gasification at the surface of the drop. This combination of effects causes the effective burning rate to be highest at the lowest pressure, where bursting dominates the process, and then to show relatively little change with pressure over most of the region considered during present tests. The strand burning results of McBratney[4,5] and Vosen[6] are also illustrated in Fig. 6. The present results are a crude extension of McBratney's[4,5] measurements of gelled propellants at higher pressures. The results of Vosen[6] are much higher than the rest of the measurements due to effects of liquid surface disturbances of burning liquid strands at high pressures, noted earlier.

Spray Combustion

Experimental Methods

Apparatus. The present spray combustion test apparatus was similar to the arrangement used by Birk and Reeves.[19] A sketch of the apparatus appears in Fig. 7. The experiments were conducted in the same chamber as the drop combustion tests. The combustion environment was produced by filling the chamber with a combustible mixture and then igniting it with two sparks to achieve the combustion gas properties summarized in Table 1 (denoted spray). The pressure of the spray tests was adjusted by varying the initial pressure of the combustible gas mixture since combustion of this gas approximated a constant volume process. The combustible gas mixture had temperatures that were somewhat greater than adiabatic combustion temperature of the monopropellant.

The spray was pressure atomized using injectors having exit diameters of 0.31, 0.58, 1.08 and 1.17 mm. The inlet of the injectors had baffles, to control any swirl in the liquid, and smooth entries, to reduce effects of cavitation. Injectors having length-to-diameter ratios of 2, 17 and 42 were considered since earlier work indicated that the degree of flow development at the injector exit influenced spray mixing properties.[2,3,13] The injectors were directed vertically upward.

A test was run by placing a propellant sample (3-4 ml) in the fuel delivery tube and filling the injector passage up to its exit. A cap was then placed over the exit to prevent gas inflow when the chamber was filled with the combustible gas mixture and further pressurized as this gas burned. The propellant flow was initiated by venting nitrogen from an accumulator into the fuel delivery tube by opening a solenoid valve. Once the pressure of the propellant was greater than the chamber pressure, the cap popped off and the resulting propellant flow generated a spray in the hot gas mixture. The process ended when all the propellant was consumed. The injector passage continued to be purged by the nitrogen flow from the accumulator for a time before the accumulator flow was ended.

Instrumentation. The combusting sprays were observed using motion picture shadowgraphs as illustrated in Fig. 7. Backlighting was provided by a flash lamp source, ca. 1 μs flash duration, which was synchronized with the camera; therefore, the image of the spray was effectively stopped on the film. The shadowgraphs were recorded with a 16 mm high-speed camera operating at roughly 1000 pictures per second, using Tri-X negative film. The camera optics yielded a 25 mm diameter field of view; therefore, it was necessary to adjust the position of the injector to observe the full length of the liquid containing region.

Since propellant combustion does not produce particulates and gas temperatures are relatively uniform in monopropellant spray flames, the boundaries of the spray were reasonably well defined -- similar to past measurements of Birk and Reeves.[19] The films were analyzed to yield mean and fluctuating time averaged liquid volume fractions, assigning dark zones to unburned liquid reactant and light zones to gaseous combustion products. For each test, 10-30 frames were available for analysis during the steady flow portion of the spray combustion process. Separating dark and light zones was somewhat subjective; and since the measurements correspond to line-of-sight projections, they are biased downstream and radially outward from correct point measurements of mean and fluctuating liquid volume fractions. Predictions were analyzed to estimate the line-of-sight biases, as discussed in the next section.

Test Conditions. Test conditions for the spray combustion tests are summarized in Table 2. Most of the injector flows correspond to fully developed flow at the injector exit, which due to the Reynolds number of the passage flow corresponds to turbulent pipe flow. Injection velocities were in the range 49-65 m/s: these conditions correspond to the atomization break-up regime, i.e., a drop-containing shear layer begins to develop at the liquid surface immediately at the injector exit.[t2,t3]

Theoretical Methods

Present measurements were compared with the monopropellant spray combustion analysis developed earlier in this laboratory.[1,3] Drop trajectory calculations were also carried out in order to help assess effects of separated-flow phenomena. Both analyses are described in the following.

Spray Analysis. The main features of the spray analysis will be only briefly described in the following, original sources should be consulted for details.

The analysis involves use of the LHF approximation of multiphase flow theory[t1-t3] and the thin laminar flamelet approximation of premixed turbulent flame theory.[t4,15] Turbulent mixing was treated using a Favre-averaged turbulence model.[14-t7] This approach provides a useful limit since both multiphase and chemical reaction phenomena are controlled by turbulent mixing which minimized the empiricism needed for predictions, e.g., initial drop size and velocity distributions, chemical kinetic properties, etc., are not needed to define the problem. The main limitation of the LHF approximation is that its use generally tends to overestimate the rate of development of sprays, particularly in dilute-spray regions far from the injector exit.[t1-13] However, Ruff et al.[13] find that the LHF approach, using the present turbulent-mixing model, provided reasonably good estimates of mixing properties in the near-injector dense-spray region of nonevaporating pressure-atomized sprays in the atomization breakup regime -- conditions that are representative of present tests.

The thin laminar flamelet approximation implies that heterogeneous monopropellant flames cover all liquid surfaces. Except for very near the liquid surface, the liquid is at the same state as in the injector while beyond the outer edge of the thin flame the gas has uniform properties equivalent to adiabatic flame conditions noted in Table 1. Under the LHF approximation, relative velocities between the phases (slip) are neglected.

Other major assumptions of the analysis are as follows: (1) steady (in the mean) axisymmetric flow with no swirl; (2) low Mach numbers with negligible potential and kinetic energy changes, and negligible viscous dissipation; (3) boundary-layer approximations apply; (4) negligible effects of radiant energy exchange; (5) equal exchange coefficients of all species and heat; and (6) high Reynolds numbers, so that laminar transport is negligible in comparison to turbulent transport. Justification of these assumptions is presented in Refs. 1 and 3.

Under these assumptions, flow properties can be found by solving governing equations for conservation of mass, momentum and reaction progress variable, in conjunction with second-order turbulence model equations for turbulence kinetic energy and its rate of dissipation.[t4,t5] The formulation, all empirical constants used in the turbulence model, and the method of solution, can be found in Ref. 3.

The predictions were also used to estimate potential effects of line-of-sight biasing on the measured distributions of liquid volume fractions using a stochastic approach developed for radiation calculations in this laboratory.[21] Knowing the time-averaged probability density function of the reaction progress variable along paths through the flow, the reaction progress variable was simulated for a series of statistically-independent eddies along the path. Counting the presence of any liquid in the path as a condition which would block the light, giving a dark image on the film, yielded estimates of time averaged mean and fluctuating liquid volume fractions for the path. This procedure has not been calibrated using known flows, however, it does provide at least a qualitative indication of potential effects of line-of-sight bias.

Table 2. Summary of Combusting Spray Test Conditions

Diameter (mm)	L/d	Flow Type[a]	Amb. Pres. (MPa)	Pressure Drop (MPa)	Inj. Velocity[b] (m/s)	Re[c]	Oh[d]	We_f[e]
Radial Measurements:								
1.17	17	FDF	3.11	2.02	52.7	12600	0.021	70700
1.17	17	FDF	7.07	1.79	49.3	11800	0.021	62400
1.17	17	FDF	9.10	1.81	49.7	11900	0.021	63300
1.08	2	SF	6.83	1.93	51.4	11400	0.022	62200
0.58	42	FDF	3.19	2.07	53.2	6300	0.030	35800
0.58	42	FDF	6.15	2.76	61.6	7300	0.030	47900
Axial Measurements:								
0.58	42	FDF	3.22	2.33	56.6	6700	0.030	40400
0.58	42	FDF	6.16	1.81	49.5	5900	0.030	30900
0.58	42	FDF	8.99	2.14	54.3	6400	0.030	37100
0.31	42	FDF	6.51	3.05	64.8	4000	0.041	27800

[a]FDF = fully developed flow; SF = slug flow.

[b]Unity flow coefficient.

[c]$Re = \rho_f u_o d/\mu_f$, $\mu_f = 0.0071$ kg/ms.

[d]$Oh = \mu_f / \sqrt{\rho_f d\sigma}$, $\sigma = 0.0669$ kg/s^2.

[e]$We_f = \rho_f u_o^2 d/\sigma$.

Drop Trajectory Analysis. Direct assessment of the approximations of the LHF approach for the monopropellant sprays was undertaken using drop trajectory calculations, similar to the approach used by Shearer et al.[22] and Mao et al.[23] for nonpremixed spray flames. These calculations were limited to drops moving along the axis of the spray. The drops were assumed to be always in contact with the gas phase which was taken to have the properties summarized in Table 1. Estimates of the gas velocity variation along the axis were obtained from the LHF analysis.

Drop trajectory calculations were limited to deterministic calculations, ignoring effects of turbulence/drop interactions; therefore, mean gas velocities from the LHF analysis were used in the governing equations for drop motion. Drops were assumed to be surrounded by gas immediately at the injector exit, ignoring the all-liquid core present in these sprays.[13] Effects of drop heat-up were also ignored: the drop radius was assumed to decrease throughout the entire trajectory at 10 mm/s -- based on the results of Fig. 6 for the present test range. This high burning rate implies that the decomposition flame is located near the drop surface, well within the boundaries of the flow field around the drop; therefore, gas-phase properties used to estimate drop drag were taken to be ambient gas properties and effects of forced convection or drop burning rates were ignored. Other aspects of the analysis were similar to Refs. 22 and 23: the flow field around the drop was assumed to be quasi-steady; virtual mass, pressure-gradient, Basset history and gravitational forces were ignored; swelling of the drops was ignored; and drop drag was estimated using the standard drag correlation for solid spheres.

Under these assumptions, the governing equations of drop motion along the axis are as follows:

$$dx_p/dt = u_p \tag{1}$$

$$dd_p/dt = -2\,K_p \tag{2}$$

$$du_p/dt = -3\rho_g\,C_D\,|\,u_p - \tilde{u}\,|\,(u_p - \tilde{u})/4 \tag{3}$$

where

$$C_D=24\,(1+Re_p^{2/3}/6)/Re_p,\ Re_p \le 1000;\ C_D=0.44,\ Re_p>1000 \tag{4}$$

The initial condition is $u_p = u_o$, $d_p = d_{po}$ and $x_p = 0$ at $t = 0$. Equations (1) - (3) were integrated using a Runge-Kutta algorithm.

Results and Discussion

Due to strong background lighting, it was not possible to determine that ignition had taken place from flame luminosity. Nevertheless, ignition was readily identified from the pressure trace: inert liquid (like water or unignited monopropellant spray liquid) caused the hot combustion products of the premixed gas flame to be quenched which resulted in a rapid reduction of the chamber pressure; in contrast, energy release from the combusting monopropellant spray caused an increase of chamber pressure in the period when the propellant was flowing. It was possible to consistently ignite the spray at pressures as low as 2.7 MPa, however, the bulk of spray measurements were obtained at pressures of 3-9 MPa.

Measured and predicted time-averaged liquid volume fractions along the axis, $\bar{\alpha}_{fc}$, are plotted as a function of normalized distance from the injector exit, x/d, in Fig. 8. Both present measurements and those of Birk and Reeves[19] are shown on the plot. Predictions include direct values of $\bar{\alpha}_{fc}$ as well as results allowing for line-of-sight bias, as noted earlier.

Test conditions used by Birk and Reeves[19] were similar to present test conditions, except that injector L/d were in the range 1.2-2.4 and the injector inlet was not rounded (see Lee et al.[3] for a sketch of the injectors), and injector pressure drops were 1.5-2.0 times higher than the present study. The motion picture shadowgraphs of both investigations were obtained in a similar manner and were analyzed in this laboratory. Each set of experimental results also exhibits a significant degree of internal consistency and repeatability when plotted in the manner of Fig. 8. Finally, pressure traces indicated that measurements were obtained for combusting sprays for both studies. Nevertheless, present measurements exhibit a much longer liquid-containing region than those of Birk and Reeves,[19] e.g., $\bar{\alpha}_{fc} = 0.5$ at x/d roughly 150 and 25 for the two sets of measurements. Specific reasons for these differences are not obvious since so many features of the two studies were the same, however, changes in injection properties offer the most plausible explanation. In particular, the sharper injector inlet used by Birk and Reeves[19] could have caused cavitation in the injector passage resulting in a more finely atomized spray with a rapid rate of radial spread. Similarly, the injector used by Birk and Reeves[19] did not have a flow straightener and swirl induced in the injector flow passage could have resulted in unusually high radial spread rates; although the fuel-injection system only involved rectilinear motion and doesn't appear to be fundamentally prone to induce swirl. Finally, Birk and Reeves[19] employed somewhat higher injector pressure drops which would be expected to yield smaller drop sizes in the spray; nevertheless, spray conditions for both investigations were in the atomization breakup regime and the pressure drop increase doesn't appear to be sufficient to explain the differences seen in Fig. 8 based on the relatively small effect of pressure drop variations observed during this investigation. In any event, extensive rechecking of measurements using the present injectors could not reproduce the results of Birk and Reeves.[19]

Present measurements in Fig. 8 are roughly similar (in terms of x/d) at all test conditions, with the downstream limit of the liquid-containing region at x/d ca. 350. Since these results involve a range of pressures and injector diameters, this behavior suggests a mixing-controlled process supporting the use of LHF analysis -- a conclusion reached in Ref. 3, based on the measurements of Birk and Reeves.[19] Closer examination of the data, however, reveals trends that suggest significant separated-flow effects. First of all, results for the 0.31 mm diameter injector consistently exhibit higher values of $\bar{\alpha}_{fc}$ at a particular x/d than the 0.58 mm diameter injector. This is a separated-flow property since drop diameters are not strongly affected by injector diameters while drops of a particular size must penetrate a certain distance in order to disappear: this causes in a tendency for penetration distances, x, to be constant for separated flows rather than x/d.[11] Another effect is that $\bar{\alpha}_{fc}$ at a particular x/d is lower for a chamber pressure of 8.99 MPa than the other pressures considered for the 0.58 mm diameter injector: this behavior parallels the effective burning rate results of Fig. 6 where drop burning rates at 9 MPa are higher than for pressures in the range 3-6 MPa, which are roughly the same. A final effect is that use of long and short L/d injectors yielded roughly the same results while mixing-controlled flows would result in much faster mixing rates for the long L/d injector.[13]

Predictions illustrated in Fig. 8 are for fully-developed flow at the injector exit, which corresponds to the bulk of present test conditions. Effects of ambient pressure, injector diameter and injector Reynolds number had little effect on the predictions; therefore, only single lines are shown for results with and without the line-of-sight bias correction. Comparing predictions with and without the line-of-sight bias correction indicates significant effects of bias for intermediate values of $\bar{\alpha}_{fc}$; however, predictions of the downstream end of the liquid-containing region are not strongly influenced by the bias.

In view of the bias uncertainties, the predictions illustrated in Fig. 8 are in fair agreement with the measurements of Birk and Reeves.[19] This observation prompted earlier encouragement concerning the value of the LHF and thin laminar flamelet approximations for analyzing flows of this type. However, comparison of predictions with present measurements implies that use of the LHF approximation causes the rate of development of the spray to be substantially overestimated, in agreement with most other evaluations of the LHF approximation for sprays.[11-13]

Radial profiles of time-averaged liquid volume fractions at various distances from the injector are illustrated in Fig. 9. All measurements shown in the figure were obtained during the present investigation. Predictions shown on the figure account for line-of-sight bias and are for fully-developed flow at the injector exit. Similar to results along the axis, predictions were relatively independent of test conditions and only a single line is shown for each streamwise position. Results ignoring line-of-sight bias are narrower than the plots illustrated in Fig. 9, however, the outer extent of the liquid-containing region is about the same.

Similar to results along the axis, the measured radial profiles are crudely similar for all the test conditions when plotted in the manner of Fig. 9. In terms of r/x, the radial similarity variable of turbulent jets, the liquid-containing region extends to 0.05-0.07, rather than 0.15 which is the typical width based on scalar properties in turbulent jets. Predictions provide a fair estimate of flow widths near the injector exit but progressively fail with increasing distance from the injector exit -- tending to overestimate the rate of development of the flow. This behavior is similar to other evaluations of the use of the LHF approximation for both nongasifying and gasifying sprays.

Potential effects of separated flow are examined directly by the drop trajectory computations illustrated in Fig. 10. Drop velocities and diameters along the axis are plotted as a function of distance from the injector for an ambient pressure of 10 MPa. Predictions of velocities along the axis from the LHF analysis are also illustrated on the plot, as a reference. Results are shown for initial drop diameters of 10, 20, 100 and 200 μm; drops much larger than 200 μm would be subject to secondary breakup due to excessively-high drop Weber numbers.[12] Unlike LHF predictions, drop trajectory calculations depend on the initial injector diameter, as noted earlier: the results illustrated in Fig. 10 are for an injector diameter of 1.00 mm.

The results illustrated in Fig. 10 clearly show significant effects of separated flow. The LHF predictions exhibit a decay of velocity beyond the potential-core-like region which is roughly inversely proportional to pressure -- similar to single-phase jets. Due to the small diameter of the injector, this results in a rapid deceleration rate. Only the smallest drops (initial diameters of 10 μm or less) have sufficiently fast response to approach the velocities of the continuous phase throughout most of their trajectory. With increasing drop size, the drops progressively overshoot the velocity of the continuous phase and only approach it again toward the end of their life, when they become very small. Similarly, the drops pass beyond the end of the liquid-containing region estimated by the LHF analysis (taken to be $\alpha_{fc} \geq 10^{-4}$ since liquid volume fraction never formally reaches zero in the LHF analysis due to its statistical treatment). Use of the drop burning rate estimates of Fig. 6, however, yields drop trajectories extending to x/d ca. 300 for initial drop diameters of 200 μm. This is comparable to present measurements of the extent of the liquid-containing region suggesting that the results of the drop trajectory calculations are at least reasonable.

Taken together, the results of Figs. 8-10 suggest significant effects of separated flow for combusting HAN-based monopropellant sprays over the present range of test conditions. In view of the relatively modest variation of burning rate with pressure seen in Fig. 6, the insensitivity of drop drag properties to pressure,[11,12] and the relatively high critical combustion pressure of HAN-based monopropellants (ca. 250 MPa[1,2]) it is likely that separated-flow phenomena are important for combusting HAN-based monopropellant sprays for most of their range of application.

Conclusions

The present study involved measurements of the combustion properties of the HAN-based monopropellant LGP 1845, both as drops and sprays in combustion gas environments at pressures of 0.2-9 MPa. The spray measurements, and drop trajectory calculations based on the present drop burning rate measurements, were used to evaluate earlier analysis of combusting monopropellant sprays based on the locally homogeneous flow and thin laminar flamelet approximations, due to Lee et al.[1,3] Major conclusions of the study are as follows:

1. Measurements yielded effective drop burning rates of ca. 10 mm/s for drop diameters of 300-1200 μm and pressures of 0.2-7 MPa. The effective drop burning rate involved both reaction within the bulk liquid causing bubble formation and bursting, dominating the process at low pressures; and conventional gasification from the drop surface, dominating the process at high pressures: taken together, these effects cause burning rates to be relatively independent of pressure over the present test range.

2. Present measurements of drop burning rates at pressures of 0.7-7 MPa are generally consistent with earlier strand burning rate measurements of gelled propellants due to McBratney[4,5] at pressures greater than 10 MPa.

3. Present measurements exhibited a much larger liquid containing region for combusting sprays at pressures of 3-9 MPa than the earlier measurements of Birk and Reeves[19] even though test conditions and methods of data analysis were similar, e.g., $\bar{\alpha}_{fc} = 0.5$ at x/d roughly 150 and 25 for the two sets of experiments. Reasons for these differences have not been firmly established but different injector passage conditions, possibly leading to effects of cavitation,swirl and finer atomization for the measurements of Ref. 19, have been advanced as a possible explanation.

4. While earlier evaluation of analysis using the LHF and thin laminar flamelet approximations appeared promising based on the measurements of Birk and Reeves;[19] current findings suggest that this approach substantially overestimates the rate of development of the flow which is consistent with recent findings for other pressure-atomized spray processes.[11-13] Separated flow phenomena appear to be important combusting for HAN-based monopropellant sprays over much of their range of application.

Acknowledgements

This research was sponsored by the Army Research Office and the U.S. Army Armament Research, Development and Engineering Center, Picatinny Arsenal, NJ under Contract No. DAAL03-86-K-0154.

References

[1]Faeth, G. M., Lee, T.-W. and Kounalakis, M. E., "Mixing and Thermodynamic Critical Phenomena of Combusting Monopropellant Sprays," Proceedings of the 24th JANNAF Combustion Meeting, October 1987.

[2]Kounalakis, M. E., and Faeth, G. M., "Combustion of HAN-Based Liquid Monopropellants Near the Thermodynamic Critical Point," Combust. Flame, in press.

[3]Lee, T.-W., Gore, J. P., Faeth, G. M., and Birk, A., "Analysis of Combusting High-Pressure Monopropellant Sprays," Combust. Sci. and Tech., Vol. 57, 1988, pp. 95-112.

[4]McBratney, W. F., "Windowed Chamber Investigation of the Burning Rate of Liquid Monopropellants for Guns," Report No. ARBRL-MR-03018, Ballistic Research Laboratory, Aberdeen Proving Ground, 1980.

[5]McBratney, W. F., "Burning Rate Data LGP 1845," Report No. ARBRL-MR-03128, Ballistic Research Laboratory, Aberdeen Proving Ground, 1981.

[6]Vosen, S. R. "The Burning Rate of HAN-Based Liquid Propellants," Twenty-Second Symposium (International) on Combustion, The Combustion Institute, Pittsburgh, in press.

[7]Zhu, D. L. and Law, C. K., "Aerothermochemical Studies of Energetic Liquid Materials: 1. Combustion of HAN-Based Liquid Gun Propellants Under Atmospheric Pressure," Combust. Flame, Vol. 70, 1987, pp. 333-342.

[8]Beyer, R. A., "Atmospheric Pressure Studies of Liquid Monopropellant Drops in Hot Flows," Technical Report BRL-TR-2768, Ballistic Research Laboratory, Aberdeen Proving Ground, 1986.

[9]Beyer, R. A., "Single Droplet Studies in a Hot, High Pressure Environment," Technical Report BRL-TR-2900, Ballistic Research Laboratory, Aberdeen Proving Ground, 1988.

[10]Beyer, R. A., and Teague, M. W., "Studies of Single Liquid Propellant Drops in Hot, High Pressure Environments," 22nd JANNAF Combustion Meeting, CPIA Publication 457, Vol. 2, p. 429, 1986.

[11]Faeth, G. M., "Evaporation and Combustion in Sprays," Prog. Energy Combust. Sci., Vol. 9, 1983, pp. 1-76.

[12]Faeth, G. M., "Mixing, Transport and Combustion in Sprays," Prog. Energy Combust. Sci., Vol. 13, 1987, pp. 293-345.

[13]Ruff, G. A., Sagar, A. D. and Faeth, G. M., "Structure and Mixing Properties of Pressure-Atomized Sprays," AIAA J., in press.

[14]Bray, K.N.C., "Interaction Between Turbulence and Combustion," Seventeenth Symposium (International) on Combustion, The Combustion Institute, Pittsburgh,, 1978, pp. 223-233.

[15]Bray, K.N.C., "Turbulent Flows with Premixed Reactants," Turbulent Reacting Flows (P. A. Libby and F. A. Williams, Eds.), Springer, Berlin, 1980, pp. 115-135.

[16]Bilger, R. W., "Turbulent Jet Diffusion Flames," Prog. Energy Combust. Sci., Vol. 1, 1976, pp. 87-109.

[17]Jeng, S. M. and Faeth, G. M., "Species Concentrations and Turbulence Properties in Buoyant Methane Diffusion Flames," J. Heat Trans., Vol. 106, 1984, pp. 721-727.

[18]Lockwood, F. C. and Naguib, A. S., "The Prediction of Fluctuations in the Properties of Free, Round Jet, Turbulent Diffusion Flames," Combust. Flame, Vol. 24, 1975, pp. 109-124.

[19]Birk, A. and Reeves, P., "Annular Liquid Propellant Jets — Injection, Atomization and Ignition," Report No. BRL-TR-2780, Ballistic Research Laboratory, Aberdeen Proving Ground, 1987.

[20]Gordon, S. and McBride, B. J., "Computer Program for Calculation of Complex Chemical Equilibrium Compositions, Rocket Performance, Incident and Reflected Shocks and Chapman-Jouguet Detonations," NASA Report SP-273, Washington, 1971.

[21]Faeth, G. M., Gore, J. P., Chuech, S. G. and Jeng, S. M., "Radiation from Turbulent Diffusion Flames," Ann. Rev. Num. Fluid Mech. and Heat Trans., Vol. 2, 1988, pp. 1-38.

[22]Shearer, A. J., Tamura, H. and Faeth, G. M., "Evaluation of a Locally Homogeneous Flow Model of Spray Evaporation," J. Energy, Vol. 3, September-October 1979, pp. 271-278.

[23]Mao, C.-P., Wakamatsu, Y. and Faeth, G. M., "A Simplified Model of High Pressure Spray Combustion," Eighteenth Symposium (International) on Combustion, The Combustion Institute, Pittsburgh, 1981, pp. 337-347.

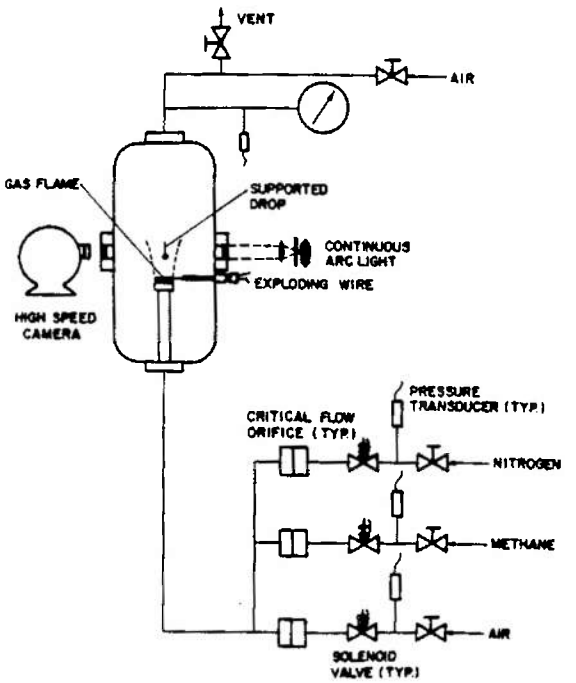

Fig. 1. Sketch of the drop combustion apparatus.

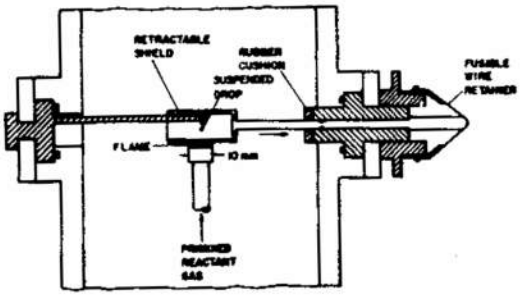

Fig. 2. Sketch of the drop support assembly.

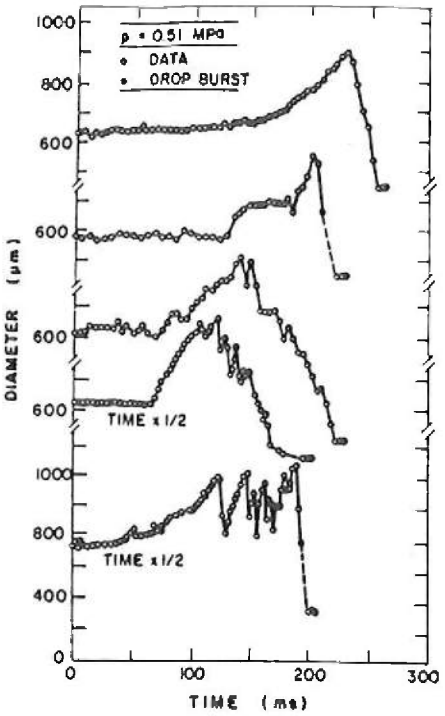

Fig. 3. Drop diameter histories at 0.51 MPa.

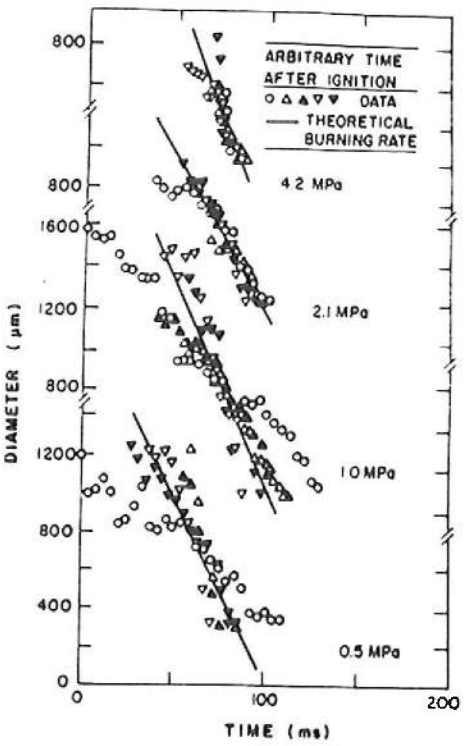

Fig. 5. Drop diameter histories in the combustion period.

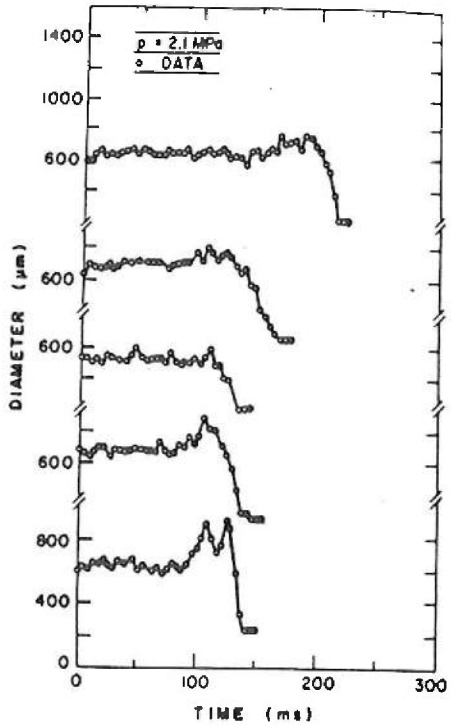

Fig. 4. Drop diameter histories at 2.1 MPa.

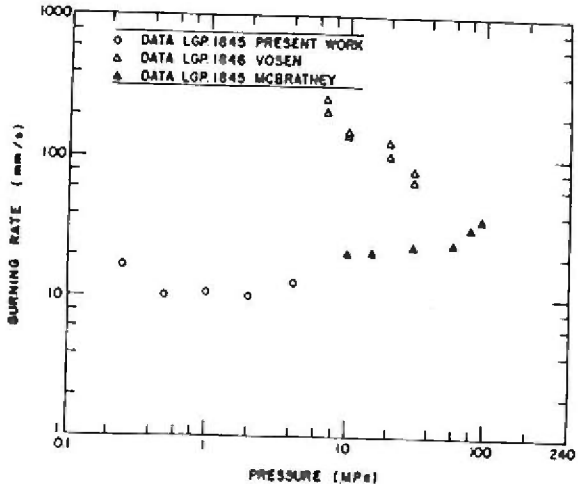

Fig. 6. Apparent drop burning rates as a function of pressure.

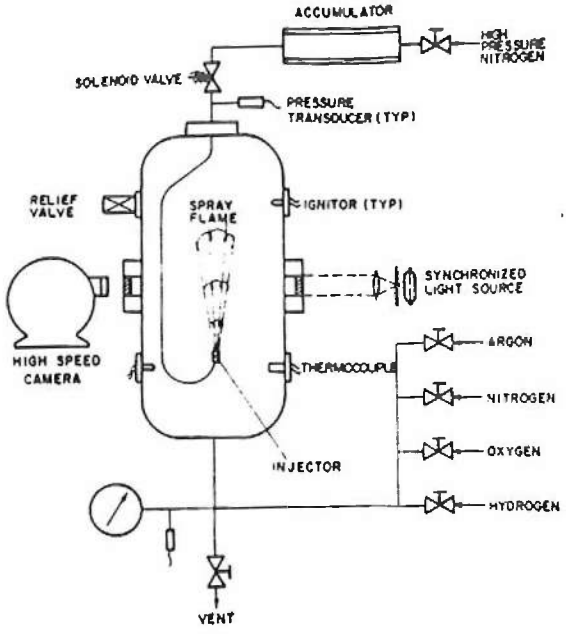

Fig. 7. Sketch of a spray combustion apparatus.

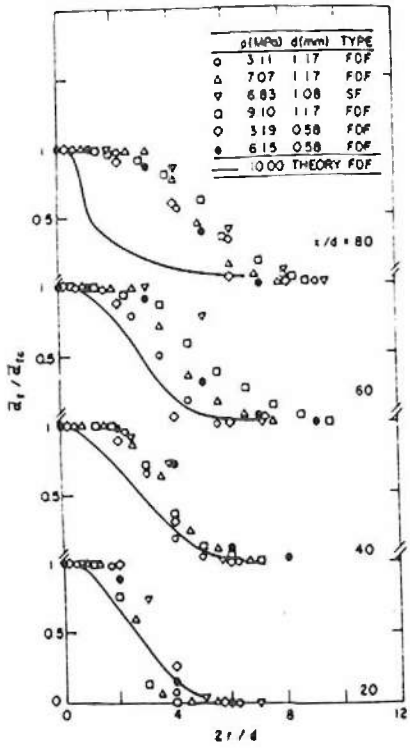

Fig. 9. Radial profiles of time-averaged liquid volume fractions. Predictions with line-of-sight bias correction.

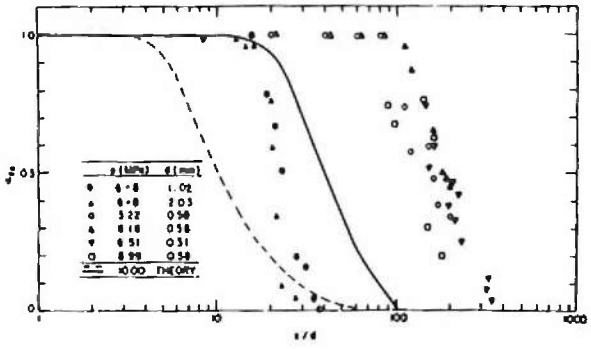

Fig. 8. Time-averaged liquid volume fractions along axis. Open symbols, present study; closed symbols, Birk and Reeves. Dashed and solid lines are predictions without and with line-of-sight bias correction.

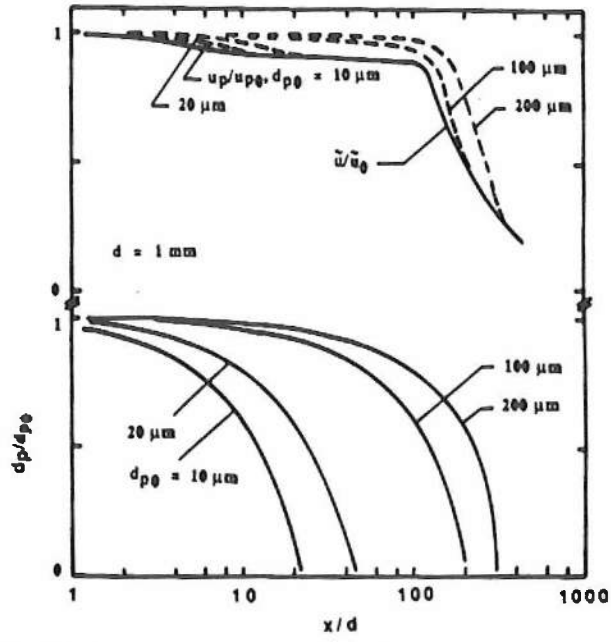

Fig. 10 Drop trajectory properties along axis. Note that $\bar{\alpha}_{fc} \sim 10^{-4}$ at x/d = 220 for the LHF calculation.

A.4 "Structure and Mixing Properties of Combusting Monopropellant Sprays," by T.-W. Lee and G.M. Faeth, AIAA Paper No. 90-0463, 1990; also, J. Prop. and Power, submitted.

AIAA-90-0463

Structure and Mixing Properties of Combusting Monopropellant Sprays

T.-W. Lee and G. M. Faeth
University of Michigan
Ann Arbor, MI

28th Aerospace Sciences Meeting
January 8-11, 1990/Reno, Nevada

Structure and Mixing Properties of Combusting Monopropellant Sprays

T.-W. Lee* and G. M. Faeth†
Department of Aerospace Engineering
The University of Michigan, Ann Arbor, Michigan

Abstract

The spray combustion properties of the HAN-based monopropellant LGP 1845 were studied both theoretically and experimentally. Drop size, liquid mass flow rate, and liquid mass flux distributions were measured for pressure-atomized sprays in the atomization breakup regime, burning within a combustion gas environment at pressures of 4.5-5.0 MPa. Two separated flow models were evaluated using the new measurements: a deterministic separated flow model where drop/turbulence interactions were ignored, and a stochastic separated flow model where drop/turbulence interactions were considered using random-walk computations for drop motion. When based on burning rates found from earlier single drop experiments, both models were in reasonably good agreement with the measurements. Separated flow effects are quite important for these sprays, with the length of the liquid-containing region being relatively independent of injector diameter and extending roughly 300 mm from the injector exit for injector diameters of 0.3 and 0.6 mm.

Nomenclature

C_B = coefficient in drop breakup correlation
C_D = drop drag coefficient
C_i = constants in turbulence model
d = injector diameter
d_p = drop diameter
d_{Pavg} = average drop diameter
k = turbulence kinetic energy
K_p = drop burning rate
L_e = characteristic eddy size
$\dot{m}$ = liquid mass flow rate
$\dot{m}''$ = liquid mass flux
m_i = drop mass of group i
$\dot{n}_i$ = number of drops per unit time in drop group i
Oh = Ohnesorge number, $\rho_f u_0 d/\mu_f$
r = radial distance
Re = Reynolds number, $\rho_f u_0 d/\mu_f$
SMD = Sauter mean diameter
S_ϕ = source term
t = time
t_e = characteristic eddy lifetime
u = streamwise velocity
u_i = velocity in coordinate direction i
v = radial velocity
v_j = volume of computational cell j
We_f = liquid Weber number, $\rho_f u_0^2 d/\sigma$
x = streamwise distance
x_i = distance in coordinate direction i
α_f = liquid volume fraction
ε = rate of dissipation of turbulence kinetic energy
μ = absolute viscosity
μ_t = turbulent viscosity
ρ = density
σ = surface tension
σ_i = turbulent Prandtl/Schmidt number
ϕ = generic property

Subscripts
c = centerline quantity
f = liquid property
p = drop property
0 = injector exit condition
∞ = ambient condition

Superscripts
$\bar{(\ )}$ = time-averaged quantity
$(\ )'$ = time-averaged root-mean-squared fluctuating quantity

Introduction

Combusting monopropellant sprays represent an important fundamental multiphase combusting flow, since they are the premixed counterpart of more common spray diffusion flames. Additionally, combusting monopropellant sprays have applications to regenerative liquid-propellant guns, throttable thrustors, and underwater propulsion systems. Motivated by these considerations, the present investigation considered the structure of combusting pressure-atomized monopropellant sprays both theoretically and experimentally, seeking to extend earlier work in this laboratory.[1-3] Similar to the earlier studies,[1-3] the investigation was limited to a hydroxyl-ammonium-nitrate (HAN)-based monopropellant (LGP 1845) which is of interest for several high-pressure monopropellant combustion systems.

The importance of multiphase flow phenomena is a significant issue for combusting monopropellant sprays. In particular, most applications involve high-pressure combustion (greater than 10 MPa) so that drops can approach their thermodynamic critical point where multiphase flow characteristics would disappear. Thus, combustor pressures required to reach near-critical conditions have been theoretically studied for HAN-based monopropellants.[1] It was found that these pressures are unusually high, ca. 250 MPa with an uncertainty of 50 percent due to uncertainties of thermochemical properties. As a result, multiphase effects are important for most applications involving these monopropellants.

The importance of finite interphase transport rates (separated-flow effects) is also a significant issue for high-pressure combusting sprays. This has been examined during earlier work in this laboratory.[2,3] Initial work involved development of a locally-homogeneous flow (LHF) model for combusting HAN-based monopropellants, where interphase transport rates are assumed to be infinitely fast.[2] This approach yielded reasonably good agreement with flow visualization measurements of Birk and Reeves[4] for combusting LGP 1845.[2] However, later evaluation in this laboratory suggested significant separated-flow effects using similar measurements as well as drop trajectory calculations.[3] Thus, the need for a separated-flow treatment of these sprays has been established although models of this type have not

---

* Graduate Assistant, currently Postdoctoral Fellow, Department of Mechanical Engineering, The Pennsylvania State University, University Park, Pennsylvania.
† Professor, Fellow AIAA.

been reported.

Information concerning the combustion properties of individual drops is needed to treat effects of separated flow; therefore, several studies relevant to drop combustion have been undertaken for the HAN-based monopropellants.[3,5-11] This includes measurements of strand burning rates,[5-7] as well as observations of individual drop combustion in heated or combustion gas environments.[3,8-11] Drop combustion at low pressures (less than 2 MPa) involves considerable subsurface liquid reaction with bubble formation and mechanical removal of liquid by microexplosions being the main mechanism for the reduction of the drop diameter.[3,8-11] This behavior follows since the liquid surface temperatures of HAN-based monopropellants are unusually high, ca. 1000 K, tending to promote liquid phase reactions.[1] At higher pressures (greater than 2 MPa) within combustion gas environments, however, conventional surface gasification as a heterogeneous premixed flame is more dominant.[3,5,6] The combined effect of the two mechanisms yields relatively high monopropellant drop burning rates, 10-40 mm/s, with a weak pressure dependence, ca. $p^{1/3}$, over the pressure range of 0.4-100 MPa.[3]

Finally, recent studies of the near-injector (dense spray) region of pressure atomized sprays are helpful for identifying initial conditions for separated-flow predictions of spray properties.[12-16] It is generally agreed that this region involves a liquid core, somewhat like the potential core of single-phase jets, surrounded by a multiphase mixing layer. Flow properties approximate estimates based on the LHF approximation at high liquid volume fractions, since the liquid dominates mixing properties due to its larger density, however, the bulk of the multiphase mixing layer exhibits significant effects of separated flow.[12-16] Finally, when effects of liquid turbulence are small, average drop sizes near the liquid surface approximate estimates based on aerodynamic breakup theory due to Reitz and Bracco;[12] while larger drops observed when liquid turbulence is present eventually break up to yield similar drop sizes.[16]

The present investigation sought to extend past work on the structure of combusting HAN-based monopropellant sprays. Spray combustion was observed in combustion gas environments near 5 MPa, using slide impaction to measure drop size, liquid mass flow rate and liquid mass flux distributions. These measurements were used to evaluate separated-flow models of the process considering two limits, analogous to methods used for evaporating sprays:[17] deterministic separated flow (DSF) where drop/turbulence interactions are ignored, and stochastic separated flow (SSF) where drop/turbulence interactions are considered using random-walk computations for drop motion. The present description of the study is brief, more details and tabulations of data can be found in Lee.[18]

Experimental Methods

Apparatus

The present spray combustion apparatus was similar to Lee et al.[3] and Birk and Reeves.[4] A sketch of the apparatus appears in Fig. 1. The experiments were conducted within a windowed pressure vessel having an inside diameter and length of 130 and 430 mm. The sprays were injected vertically upward in a combustion gas environment. The combustion gas environment was produced by filling the chamber with a combustible gas mixture and igniting it with a spark to achieve the combustion gas properties summarized in Table 1 (these properties were computed assuming thermodynamic equilibrium).[19] The pressure of the combusting spray was set by adjusting the initial pressure of the combustible gas mixture, since combustion of this gas approximated a constant volume process.[3] The adiabatic combustion temperature of the gas mixture was somewhat greater than the adiabatic constant-pressure combustion temperature of the monopropellant (see Table 1), however, temperature variations in this range do not have a large effect on drop burning rates.[3]

The spray was pressure-atomized using injectors having the diameters listed in Table 1. The inlets of the injectors were baffled, to eliminate swirl, and smooth, to reduce effects of cavitation. Length-to-diameter ratios were 42, yielding nearly fully-developed turbulent pipe flow at the exit.

The apparatus operated by placing a 3-4 ml sample of the propellant in the injector feed line so that the passage was filled right up to the exit. A cap was placed over the exit to prevent gas inflow when the chamber was pressured by filling or burning the combustion gas mixture. Injection was initiated by venting nitrogen from an accumulator into the delivery tube. Once the pressure of the propellant exceeded the chamber pressure, the cap popped off and the spray flowed into the combustion gas environment. The process ended when all the propellant was injected, after which the injector passage continued to be purged by nitrogen.

Instrumentation

The operation of the apparatus was monitored by measuring injector inlet and chamber pressures using pressure transducers.[18] Earlier measurements involved flash shadowgraph motion pictures of the spray, however, present measurements were limited to slide impaction.

A sketch of the slide impaction system appears in Fig. 2. The arrangement involves a translating shield with a shutter slot, and a stationary probe on which a MgO-layered glass slide (12 × 25 mm) was mounted facing downward toward the injector. Initially, the translating shutter was to the left of the slide (when viewed in Fig. 2) so that the slide was protected from initial disturbances by the shield. Once the spray was burning steadily, the wire retainer of the shield was fused by an electrical current, so that the unbalanced pressure force accelerated the shutter across the probe. The shutter opening (3.2 mm wide) traversing across the probe allowed drops to impact on the MgO layer, leaving cavities in the layer. The motion of the shutter was stopped by a rubber cushion after it had completely traversed the slide, leaving the slide protected once again by the shield. The motion of the shutter was recorded by a linear displacement transducer (not shown in Fig. 2) so that the time of passage across various portions of the slide was known.

The MgO layer was produced by passing the slide back and forth through the plume of an Mg flame from a 3 × 25 mm Mg strip burning in air. Wetting the slide with water prior to coating it was found to produce a layer with reasonably good resistance to shock disturbances and the high-temperature environment. The relationship between drop and impact crater size was found by calibrations using a Berglund-Liu monodisperse drop generator. The calibrations yielded a ratio of roughly 2.0 between the impact crater and drop diameters for drops up to 600 μm in diameter. Crater diameters were measured using a Unitron inverted metallurgical microscope at X50 magnification, with a linear micrometer reticle scale on the eyepiece. Only drops having diameters larger than 10 μm could be collected and sized; therefore, measured distributions are biased toward larger

drop diameters, although this does not affect estimates of SMD appreciably.

The slide impactor was positioned at various distances from the injector exit, by moving the injector. Due to excessively-high liquid fluxes, which resulted in overlapping craters and washing out of the slide at the shortest feasible shutter-opening times, it was not possible to make measurements closer than 135 mm from the injector. By accumulating data for several slides at a particular condition, 50-200 drops were sized to find drop size distributions and the SMD. Knowing the drop sizes and slide exposure times, these measurements could be used to find liquid fluxes and the total liquid flow rate over the crossection of the spray.

Experimental uncertainties of the slide impaction measurements were dominated by difficulties of overlapping impaction craters in the dense portion of the spray near the axis, and limitations of finite sample sizes. In particular, excessive liquid fluxes often required extrapolation of findings away from the axis to infer spray properties over the crossection.[18] The experimental uncertainties (95 percent confidence) were large as a result and are estimated as follows: SMD less than 25 percent, liquid fluxes less than 40 percent, and liquid flow rates only within a factor of two since flow rates near the axis involved extrapolation. These uncertainties are substantially greater than earlier work in evaporating air atomized sprays at atmospheric pressure,[17] reflecting the increased problems of the slide impaction technique in high-pressure and high-temperature environments within dense pressure-atomized sprays.

Test Conditions

Test conditions are summarized in Table 1. Injector Reynolds numbers are high enough to yield turbulent flow at the injector exit, well within the atomization breakup regime where the multiphase mixing layer begins to form right at the injector exit.[12-16] Combustor pressures were in the range 4.6-4.9 MPa, which is high enough for drop combustion to be dominated by surface gasification rather than microexplosions, based on single-drop combustion studies.[3]

Theoretical Methods

Gas-Phase Formulation

In view of the large monopropellant burning rates for present est conditions, ca. 10 mm/s, the heterogeneous premixed flame that covers all liquid surfaces is relatively thin, ca. 1 μm.[2] Thus the flow largely involves two states, unreacted liquid at its injection temperature, and completely reacted gaseous combustion products, if the ambient state also consists of products of adiabatic combustion. Since drop combustion properties were not strongly influenced by ambient temperatures,[3] this approximation is made in the following. Then, both phases have constant densities and there is no need to treat scalar mixing, which substantially simplifies the formulation. The present approach involves Eulerian calculations for the properties of the gas phase, and Lagrangian calculations of drop trajectories within the gas phase. Drop source terms in the governing equations for the gas phase account for interphase transport of mass and momentum.

Major assumptions of the gas phase formulation are as follows: axisymmetric and steady (in the mean) flow with no swirl, boundary-layer approximations apply, constant density gas, and negligible effects of buoyancy. The first of these is a condition of the experiments while pressure-atomized sprays, like single-phase jets, generally satisfy the boundary layer approximations. The constant density approximation follows from the assumption of thin heterogeneous flames as discussed earlier. Finally, injector velocities are ca. 70 m/s while the multiphase flow region was only roughly 300 mm long; therefore, it is reasonable to neglect effects of buoyancy. Similar to Solomon et al.,[17] the gas phase velocity field was found using a k-ε turbulence model that has been well calibrated for constant density turbulent round jets.[20-22]

Boundary conditions along the liquid core are specified as described later. Within the multiphase flow region, drop properties were found by solving Lagrangian equations of motion for the size and trajectories of a statistically significant sample of individual drops and then computing source terms for mass and momentum exchange from drops in the governing equations for the gas phase. This involves dividing the drops into n groups (defined by initial position, size and velocity) and then computing their subsequent motion in the flow. Based on recent findings for pressure-atomized non-evaporating sprays,[4-16] effects of collisions don't appear to be important even in the dense portion of pressure-atomized sprays and were ignored. Similarly, effects of adjacent drops are not likely to influence the heterogeneous flames, since they are thin, and were ignored as well. Effects of secondary drop breakup may be important for present sprays,[16] however, this still was neglected due to the lack of information concerning this phenomenon. Since initial drop size distributions were based on measurements downstream of the region where secondary breakup would be important, the effect was accommodated in any event. Additionally, direct effects of drops on turbulence properties (called turbulence modulation) were ignored since the bulk of the flow is relatively dilute and methods to treat these phenomena are not well established.[22] Finally, drop/turbulence interactions are known to influence the structure of noncombusting sprays,[17,22] therefore, this was evaluated for combusting monopropellant sprays by carrying out both DSF and SSF computations, which ignore and consider drop/turbulence interactions as noted earlier.

Formulations

Under present assumptions, the gas phase governing equations are the same for the DSF and SSF formulations, and can be written as follows:[17,22]

$$r\,\partial/\partial x(\bar{\rho}\,\tilde{u}\,\tilde{\phi}) + \partial/\partial r(r\bar{\rho}\,\tilde{v}\,\tilde{\phi}) = \partial/\partial r((r\mu_t/\sigma_\phi)\partial\tilde{\phi}/\partial r) + rS_\phi \qquad (4)$$

where there is no need to consider Favre-averaged variables, since the density of the gas phase is constant. The parameters ϕ and S_ϕ appearing in Eq. (1) are summarized in Table 2, along with all empirical parameters used in the calculations. Since the Reynolds numbers of present flows are relatively high, laminar transport has been ignored. The source terms for $\phi = 1$ (conservation of mass) and $\tilde{u}$ in Table 2 are the drop source terms found by computing the net change of mass and momentum of each drop group i passing through computational cell j, having a volume V_j. The boundary conditions for Eq. (1) involve a constant property ambient environment and symmetry at the axis (aside from the liquid core region which will be taken up later), as follows:

$$r \to \infty, \quad \phi = 0; \qquad r = 0, \quad \partial\phi/\partial r = 0 \qquad (2)$$

Drop Formulation

Drop trajectories were computed similar to earlier

work.[3] Drops were assumed to be surrounded by gas in the multiphase flow region. Effects of drop heatup were ignored and the drop radius was assumed to decrease at 10 mm/s, based on drop burning rate measurements at the pressure of present tests.[3] The high monopropellant burning rate implies a thin decomposition flame near the surface, well within the boundaries of the drop flow field; therefore, ambient gas properties were used to estimate drop drag and effects of forced convection on drop burning rates were ignored. Similarly, the eventual loss of the linear burning rate law for monopropellants ($K_p = -dr_p/dt$ = constant) for small drops was ignored, since this would occur for drop diameters of ca. 1 μm.[3] Other assumptions were similar to earlier separated flow models:[17,22] the flow field around the drops was assumed to be quasisteady; virtual mass, pressure-gradient, Basset history and gravitational forces were ignored; drop swelling was ignored; and drop drag was estimated using the standard drag correlation for solid spheres.

Under these assumptions, the governing equations for drop motion are as follows:[22]

$$d x_{pi}/dt = u_{pi}, \quad i=1,2,3 \tag{3}$$

$$d d_p/dt = -2 K_p \tag{4}$$

$$du_{pi}/dt = (3\rho C_D/4\, d_p\rho_p)(u_i-u_{pi})\, |u-u_p|, \quad i=1,2,3 \tag{5}$$

where a Cartesian coordinate system has been used and $|u-u_p|$ denotes the magnitude of the relative velocity between the drop and the gas. The drag coefficient expression was identical to past work.[22]

Equations (3) and (5) were solved using time-averaged gas phase velocities for the DSF model. In contrast, the SSF model involves an approximate approach to treat turbulence/drop interactions that has been reasonably successful during past evaluations.[17,22] This involves computing drop trajectories as they encounter a succession of turbulent eddies. The properties of each eddy are assumed to be uniform and to change randomly from one eddy to the next. The gas velocities within the eddies were found by making a random selection from the probability density function (PDF) for velocity, assuming an anisotropic Gaussian PDF with streamwise and crosstream variances of k and k/2. A drop was assumed to interact with an eddy as long as the time of interaction did not exceed the eddy lifetime t_e, or the displacement of the drop did not exceed the characteristic eddy size, L_e. These quantities were estimated, as follows:[22]

$$L_e = C_\mu^{3/4} k^{3/2}/e, \quad t_e = L_e/(2k/3)^{1/2} \tag{6}$$

All quantities needed for these procedures can be found from the gas phase turbulence model.

Initial Conditions

Initial conditions were specified in the region of the liquid core as illustrated in Fig. 3. The present approach is somewhat similar to Chatwani and Bracco.[13] Since the LHF approach is expected to give reasonable estimates of flow properties at large liquid volume fractions,[14] the earlier LHF monopropellant combustion model was used to estimate the flow field in the near-injector region.[3] The boundary of the liquid core was then defined by locations where the time-averaged liquid volume fraction was 0.997, with mean and fluctuating streamwise and radial velocities identified at 40 locations from the LHF predictions (see Table 3 for representative data at these boundary points). The velocities of drop groups emanating from these positions were then estimated by either the mean velocities (DSF approach) or by a random selection from the velocity PDF's (SSF approach). The drop size distributions at the boundary of the liquid core were extrapolated back from the position nearest to the injector where they were measured, assuming an average drop velocity and the linear burning rate law, see Table 3 for the distribution used for d = 0.6 mm. This translation procedure biases out drops that burn completely before reaching the first measurement location, however, measured spray properties are dominated by large drops and this effect is expected to be small.

Drop size estimates obtained at the boundary of the liquid core in this manner appear to be reasonable. Using either aerodynamic breakup theory, due to Reitz and Bracco,[12] or estimates based on maximum stable drop sizes for secondary breakup near the liquid surface, average drop sizes near the liquid surface for pressure-atomized nonevaporating sprays are correlated by:[16]

$$d_{p_{avg}} = C_B\sigma/(\rho\, u_0^2) \tag{7}$$

where C_B is roughly 10 and 40 for slug and fully-developed flows at the injector exit. Taking the latter value as representative of present test conditions yields $d_{p_{avg}}$ = 250 μm, which is comparable to present estimates of SMD along the boundary of the liquid core, see Table 3.

Computations

Calculations for the continuous phase were performed with a modified version of the GENMIX algorithm,[23] with a computational grid similar to past work.[17,22] Roughly 1000 drop groups were used for both the DSF and SSF predictions, with Eqs. (3)-(5) integrated by a second-order Runge-Kutta algorithm. Numerical accuracy was evaluated by doubling and halving the grid size and the number of drop groups, indicating that the results reported here are numerically closed within 3 percent.

Results and Discussion

Drop Size Properties

Predicted and measured SMD over the spray crossection are plotted as a function of x/d in Fig. 4 for injector diameters of 0.3 and 0.6 mm. Predictions include results from both the DSF and SSF models. The first observation is that liquid extends substantially beyond the region where liquid was seen during spray shadowgraph observations of liquid volume fractions,[3] e.g., x/d = 500-1000 for d = 0.3 and 0.6 mm, as opposed to x/d ca. 350 for a similar range of pressures and injector diameters. It is clear that earlier spray shadowgraphs did not record drops within the dilute portions of the spray far from the injector exit and really don't offer a quantitative evaluation of predictions. Another feature of the measurements is that SMD does not scale with x/d as d is changed, which would be indicative of mixing-controlled behavior that might satisfy the LHF approximation. Instead, the scaling more closely approximates completion of combustion at a fixed distance from the injector with x/d at the end of the liquid-containing region increasing from ca. 580 to ca. 980 as d is reduced from 0.6 to 0.3 mm. Since initial drop sizes and velocities of the two injectors are estimated to be nearly the same, this behavior is indicative of strong effects of separated flow.

Predictions using the DSF and SSF models are not very different from each other in Fig. 4 and are in reasonably good agreement with the measurements. The agreement between predictions and measurements is best toward the downstream end of the spray where the slide impaction

technique was more reliable due to lower liquid fluxes. Discrepancies between predictions and measurements are largest for near injector positions and d = 0.3 mm, where drop sizes are felt to be biased downward to difficulties of measuring large drops near the axis due to high rates of drop impaction since these positions were relatively close to the injector exit. The predictions were strongly dominated by effects of drop burning rates, while initial drop size distributions were calibrated; therefore, present findings suggest that drop burning rates observed in the combusting sprays are consistent with the single drop results reported earlier.[3]

Measured and predicted (both DSF and SSF methods) drop size distributions are illustrated in Figs. 4 and 5 for the two injector diameters. As noted earlier, the measurements at positions nearest the injector were extrapolated to the injector exit in an approximate manner to provide initial conditions for the predictions. Reversing the process to yield the predictions illustrated in Figs. 5 and 6 does not exactly reproduce the distributions at the smallest x/d due to different rates of deceleration experienced by various drop groups. This yields somewhat whimsical variations of predicted drop size distributions at the smallest x/d, due to limited drop size statistics, but the predictions are still in reasonably good agreement with the measurements.

Aside from limitations in resolving drop sizes near 10 μm, the subsequent evolution of the drop size distributions with increasing x/d is also predicted reasonably well in Figs. 5 and 6. In particular, the distributions become skewed toward smaller drop sizes as the end of the liquid-containing region is approached, which is represented reasonably well by the predictions.

Liquid Flow Properties

As noted earlier, measurements of liquid flow rates and fluxes are less accurate than measurements of SMD, however, in spite of these limitations, the results help provide a more complete picture of the structure of the sprays. Measured and predicted normalized liquid flow rates over the spray crossection are plotted as a function of x/d in Fig. 7 for the two injectors. Measurements at one position for each of the injectors are significantly higher than the rest and are felt to be anomalous due to problems with the slide impactor in the period where these results were obtained. The remaining results show the expected trend of decreasing liquid flow rates with increasing x/d. Although liquid is observed for x/d > 500, the flow-rate is generally less than 10 percent of the original flow rate at the injector exit. This comes about due to both consumption of drop liquid, as well as reduced drop velocities in the relatively slow gas flow far from the injector.

The comparison between predictions and measurements for liquid flow rates in Fig. 7 is not as good as for SMD in Fig. 4. This is typical of evaluations of spray models using liquid flow rates and fluxes: these quantities are difficult to measure accurately in pressure atomized sprays and are particularly sensitive to uncertainties in model predictions.[15,17,22] As before, there is little to choose between the DSF and SSF methods, with the latter yielding a somewhat shorter spray length. This comes about due to higher mean drag when instantaneous gas velocities are used to estimate drop trajectories (since drag forces are nearly quadratic functions of relative velocities for present conditions), as well as effects of turbulent dispersion which transports drops laterally into slower moving gas near the edge of the flow. However, effects of turbulent/drop interactions are much reduced for the present monopropellant sprays in comparison to evaporating sprays,[17] since the rate of drop gasification is not influenced by the radial position of the drops within the flow.

An indication of the width of the sprays can be seen from the plot of normalized liquid mass flux in Fig. 8 for d = 0.3 mm. Results for d = 0.6 mm are similar.[18] These results are plotted in terms of the radial similarity variable for turbulent jets, r/x, so that the actual width of the flow can be seen. However, similarity of liquid mass fluxes in these coordinates is neither expected nor observed. Spray widths extend to r/x ca. 0.12 at x/d = 460, but the liquid becomes progressively more confined near the axis at larger distances from the injector.

Liquid fluxes are difficult to predict accurately, as noted earlier,[15,17,22] and there is only qualitative agreement between predictions and measurements in Fig. 8. In fact, predictions underestimate the spray length for these conditions, see Figs. 4 and 7, so that no predictions are available for comparison with the measurements at the highest position. Consideration of turbulent dispersion using the SSF model does not yield a wider liquid flux distribution. Instead, separated flow effects dominate the process, causing small drops to disappear more quickly in the low velocity region near the edge of the flow.

Additional Predictions

The comparison between predictions and measurements indicates that both the DSF and SSF models provide the general features of the combusting monopropellant sprays, particularly for drop size properties where predictions are less sensitive to model parameters and measurements are more reliable. Thus, additional computations were performed to help gain insight concerning spray properties where measurements were not available. This included predictions of phase velocities and the sensitivity of predictions to variations of model parameters and spray operating conditions.

Predicted phase velocities for present test conditions are plotted in Fig. 9. Number-averaged drop velocities and time-averaged gas velocities along the axis, found from the DSF model, are plotted as a function of distance from the injector for d = 0.3 and 0.6 mm. Effects of separated flow are evident, with liquid velocities decaying much more slowly than gas velocities. The relative velocities are larger for d = 0.3 mm, since the smaller diameter injector involves higher rates of deceleration of the gas, which cannot be followed by the drops due to their limited response properties. In fact, liquid velocities remain nearly constant until x/d > 100, since both gas velocities and drop diameters are largest in this region. Farther from the injector, drop velocities decrease rapidly toward gas velocities, due to increased drop response as the drops become smaller. This increases drop residence times for a particular penetration length and makes estimates of properties like liquid flow rates and fluxes at large x/d very sensitive to model parameters, as noted earlier.

The sensitivity of predictions to variations of model parameters and spray operating conditions can be seen more quantitatively from the results summarized in Table 4. The percent increase of x/d at the points where SMD = 0 and $\dot{m}/\dot{m}_o$ = 1/2 are tabulated for various changes of parameters. These results involve use of the DSF model (except for the last item) and d = 0.6 mm, however, they are typical.

As expected, results in Table 4 show that the drop burning rate has a strong effect on the axial penetration of spray liquid, with a nearly one-to-one correspondence for changes of drop burning rates by a factor of two. Results are less sensitive to initial SMD, however, since reduction of drop sizes increases momentum exchange to the gas causing gas velocities to increase. The resulting larger drop velocities tend to compensate for smaller drop lifetimes when evaluating

spray penetration. Raising the ambient density by a factor of 10, for a fixed initial SMD, only decreases penetration lengths by 30-40 percent, largely due to increased entrainment rates which reduce gas phase velocities in the spray. Varying ambient density is actually likely to have a greater effect, however, by reducing drop sizes through the drop breakup criterion, e.g., Eq. (7). Based on effects of SMD in Table 4, this would considerably shorten spray penetration lengths from results measured during the present investigation. Effects of injector diameter variations follow from the nearly constant spray penetration length for various injector diameters, i.e., increasing the diameter by a factor of ten reduces the penetration length, in terms of x/d, by nearly the same ratio. Finally, effects of including turbulent dispersion are relatively small, particularly in view of uncertainties in estimating initial conditions for separated flow calculations.

Conclusions

Major conclusions of the study are as follows:

1. Present slide impaction measurements show that the liquid-containing region is 2-4 times longer than found during earlier measurements using flash shadowgraphs by Lee et al.,[3] due to the inability of the shadowgraph approach to detect dilute portions of the spray.

2. Present measurements of combusting spray properties show that monopropellant drop burning rates within the sprays, $- dr_p/dt$ ca. 10 mm/s, are consistent with earlier single drop burning rate measurements at the same pressure, ca. 5 MPa. Due to its dominance of spray combustion properties, additional study of the drop combustion properties of HAN-based monopropellants is recommended.

3. The combusting monopropellant sprays exhibited strong effects of separated flow, with the length of the liquid containing region being nearly the same, ca. 300 mm, for injector diameters of 0.3 and 0.6 mm when initial SMD and injector exit velocities were nearly the same.

4. Estimated mean drop sizes near the injector exit were consistent with recent measurements for nonevaporating pressure-atomized sprays.[16] This suggests that initial mean drop sizes (SMD) can be estimated from either the aerodynamic breakup theory of Reitz and Bracco,[12] or analogous secondary breakup criteria,[16] through Eq. (7). However, this approach is only provisional, pending additional study of effects of liquid turbulence at the injector exit and approach of the flow to the LHF limit.

5. Predictions using the DSF and SSF models were in reasonably good agreement with each other and with the measurements, particularly in view of the relatively large uncertainties of estimates of initial drop properties and the slide impaction measurements. Thus, the DSF approach is favored, since it requires less extensive computations. The relatively small effects of drop/turbulence interactions follows since the gas phase has constant properties and drop burning rates are relatively independent of the properties of their surroundings for combusting monopropellant sprays.

Acknowledgements

This research was sponsored by the Army Research Office and the U.S. Army Armament Research, Development and Engineering Center, Picatinney Arsenal, NJ under Contract No. DAAL03-86-K-0154.

References

[1]Kounalakis, M. E. and Faeth, G. M., "Combustion of HAN-Based Liquid Monopropellants near the Thermodynamic Critical Point," Combust. Flame, Vol. 74, November 1988, pp. 179-192.

[2]Lee, T.-W., Gore, J. P., Faeth, G. M. and Birk, A., "Analysis of Combusting High-Pressure Monopropellant Sprays," Combust. Sci. and Tech., Vol. 57, 1988, pp. 95-112.

[3]Lee, T.-W., Tseng, L.-K. and Faeth, G. M., "Separated-Flow Considerations for Pressure-Atomized Com-busting Monopropellant Sprays," J. Prop. Power, in press.

[4]Birk, A. and Reeves, P., "Annular Liquid Propellant Jets—Injection, Atomization and Ignition," Report No. BRL-TR-2780, Ballistic Research Laboratory, Aberdeen Proving Ground, March 1987.

[5]McBratney, W. F., "Windowed Chamber Investigation of the Burning Rate of Liquid Monopropellants for Guns," Report No. BRL-TR-03018, Ballistic Research Laboratory, Aberdeen Proving Ground, April 1980.

[6]McBratney, W. F., "Burning Rate Data LGP 1845," Report No. BRL-TR-03128, Ballistic Research Laboratory, Aberdeen Proving Ground, August 1981.

[7]Vosen, S. R., "The Burning Rate of HAN-Based Liquid Propellants," Twenty-Second Symposium (International) on Combustion, The Combustion Institute, Pittsburgh, pp. 1817-1825, 1988.

[8]Zhu, D. L. and Law, C. K., "Aerothermochemical Studies of Energetic Liquid Materials: 1. Combustion of HAN-Based Liquid Gun Propellants under Atmospheric Pressure," Combust. Flame, Vol. 70, December 1987, pp. 333-342.

[9]Beyer, R. A., "Atmospheric Pressure Studies of Liquid Monopropellant Drops in Hot Flow," Report No. BRL-TR-2768, Ballistic Research Laboratory, Aberdeen Proving Ground, October 1986.

[10]Beyer, R. A., "Single Droplet Studies in a Hot, High Pressure Environment," Report No. BRL-TR-2900, Ballistic Research Laboratory, Aberdeen Proving Ground, March 1988.

[11]Beyer, R. A. and Teague, M. W., "Studies of Single Liquid Propellant Drops in Hot, High Pressure Environments," 22nd JANNAF Combustion Meeting, CPIA Publication 457, Vol. 2, October 1986, p. 429.

[12]Reitz, R. D. and Bracco, F. V., "Mechanism of Atomization of a Liquid Jet," Phys. Fluids, Vol. 25, October 1982, pp. 1730-1742.

[13]Chatwani, A. V. and Bracco, F. V., "Computation of Dense Spray Jets," Third International Conference on Liquid Atomization and Spray Systems, Imperial College, London, 1985.

[14]Ruff, G. A., Sagar, A. D. and Faeth, G. M., "Structure and Mixing Properties of Pressure-Atomized Sprays," AIAA J., Vol. 27, July 1989, pp. 901-908.

[15]Ruff, G. A., Bernal, L. P. and Faeth, G. M., "Structure of the Near-Injector Region of Non-Evaporating Pressure-Atomized Sprays," J. Prop. Power, in press.

[16]Ruff, G. A. and Faeth, G. M., "Continuous-Phase Properties of the Near-Injector Region of Non-Evaporating Pressure-Atomized Sprays," AIAA Paper No. 90-0464, 1990.

[17]Solomon, A.S.P., Shuen, J.-S., Zhang, Q.-F. and Faeth, G. M., "Measurements and Predictions of the Structure of Evaporating Sprays," J. Heat Trans., Vol. 107, August 1985, pp. 679-686.

[18]Lee, T.-W., "Structure of Combusting Monopropellant Sprays at High Pressures," Ph.D. Thesis, The University of Michigan, Ann Arbor, Michigan, 1990.

[19]Gordon, S. and McBride, B. J., "Computer Program for Calculation of Complex Chemical Equilibrium Compositions, Rocket Performance, Incident and Reflected Shocks and Chapman-Jouguet Detonations," NASA Report SP-273, Washington, 1971.

[20]Jeng, S. M. and Faeth, G. M., "Species Concentrations and Turbulence Properties in Buoyant Methane Diffusion Flames," J. Heat Trans., Vol. 106, November 1984, pp. 721-727.

[21]Lockwood, F. C. and Naguib, A. S., "The Prediction of Fluctuations in the Properties of Free, Round Jet, Turbulent Diffusion Flames," Combust. Flame, Vol. 24, February 1975, pp. 109-124.

[22]Faeth, G. M., "Mixing, Transport and Combustion in Sprays," Prog. Energy Combust. Sci., Vol. 13, 1987, pp. 293-345.

[23]Spalding, D. B., GENMIX: A General Computer Program for Two-Dimensional Parabolic Phenomena, Pergamon Press, Oxford, 1978.

Table 1 Summary of test conditions[a]

Injector Diameter[b] (mm)	Ambient Pressure[c] Re (MPa)	Pressure Drop Oh (MPa)	Injector Velocity[d] Wef (m/s)
Drop Size Measurements:			
0.58	4.89	3.13	65.5
	7800	0.030	54200
0.31	4.69	3.96	73.8
	4700	0.041	36700
Liquid Flux Measurements:			
0.58	4.63	3.56	70.0
	8300	0.030	61700
0.33	4.75	3.70	71.4
	4800	0.040	36500

[a]Combustion of LGP 1845, consisting of 63.2% HAN, 20% TEAN and 16.8% H_2O (by mass). Adiabatic combustion yields product temperature of 2150 K, consisting of 69.2% H_2O, 12.9% CO_2 and 17.4% N_2 (by volume). Liquid properties: ρ_f = 1454 kg/m^3, μ_f = 0.0071 kg/ms, σ = 0.067 N/m.
[b]Injector length-to-diameter ratio of 42, yielding fully-developed turbulent pipe flow at exit.
[c]Combustion product environment at 2790 K and consisting of 19.8% H_2O, 38.3% N_2 and 40.9% Ar (by volume).
[d]For a flow coefficient of unity.

Table 2 Source terms and empirical constants for separated-flow predictions

ϕ	S_ϕ
1	$\sum_{i=1}^{n} \dot{n}_i (m_{i_{in}} - m_{i_{out}})_j / V_j$
$\bar{u}$	$\sum_{i=1}^{n} \dot{n}_i ((m_i u_{pi})_{in} - (m_i u_{pi})_{out})_j / V_j$
k	$\mu_t(\partial\bar{u}/\partial r)^2 - \bar{\rho}\varepsilon$
ε	$(C_{\varepsilon 1}\mu_t(\partial\bar{u}/\partial r)^2 - C_{\varepsilon 2}\bar{\rho}\varepsilon)\varepsilon/k$

μ_t	C_μ	$C_{\varepsilon 1}$	$C_{\varepsilon 2}$	σ_k	σ_ε	K_b(mm/s)
$C_\mu\bar{\rho}k^2/\varepsilon$	0.09	1.44	1.87	1.0	1.3	10

Table 3 Initial conditions for separated-flow predictions[a]

Location Index	x/d	r/d	$\Delta\dot{m}_j/\dot{m}_o$	$\bar{u}_p/u_o$	$\bar{v}_p/u_o$	$\bar{u}_{p'}/u_o$	$\bar{v}_{p'}/u_o$
1	0.31	0.47	0.0358	0.974	0.008	0.121	0.060
10	3.13	0.39	0.0315	0.801	0.076	0.074	0.037
20	6.25	0.29	0.0264	0.858	0.072	0.057	0.028
30	9.37	0.15	0.0238	0.904	0.016	0.045	0.023
40	10.8	0.00	0.0075	0.914	0.000	0.041	0.020
d_{po}	%[b]	d_{po}	%[b]	d_{po}	%[b]	d_{po}	%[b]
185	1.20	215	7.72	245	4.21	285	2.01
190	2.91	220	6.92	250	3.91	295	1.71
195	5.32	225	6.42	255	3.51	305	1.40
200	7.92	230	5.72	260	3.21	315	1.10
205	9.73	235	5.22	265	2.81	325	0.80
210	8.73	240	4.71	275	2.31	335	0.50

[a]Drop size distribution for a 0.6 mm diameter injector.
[b]Percentage of total drop number flow rate.

Table 4 Parameter sensitivity of separated-flow predictions[a]

Input Parameter	Factor of Variation	Percent increase of x/d	
		SMD = 0	$\dot{m} = \dot{m}_o/2$
Drop burning rate	1/2	41	56
Drop burning rate	2	- 32	- 40
Initial SMD	1/2	- 28	- 38
Ambient density	10	- 42	- 30
Injector diameter	10	- 80	- 84
Turbulent dispersion[b]	---	- 9	- 11

[a]Results for d = 0.6 mm using the DSF model except as noted.
[b]The effect of including turbulent dispersion is shown.

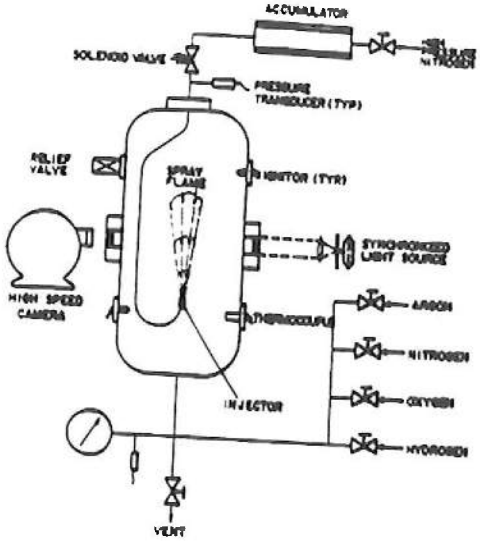

Fig. 1 Sketch of spray combustion apparatus.

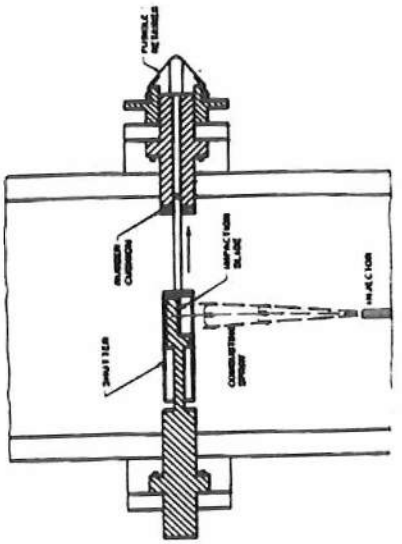

Fig. 2 Sketch of slide impactor assembly.

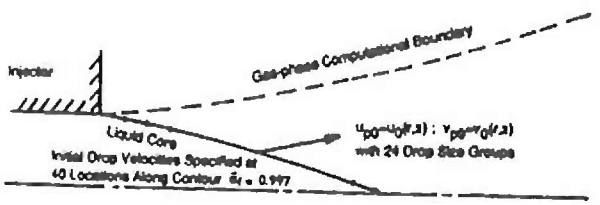

Fig. 3 Specification of initial conditions for separated-flow computations.

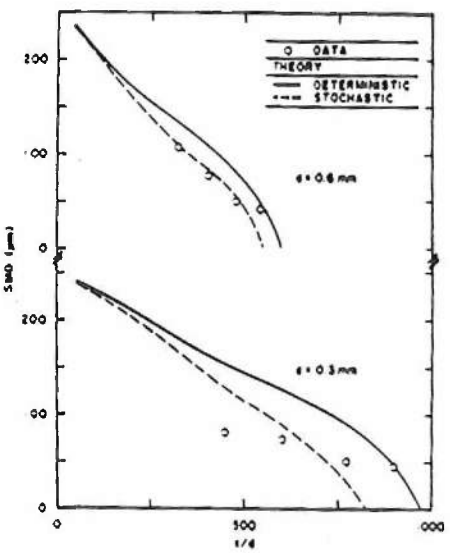

Fig. 4 Predicted and measured SMD variation with streamwise distance.

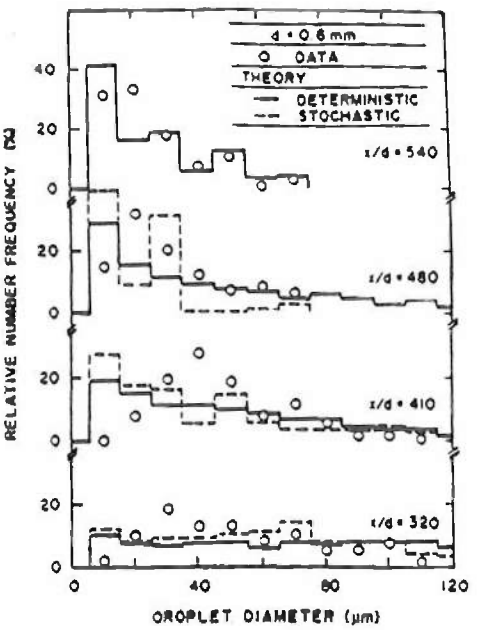

Fig. 5 Predicted and measured drop size distributions at various streamwise distances, d = 0.6 mm.

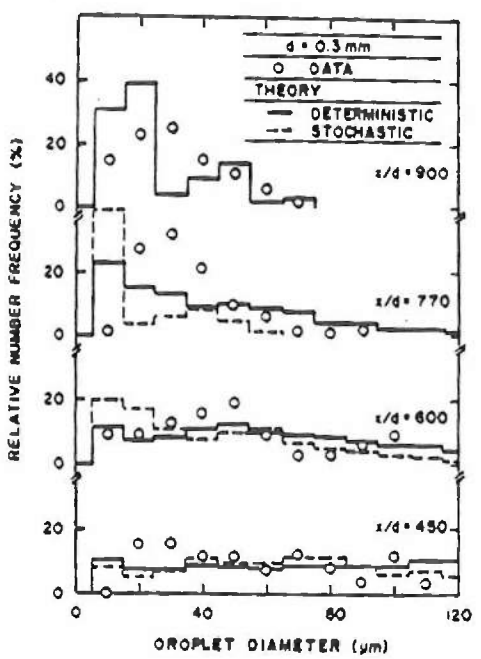

Fig. 6 Predicted and measured drop size distributions at various streamwise distances, d = 0.3 mm.

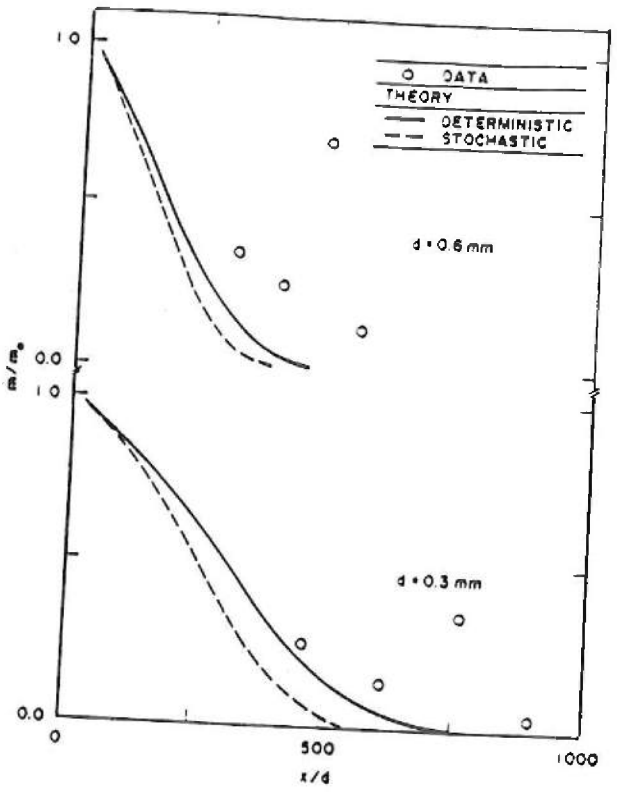

Fig. 7 Predicted and measured liquid mass flow rate variation with streamwise distance.

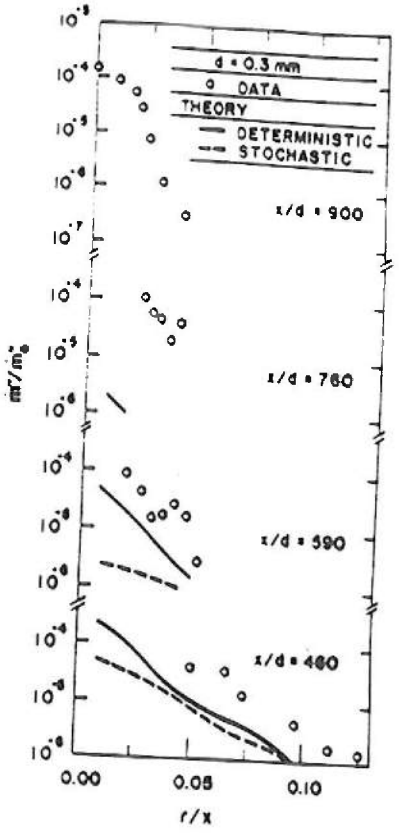

Fig. 8 Predicted and measured liquid mass flux distributions at various streamwise distances, d = 0.3 mm.

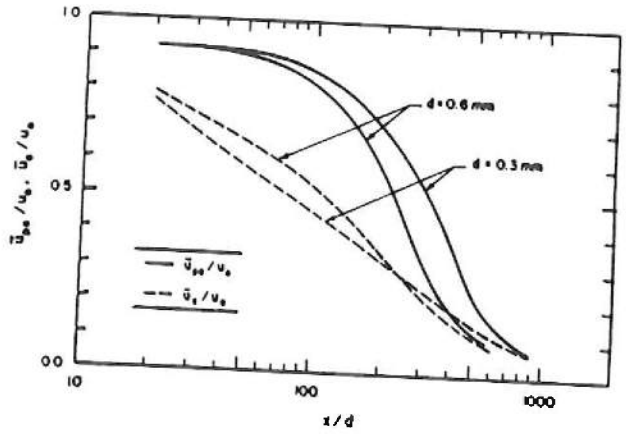

Fig. 9 Predicted mean phase velocity variation with streamwise distance.